

**TREATMENT STRATEGY FOR COMPOSITE TISSUE LIMB  
TRAUMA**

A Dissertation

Presented to

The Academic Faculty

by

Mon Tzu (Alice) Li

In Partial Fulfillment

of the Requirements for the Degree

Doctor of Philosophy in the

School of Biomedical Engineering

Georgia Institute of Technology

May 2015

**COPYRIGHT © 2015 BY MON TZU LI**

**TREATMENT STRATEGY FOR COMPOSITE TISSUE LIMB  
TRAUMA**

Approved by:

Dr. Robert E. Guldberg, Advisor  
School of Mechanical Engineering  
*Georgia Institute of Technology*

Dr. Gordon L. Warren  
Department of Physical Therapy  
*Georgia State University*

Dr. Andrés J. García  
School of Mechanical Engineering  
*Georgia Institute of Technology*

Dr. Linda C. Cendales  
Department of Surgery  
*Duke University*

Dr. Johnna S. Temenoff  
Department of Biomedical Engineering  
*Georgia Institute of Technology*

Date Approved: Dec 11, 2014

*Dedicated to my family, friends, and most of all, my fiancé,  
for their love and support.*

## ACKNOWLEDGEMENTS

Many have told me over the years that graduate school years were the best years of their lives, and I have no doubt that they were the best of mine. I am grateful to have had this opportunity to research at a top-notch university, learn from the best in the field, and meet so many amazing people.

First of all, it has been a great honor to have worked with Bob these last few years. His emphasis on clear communication of the science really makes him a unique advisor, and I know I am definitely a better presenter and communicator because of it. I appreciate the amount of freedom he gives his students to pursue their interests within the purview of the lab's research, even though it does make the path more winding at times. His high standards for quality challenge all of us to work harder and set higher bars for ourselves. Likewise, I would like to thank all of my committee members for their help and guidance through the last few years. Gordon has spent hundreds of hours traveling to Tech, helping with surgeries, and working out the kinks with the muscle testing. His dry humor has gotten me through many 10-hour days in the PRL, and his willingness to work those 10-hour days with me was extraordinary. Words cannot describe how much I have appreciated his support and guidance throughout this project. Johnna has been an amazing mentor; when I attended the Society for Biomaterials annual meeting as an undergraduate senior, she sought me out to offer some words of encouragement. She challenged me to gain a more thorough understanding of the mechanisms behind my work. Andrés always had great stories to tell that were incredibly entertaining. His belief in my abilities near the end of my PhD was a great motivating factor, especially when I was starting to burn out. I also had the great opportunity to benefit from his NIH Cell/Tissue Engineering training grant, where I learned to critically analyze a wide variety of biomedical research. Dr. Cendales was extremely supportive and offered a unique clinical perspective to my work. I'm also very grateful for her willingness to work

around my schedule, which facilitated many milestones through my graduate career. Additionally, Dr. Guijun Dong and Kefeng Li, visiting scholars from China, have been amazing help to me, particularly for the muscle homogenizing and assays. They were kind enough to not point out my butchering of the Chinese language trying to hold a conversation while working non-stop on my muscle samples.

I also had the opportunity to intern at MiMedx. I am thankful to Tom, Michelle, Nicole, and Lisa for taking their time to train me and to guide me through my work at the company. I am very glad to have seen the inner workings of a mid-sized start-up in the challenging field of tissue engineering. And I'm so thankful that my carpool buddy Apoorva was there with me --- I loved our talks while stuck in traffic trying to get home.

A big part of my graduate career involved leadership opportunities that I was lucky enough to participate in. I had the honor of working closely with Meg and Colly while heading some of the committees in the Bioengineering and Biosciences United Graduate Students (BBUGS) group. They were huge advocates for graduate students, helping to secure funds and support for student-centric activities. Through BBUGS, I was able to work with other talented graduate students that really took the initiative to organize events that benefit the graduate community. Through organizing the Biotechnology Career Fair and BME recruiting events, I was able to learn a lot about leadership by working with Sally and Shannon, who manage to organize amazing things in a surprisingly short amount of time. My participation in the Graduate Leadership Program opened my eyes to various elements of self reflection and leadership through service. In this program, Ravi not only convinced me to go through the ropes course despite my fear of heights and falling, he also participated and were side-by-side with us as we completed the challenges.

The amount of research presented here could not have been possible without a whole host of people, particularly in IBB, that helped throughout the way. James and Floyd were always so helpful whenever I had a presentation in the Suddath room, and

they would stay until everything was set up perfectly. Janice and Sandra have been incredibly helpful and responsive with the finances, whether it was for BBUGS or for the training grant or dispensing IBB funds. Aqua has seen me so many times over the years in the histology lab, and she was always so concerned with making sure that my samples were processed and sectioned correctly. Andrew was so patient with us as we learned confocal microscopy, and he was always there to help figure out how to image the right samples. Thank you all for your assistance and care --- it really did make the research that much easier with your support.

The people of the Guldberg lab have been amazing. I can't imagine having to do this PhD in any other lab. Everyone is so collaborative and willing to help each other. This kind of support is really extraordinary, and I'm thankful to have had this experience with all these people. Hazel has given such great guidance to me throughout the years. She always had words of encouragement when things weren't working well, and she ensured that the science was done well and done right. Her dry humor was much appreciated, and I will definitely miss her and our impromptu discussions. Angela was always so willing to help me brainstorm or think through my CT analysis. Her impeccable taste in food and restaurants has allowed me to sample amazing fare at the ORS conferences. Nick W really helped me get started with my project, from surgeries, muscle testing, perfusions, and dissections. Laxmi was an amazing sounding board, which was essential in getting me through my proposal and defense, and he somehow always found the positive side of the data even when I couldn't see it. I couldn't have survived my final years without my amazing undergrads Sukhita and Nick S. They have spent endless hours helping me collect data and were so good at tackling any challenge that came their way. I know that they will do wonderful things no matter where they end up. Vivian always took care of me whenever I had to schedule meetings with Bob, paperwork to sign, or had reimbursement issues. Joel, Brent, and Dosier were amazing and taught me so many new techniques. Their hard work and dedication were something

for me to aspire to. I really admire Jason for his persistence to finish the PhD even with difficult hurdles. I will definitely miss David's (and Rachel's) amazing baked goods. Marian and Giuli have such great work ethics and are always at it --- I have no doubt they will be wonderful professors one day. I know that Albert and Brennan will live up to the crazy Guldberg lab alums while still doing brilliant work in lab. And Brett and Marissa, the newest recruits, are off to an amazingly productive start --- they are very fitting additions to the lab. I really have to thank Lauren for sitting through all my rants and talks and questions throughout the years --- even though I'm sure I talked way too much and bothered her during busy times. She will make an amazing professor and teacher someday soon! Ashley and Tanu, my incoming classmates --- we've had great times over the years. I'm in awe of how Ashley (my now neighbor) always bounces back after countless challenges --- and not only that, she still has such a bright infectious personality. Tanu and I have had some ridiculous times together. We made such a great team (you write with speed, I refine) --- and I'm so glad that you were there to push me to go work out because I am sure that I wouldn't have gone without you. I can't wait until our Michelin star tour (another 15 years, right?)!

A big part of what makes grad school the best times of my life is the friendships I've made over the last few years. My incoming BME class bonded over the pain and stress of our core classes. Inthu, Kristin, Mei, Eric, Akhil --- we've had some great times together, and it's great to have someone to talk to about problems and concerns throughout the PhD that is also experiencing something similar. All of our birthday and food celebrations (from Thanksgiving to New Years to Bollywood movies) have been delicious and great fun! James and Kyuyun have become very good friends with us, sharing our love for food and pets. I hope to visit them (and their newborn baby) soon in DC. Patricia, our honorary BME and lab member who borrows all of our equipment --- I will miss the days when your laughter filled the halls and seeped into the lair. And I couldn't have picked a better person to train with for our first 5k (and there's no better

trainer than Ashley)! Jessica, I'm so glad that we took that management class together because I wouldn't have had the opportunity to get to know you without it. You've been a great host for so many of your house parties, and I love that we could share our love of food (and counteracting it by working out).

Tiffany, Stacie, Shu, and Gen --- we've really had some great times together over the years. Your consistent running regimen of going to the 5k Chattahoochee trail every weekend finally got me to cross the milestone of running a mile, and our post-running tofu soup and bubble tea feasts at So Kong Dong and Sweet Hut made it that much better. Our Thanksgiving celebrations, whether we have turkey or Peking duck, have been so much fun these last few years. Our cabin trips up to Blue Ridge are still some of my favorite times during grad school, and I will definitely miss our food-based birthday celebrations together. Our Starbucks work marathons really got me on track on writing, and our late night Sweet Hut runs gave me motivation to keep going. Our ranting sessions were great ways to let off steam after long days of work and frustration. Tiffany, I wouldn't have a job now if it weren't for you, and I love our discussions because we could always build ideas on top of each other's ideas. I'm excited to be see you again soon! Stacie, I admire your impeccable organization --- you were always prepared for everything because you feared and prepared for the worst. Gen, I'm so glad that you are finally happy with work and doing what you love --- you deserve it after all those persistent years through the roadblocks to obtaining your nursing degree. Shu, you are extremely smart and talented, and best of luck to you finishing up. I know you will do great things --- just trust in yourself and be confident enough to express yourself. I couldn't have found better friends than you, and I really can't imagine going through the graduate years without you.

Last but not least, I need to thank my family. My parents gave me financial support through the years, even paying for expensive school trips even though they had barely enough to get by. Though we've had our differences, my mom has always given

me the freedom I needed to do what I want. I still remember her determination to get me to school on time, just because I hated getting there late. She drove me to and from school every day and spoiled me by doing all the chores so that I could concentrate on schoolwork. She instilled in me a high standard of quality when I was young, and it has never left, even though my standard of quality isn't quite as high as hers. For her sacrifices and her time raising me, I will be forever grateful. I have to thank my brother Tom, who has given me opportunities to explore the world and continues to be a role model for me. And, of course, my fiancé Si, who has taken care of me through the best and worst times of this graduate career. He allowed me to get my kitties Momo and Shadow even though he is somewhat allergic to cats, and they have been my desk buddies and de-stressors on those long nights of writing. I thank him for being understanding, even when I'm being unreasonable or when I'm in a bad mood. He basically took care of everything from the laundry to cooking to taking care of the cats when I was finishing up, and I really couldn't have done it without him. He has been amazingly supportive through these years, and I hope that I can do the same for him as he works through his PhD as well. I love him for everything he is, and I wish that I can be as understanding and supportive as he has been for me.

Thank you all for everything!

## TABLE OF CONTENTS

ACKNOWLEDGEMENTS .....	IV
LIST OF FIGURES .....	XIII
LIST OF SYMBOLS AND ABBREVIATIONS .....	XV
SUMMARY .....	XVII
CHAPTER 1      SPECIFIC AIMS .....	1
Aim 1 .....	1
Aim 2 .....	2
Aim 3 .....	3
CHAPTER 2      LITERATURE REVIEW .....	5
2.1    Traumatic Injuries to the Extremities .....	5
2.1.1    Volumetric Muscle Loss .....	5
2.1.2    Open Fractures/Composite Injuries.....	7
2.2    Animal Injury Models .....	9
2.2.1    Volumetric Muscle Loss .....	9
2.2.2    Composite Bone & Muscle Injuries .....	11
2.3    Current Tissue Engineering Strategies Tested in Pre-Clinical Injury Models .....	14
2.3.1    Treatments for Volumetric Muscle Loss .....	14
2.3.2    Treatments for Composite Injury Models.....	21
2.4    Motivations for Research .....	22
CHAPTER 3      VOLUMETRIC MUSCLE LOSS MODEL IN THE RAT QUADRICEPS .....	24
3.1    Abstract.....	24
3.2    Introduction.....	25
3.3    Materials/Methods .....	27
3.4    Results .....	31
3.5    Discussion.....	38
CHAPTER 4      COMPOSITE MUSCLE & BONE INJURY MODEL IN THE RAT .....	44

4.1	Abstract.....	44
4.2	Introduction.....	45
4.3	Materials/Methods .....	48
4.4	Results .....	55
4.5	Discussion.....	68
<b>CHAPTER 5 DEVELOPMENT AND CHARACTERIZATION OF THE HAMSTRINGS VML MODEL.....</b>		<b>76</b>
5.1	Abstract.....	76
5.2	Introduction.....	76
5.3	Materials/Methods .....	79
5.4	Results .....	84
5.5	Discussion.....	92
<b>CHAPTER 6 TREATMENT OF THE BICEPS FEMORIS VML MODEL WITH MICROVESSELS .....</b>		<b>98</b>
6.1	Abstract.....	98
6.2	Introduction.....	98
6.3	Materials/Methods .....	102
6.4	Results .....	105
6.5	Discussion.....	110
<b>CHAPTER 7 EFFECTS OF MICROVASCULAR CONSTRUCTS ON THE HEALING OF COMPOSITE MUSCLE &amp; BONE INJURIES .....</b>		<b>116</b>
7.1	Abstract.....	116
7.2	Introduction.....	117
7.3	Materials/Methods .....	119
7.4	Results .....	126
7.4.1	Microvascular Construct around the Bone Defect .....	126
7.4.2	Microvascular Construct in the Quadriceps Defect .....	127
7.5	Discussion.....	131
<b>CHAPTER 8 SUMMARY AND FUTURE DIRECTIONS .....</b>		<b>137</b>
8.1	Overall Summary .....	137

8.2	Development and Characterization of Preclinical Models that Reproduce Traumatic Limb Injuries .....	141
8.3	Pursuit of a Critically-Sized VML Model.....	145
8.4	Challenges in the Use of Microvascular Constructs for Regeneration of Musculoskeletal Tissues .....	147
8.5	Final Conclusions.....	151
APPENDIX	.....	152
A.1.	Microvessel Isolation Protocol.....	152
A.1.1.	Solutions (keep all solutions on ice or in fridge).....	152
A.1.2.	Preparation of Collagenase .....	152
A.1.3.	Fat Isolation.....	153
A.1.4.	Microvessel Isolation from Fat .....	154
A.1.5.	Suspending Microvessels in a Collagen Gel.....	155
A.2.	Myoblast Isolation Protocol .....	156
A.2.1.	Solutions for Myoblast Isolation & Culture .....	156
A.2.2.	Isolation of Soleus Muscle .....	156
A.2.3.	Mechanical and Enzymatic Dissociation of the Muscle.....	157
REFERENCES	.....	159

## LIST OF FIGURES

Figure 1: Methods for Creating and Analysis of the Quadriceps VML Model. ....	28
Figure 2: MRI Visualization of the Extent of Muscle Injury.....	32
Figure 3: Quantitative Measures of Muscle Function.....	33
Figure 4: Quantitative Measures of Muscle Fatigue.....	34
Figure 5: Muscle Mass and Representative Cross-Sectional Images of Muscle. ....	35
Figure 6: Correlations between Measurements.....	36
Figure 7: Quantitative Measures of Gait and Limb Recovery.....	37
Figure 8: Fibrosis and regenerating fibers, visualized in histology.....	38
Figure 9: Representative Methods Images.....	49
Figure 10: Femur Radiographs. ....	55
Figure 11: Bone Regeneration. ....	57
Figure 12: Bone Histology.....	57
Figure 13: Muscle Histology. ....	58
Figure 14: Muscle Functional Capacity.....	60
Figure 15: Limb Function. ....	62
Figure 16: Bone Volume after Treatment with Muscle Autografts.....	63
Figure 17: Muscle Regeneration after Treatment with Muscle Autografts. ....	64
Figure 18: Early revascularization of the Thigh within the Defect Areas. ....	66
Figure 19: Vessel Diameter Distribution at Days 3, 7, and 14. ....	67
Figure 20: Representative Vessel Images within the Bone Defect Area at Day 14. ....	68
Figure 21: Enzyme Activities of Defect Tissue after Biceps Femoris VML.....	85
Figure 22: Hamstrings Muscle Function.....	86
Figure 23: Defect Revascularization 2 and 4 weeks post-injury. ....	87
Figure 24: H&E Histology at 2 weeks post-injury. ....	88
Figure 25: Masson's Trichrome Histology at 2 weeks post-injury. ....	89

Figure 26: H&E Histology at 4 weeks post-injury. ....	90
Figure 27: Masson's Trichrome Histology at 4 weeks post-injury. ....	90
Figure 28: H&E Histology of Biceps Femoris at 6 weeks post-injury. ....	91
Figure 29: H&E Histology of Biceps Femoris at 8 weeks post-injury. ....	91
Figure 30: Microvessel Culture, Construct, and Surgery. ....	106
Figure 31: Vascular Volume in Microvessel-Treated Biceps Femoris.....	107
Figure 32: Histology of Microvessel and Microvessels+Myoblasts groups at 4 weeks Post-Injury.....	108
Figure 33: Citrate Synthase Activity 8 weeks post-injury. ....	109
Figure 34: Histology of Microvessel and Microvessels+Myoblasts groups at 8 weeks Post-Injury.....	110
Figure 35: Microvascular Construct Surrounding a Nanofiber Mesh. ....	122
Figure 36: Microvascular Construct for Filling of Quadriceps Defect. ....	123
Figure 37: Early Revascularization of Thigh near the Defect Area after Microvascular Treatment around Mesh. ....	126
Figure 38: Longitudinal Analysis of Bone Regeneration after Microvascular Treatment around Mesh.....	127
Figure 39: Early Revascularization of Thigh near the Defect Area after Microvascular Treatment in the Quadriceps. ....	128
Figure 40: Bone Mineral Volume and Radiograph Images after Microvascular Treatment in the Quadriceps. ....	129
Figure 41: Bone Postmortem Biomechanical Properties after Microvascular Treatment in the Quadriceps. ....	129
Figure 42: Muscle regeneration after Microvascular Treatment in the Quadriceps. ....	131

## LIST OF SYMBOLS AND ABBREVIATIONS

ANOVA	Analysis of variance
ATP	Adenosine triphosphate
BAM	Bladder acellular matrix
BMP-2	Bone morphogenetic protein-2
CK	Creatine kinase
CS	Citrate synthase
DTNB	5'5'-dithio-bis(2-nitrogenzoic acid)
ECM	Extracellular matrix
GFP	Green fluorescent protein
H&E	Hematoxylin & eosin
IACUC	Institutional animal care and use committee
IGF-1	Insulin-like growth factor 1
LD	Latissimus dorsi
LEAP	Lower extremity assessment project
Micro-CT	Micro-computed tomography
MPC	Muscle progenitor cell
MRI	Magnetic resonance imaging
MSC	Mesenchymal stem cell
MVC	Microvascular construct
PBS	Phosphate-buffered saline
PCL	Polycaprolactone
PCSA	Physiological cross-sectional area

rh-BMP2	Recombinant human bone morphogenetic protein-2
SEM	Standard error of mean
SIP	Sickness impact profile
SIS-ECM	Small intestine submucosa extracellular matrix
TA	Tibialis anterior
TE-MR	Tissue-engineered muscle repair
VEGF	Vascular endothelial growth factor
VML	Volumetric muscle loss

## SUMMARY

Large extremity injuries that involve damage to both muscle and bone pose a significant challenge in the clinic. Even with gold standard treatment, covering the exposed bony defect with a vascularized muscle flap, these injuries often do not recover to full function, affecting patients' quality of life and their contributions to society. Patients recovering from large extremity wounds suffer from pain and mobility issues years after limb salvage, and some patients ultimately opt for late stage amputation. Thus, there is a need for tissue engineering strategies to facilitate functional recovery of large composite defects of the limb.

Despite this pressing need, few tissue engineering strategies exist and have been tested in composite defects preclinically, limiting the number of translatable treatment options. The overall goal of this dissertation is to examine the regenerative potential of engineered matrix constructs and stem cells on composite bone & muscle defects. To accomplish this goal, we first established a volumetric muscle loss model in the quadriceps and a composite muscle and bone injury model in the quadriceps and femur of the rat, designed to allow for functional measurements of tissue function. We found that a large VML in the quadriceps caused sufficient damage that an autograft within the defect space was not able to significantly recover muscle function. In the composite injury model, the addition of the muscle injury on top of the segmental bone defect compounded functional deficits and attenuated rhBMP-2 mediated bone regeneration. In the characterization of these models, we found that the VML in the quadriceps defect was complicated by multi-muscle and vessel/nerve damage and that early revascularization

was delayed in the composite injury group compared to the bone injury only group. To address these issues, we designed a separate VML model that is more suited for testing for muscle regeneration within a single, planar muscle, the biceps femoris, and further tested a vascular treatment, microvascular constructs with or without myoblasts, within this VML model. We found that though this treatment allowed for an early vascular response, the microvascular constructs treatment did not lead to a full recovery of the muscle. Third, we tested the effects of this vascular treatment in the composite injury model, either surrounding the bone or within the muscle defect. We found that the microvascular constructs surrounding the bone resulted in an early revascularization of the limb but led to decreased bone regeneration. Microvascular constructs with myoblasts, on the other hand, were implanted into the muscle and demonstrated a small increase in both bone and muscle regeneration despite a lack of increased vascularization. Taken together, these results suggest that while vascularization may play a role in regenerating tissues, the full recovery of complex limb injuries likely depend on other cellular and biochemical factors as well.

The studies presented here move the field of composite injuries forward by presenting new platforms on which to test therapeutics and measure functional outcomes. This work has led to some insights into the revascularization of large defects, and by analyzing the effects of vascular treatment on these complex injuries, we have demonstrated a potential therapeutic that may warrant further research. Overall, this work will aid in the development of tissue engineering treatments to facilitate the full functional recovery of complex limb trauma.

## CHAPTER 1 Specific Aims

Approximately 82% of all fractures in current US armed conflicts are open fractures, in which a soft tissue injury is sustained along with the bone fracture [1]. The clinical gold standard for treating such injuries with large defects in the bone and muscle involves using muscular flaps to cover the bone [2]. Despite this treatment approach, the percentage of complications remains high, and patients often do not regain normal function of their extremity [3, 4]. Though multi-tissue injuries remain a complex clinical problem, few animal models exist in which to test possible treatments, limiting assessments of tissue engineering strategies [5-9].

Due to a substantial amount of tissue damage and debridement treatment in composite injuries, a large volume of cells and extracellular matrix (ECM) proteins that are necessary for tissue healing are removed from the body. The replacement of cells and structural proteins within the defect space may aid in regeneration by facilitating the repopulation of the defect space. In the replacement of large volumes of tissue, nutrient transfer necessitates a vascular supply to maintain the viability of delivered cells. **The objective of this project is to examine the regenerative potential of engineered matrix constructs and stem cells on composite bone & muscle defects.** *We hypothesize that stem cells delivered on engineered matrix constructs into the muscle defect will aid in muscle regeneration and promote bone healing, ultimately resulting in superior functional limb recovery.* This objective will be accomplished through the following specific aims:

**Aim 1: Characterize a volumetric muscle loss model and bone & muscle composite injury model in the rat.** There is a need for animal models that recapitulate extremity

injuries seen in the clinic that involve damage to multiple muscle groups and tissues. *Our hypothesis was that a large volumetric muscle loss in the quadriceps will result in decreased muscle function and that a composite bone and muscle injury will result in a compounded functional deficit in the bone, muscle, and limb function.* To develop the volumetric muscle loss (VML) model in quadriceps, we used an 8-millimeter diameter biopsy punch to create a full-thickness defect in the antero-medial quadriceps muscle. For the composite injury model, we added this VML defect to our well-characterized critically sized segmental bone defect in the rat femur [10]. Functional outcome measures included measurements of muscle torque production, longitudinal bone volume measurements, bone mechanical testing, and gait measurements to quantify full limb recovery. Further characterization of the model examined defect revascularization, analyzed via Micro-Computed Tomography (Micro-CT) Angiography, as a possible source for the compounded functional deficits seen in the composite defect.

**Aim 2: Develop a single-muscle VML model to evaluate therapeutic strategies.**

While the quadriceps VML recapitulated the complexity of traumatic battlefield injuries, the model was very complex, involving injury of four separate muscles as well as blood vessels and nerves. This complexity may preclude any therapeutics that may regenerative potential for muscle. A single-muscle VML model with uniform alignment of muscle fibers would be a simpler test bed for evaluation of muscle regeneration strategies. In considering a therapeutic to test in this sizeable VML model, a vascular supply is very important in providing adequate perfusion to aid in graft survival and integration [11]. Microvascular constructs, consisting of microvessels isolated from adipose tissue suspended in a collagen gel, have been shown to form vascular networks *in vitro* that

inosculate with host vasculature *in vivo*. Furthermore, the addition of myoblasts, adult muscle stem cells, facilitated microvascular construct growth *in vitro* through a paracrine effect, suggesting that microvascular constructs with myoblasts may aid in both vascular response as well as provide muscle stem cells to the defect site. *Our hypothesis was that a volumetric muscle loss in the biceps femoris muscle will result in very little muscle regeneration when untreated and enhanced muscle regeneration when treated with autograft, and that microvessel treatment with or without myoblasts of the biceps femoris defect will result in increased revascularization and muscle regeneration.* Outcome measures included muscle force measurements, micro-CT angiography, histology, and biochemical assays to determine creatine kinase and citrate synthase activity as well as fat and actin/myosin content to identify the type of tissue formed in the defect space.

**Aim 3: Assess the effects of microvascular construct treatment on the early revascularization and long-term regeneration of bone and muscle tissues in the composite injury model.** Early vascularization response was diminished in limbs with the composite bone and muscle defects. Combined with literature evidence of poor vascularity impeding bone healing, the impaired bone regeneration may indeed be a result of poor early vascularization due to volumetric muscle loss. Thus, for this aim, we treated the composite defect with a microvascular construct to determine if a vascular treatment will aid in bone and/or muscle healing. *Our hypothesis was that microvascular constructs implanted into composite injuries will aid in revascularization and regeneration of both tissues.* Early revascularization of the defect areas were analyzed through Micro-CT angiography. Functional outcome measures included measurements of

muscle torque production, longitudinal bone volume measurements, and bone mechanical testing to quantify full limb recovery.

## CHAPTER 2 Literature Review<sup>1</sup>

### 2.1 Traumatic Injuries to the Extremities

#### 2.1.1 Volumetric Muscle Loss

Up to 88% of combat wounds in previous US armed conflicts involve extremity injuries, and in Operation Iraqi Freedom/Operation Enduring Freedom, 53% (or 1881 cases) of extremity wounds involved large, traumatic soft tissue injuries [1]. Tissue trauma in the civilian population often involve high impact accidents in which a energy is absorbed by soft tissue. Common causes of injury include vehicular impacts, industrial accidents, and high-energy sports [12]. Studies have shown that these injuries that involve extensive loss of muscle tissue, or volumetric muscle loss (VML), often result in a decrease in muscle performance that is difficult to recover [13].

Soft tissue trauma often results in edema and inflammation, leading to compromised vascular supply, hypoxia, and soft tissue necrosis at the site [12]. Soft tissue injuries can result in a multitude of complications. Acutely, a common complication is compartment syndrome, in which edema or hematoma within the muscle leads to an increase in tissue pressure and, in severe cases, progressive ischemia [14]. In

---

<sup>1</sup> Portions of this chapter were adapted from Uhrig B A, Li M T A, Willet N J, Guldberg R E, Models of Composite Bone and Soft Tissue Limb Trauma. Chapter in Biomaterials and Regenerative Medicine (September 2014, ISBN: 9781107012097), reprinted with permission.

Material on these pages is copyright Cambridge University Press or reproduced with permission from other copyright owners. It may be downloaded and printed for personal reference, but not otherwise copied, altered in any way or transmitted to others (unless explicitly stated otherwise) without the written permission of Cambridge University Press. Hypertext links to other Web locations are for the convenience of users and do not constitute any endorsement or authorisation by Cambridge University Press.

cases of blunt skeletal trauma, ectopic calcification may occur in injured muscle, and muscular infections may develop [14]. One multi-center study found trauma to be the number one cause of necrotizing soft-tissue infections, which are associated with high mortality rates, chronic pain, and limitations in physical function [15, 16].

#### 2.1.1.1 Gold Standard Treatments

There is currently no sufficient clinical treatment for VML and its resulting functional deficits. There is no universal consensus on how to manage orthopedic soft tissue injuries. Initial analysis of the soft tissue trauma involves assessing the viability of the extremity, often by screening for vascular injury [17]. Thorough irrigation of the injured areas and debridement of devitalized soft tissues aid in reducing chances of infection [18]. Early soft tissue coverage with the use of muscle or fasciocutaneous flaps is the gold standard treatment for large, traumatic extremity injuries [19]. These soft-tissue flaps provide vascularization and offer protection of the underlying exposed tissue [17].

Despite careful actions by reconstructive surgeons to salvage the limb, long-term outcomes for patients that suffer from severe soft tissue trauma are grim. Patients that underwent fasciotomy to relieve compartment syndrome after soft tissue injury suffer from pain (50%) and report problems with physical activities (37%) seven to ten years after treatment [20, 21]. Patients that received radical debridement after a severe crush injury were more likely to suffer from motor disability [22]. In a study that compared limb function after excision of a muscle sarcoma, larger muscle excisions resulted in lower functional scores compared to partial muscle excisions [23]. These results indicate that patients with large VML injuries are likely to experience severe functional deficits that are unlikely to recover over time, despite current treatments.

### **2.1.2 Open Fractures/Composite Injuries**

It is estimated that 185,000 persons undergo an amputation of an upper or lower limb every year, commonly caused by severe traumatic injury to the extremity [24]. In the civilian population, composite bone and muscle defects often result from motor vehicle and motorcycle accidents, falls, or crush injuries. The Lower Extremity Assessment Project (LEAP) study was conducted to study the variables in the civilian patient population that sustain traumatic injuries in the below-the-knee lower limb. 601 patients were enrolled, and their treatment and recovery were followed for 44 months [25]. From this large study, fractures caused by high-energy trauma, often involving damage to the bone and muscle, were found to have a high prevalence of complications, most notably wound infection and nonunion of fractures.

In current US armed conflicts, extremity wounds are prevalent due to the increase in use of improvised explosive devices and individual vehicular body armor, which protects the body but leaves the extremities prone to injury. Extremity injuries utilized the most resources out of any other types of wounds for injury treatment [1]. Out of 1333 soldiers in the study, 54% sustained an extremity injury, which averaged 17.9 inpatient days and utilized more than \$42 million in resources [26]. Of the extremity wounds from the conflicts, one study found that 53% were penetrating soft-tissue wounds, and 26% were fractures. A large percentage (82%) of these fractures comprised of open fractures, in which a concomitant soft tissue injury was sustained alongside a bone injury [1]. 15% of all military amputations occur at least 12 weeks post-injury, mostly due to complications in the treatment of open fractures that included soft tissue injury requiring flap coverage [27, 28].

### 2.1.2.1 Gold Standard Treatments

Orthopedic surgeons often have a hard decision between limb salvage and amputation when a patient with a traumatic limb injury is admitted. Many factors play a big role in making such a decision, such as vascular status, contamination of the injury, and long-bone instability. Though limb salvage is often preferred by patients and could result in full recovery of function in the limb, multiple operations are usually required. One study indicated recovery time for limb salvage to be about 13 months compared to only 6 months for patients that opted for amputation [29]. From the LEAP study, patients that underwent reconstruction to salvage a limb had higher chances of re-hospitalization, osteomyelitis, and more surgeries than patients that elected to amputate the limb [30]. A recent study comparing outcomes of amputation versus limb salvage in military lower-extremity trauma found that patients with an amputation had better functional and psychological scores compared to those that underwent limb salvage [31]. Additionally, it was found that patients in the LEAP study that underwent late amputation (at least 3 months post-injury) exhibited a higher level of disability compared to patients that underwent earlier amputations [32, 33]. Thus, a decision to salvage the limb may lead to severe consequences.

The gold clinical standard for treating open fractures consists of muscular flaps used to cover the bone and occupy empty space in order to reduce chances of infection [34]. Additionally, the soft tissue flaps provide a vascular supply, cells, and growth factors that may aid in the repair of the bone defect or fracture [35]. Use of the muscle flap is known to be vital in treating lower extremity composite injuries and has been shown to increase bone union rate [36]; however, the percentage of complications remain

high [2], with one 15-year study reporting 58% nonunion and 11% amputation of open tibial fractures [3]. Another study of 115 wounded soldiers reported 40% infections complications, resulting in a significantly lower rate of soldiers returning to duty [37]. In addition, patients often do not regain normal function of their extremity [4]. Though upper extremity replantation resulted in better outcomes than an upper extremity amputation and prosthetic, one study showed that the replantation group only had a 50% rate of a good or excellent functional outcome [38]. Only 23% of the patients in the LEAP study reported to be pain-free 7 years after the initial treatment [39]. This persistence of pain after traumatic musculoskeletal injury is confirmed by another study that reviewed 4388 cases, in which patients reported pain up to 84 months post-injury [40]. Without full functional recovery and pain associated with the extremity for years after the treatments, some patients elect to amputate the limb even after the many surgeries required for limb salvage. This clearly necessitates strategies in the limb salvage realm that aids in functional recovery in addition to the survival of the limb.

## **2.2 Animal Injury Models**

### **2.2.1 Volumetric Muscle Loss**

Historically, skeletal muscle was thought to have a high regenerative potential due to early experiments in which a minced skeletal muscle replaced in its bed was able to regenerate within 4 weeks. These studies were often performed on mice and using smaller muscles such as the extensor digitorum longus [41]. This does not emulate the clinical situation in which patients with damage to large muscles often have difficulties regaining function of that muscle. Thus, recent studies in the field have focused on establishing larger VML injuries that are difficult to regenerate and functionally heal.

While various groups have examined muscle regeneration after a chemical, burn, or freezing injury as well as muscle loss from the abdominal wall or latissimus dorsi, the focus here will specifically be on models that create a VML in which a large portion of muscle is resected from an extremity.

Various VML injuries have recently been characterized in rodent models. Specifically, in the mouse, models have been developed in which sections of the tibialis anterior (TA) are removed (ranging from 4 milligrams to 30 milligrams of muscle). In this TA VML models, the untreated injured leg could only produce about half the force that an intact leg could produce [42, 43]. At 6 to 10 weeks post-injury, untreated injured muscle had a smaller cross-section and larger amounts of connective tissue compared to an uninjured muscle, which indicated possible atrophy of muscle and scarring instead of regeneration. Similarly, a VML model in the quadriceps of a mouse, in which a 4 x 3 millimeter portion of the tensor fasciae latae muscle was removed, exhibited a reduction in muscle size and contained connective and adipose tissue instead of muscle fibers [44]. In the rat, removal of 20% (weight) of the TA resulted in a reduction in muscle force production in the injured leg to 2/3 of the contralateral control muscle at 4 months post-injury [45]. In contrast, removal of 10% (weight) of the TA resulted in a reduction of muscle force in the injured leg to 3/4 of the contralateral control muscle at 4 weeks post-injury, indicating that there is a correlation between the size of VML and functional outcome [46]. Removal of 300 milligrams of the gastrocnemius muscle in the rat resulted in reduction of the muscle force produced by about 20% [47]. In all rodent models of VML injury, untreated injuries resulted in excess connective tissue around muscle fibers as measured by Masson's Trichrome staining, indicating fibrosis and scar formation. Few VML models exist in larger animals. Canine and lepine models have been used to test various constructs, which will be discussed in section 2.3.1.

The development of VML models is a relatively new field; most of the aforementioned models were published in the past 5 years. In general, the VML injury is characterized by a large loss of muscle function (30-50% of contralateral control) with a relatively smaller loss of muscle size (10-20%). Masson's trichrome is often used to determine the amount of fibrosis or scarring in the muscle. Inflammatory infiltrate is often present between muscle fibers, at least at the earlier time points (2 weeks, 4 weeks post-injury). In severe cases, adipose tissue is present between the muscle fibers. This intermuscular adipose tissue is usually associated with glucose dysregulation and lower levels of muscle strength, and the presence of this fat may be an indication of reduced physical activity after injury [48, 49].

Important distinctions to note are the position and size of these VML injuries. Most of these models involve damage to 1 or 2 muscles, and the largest VML injury involved the resection of a 300 milligram piece of muscle. These injuries do not involve a full-thickness defect in which the underlying bone is revealed. Clinically, many complications arise when soft tissue trauma results in exposed bone that could then increase chances of infection. Additionally, while most of the models indicate a loss of size in the injured muscle, few showed a complete lack of regeneration in the center of the defect.

### **2.2.2 Composite Bone & Muscle Injuries**

Of the few composite injury preclinical models that have been established, the main focus appears to be the investigation of crosstalk between the healing responses of bone and muscle. These models reveal clues about the mechanisms by which the two tissues interact.

Augat et al. incorporated soft tissue blunt-impact trauma with a closed tibial fracture model in rats in order to study the influence of muscle injury in revascularization during fracture healing [50] [51]. A large area of the periosteum covered in osteoid as early as day 3 in the tibial fracture only group while very little periosteal bone formation was seen in the composite injury group, indicating an early difference in bone healing. Laser Doppler flowmetry showed a similar initial delay in blood flow in the bone from the composite injury group. However, this difference in bone healing did not persist beyond day 3; by days 14 and 28, the two groups no longer showed differences in blood flow and bone strength. This study showed that a closed fracture with blunt muscle trauma may cause a slight delay in healing, but it may not be as severe as open fractures seen in the clinic.

Landry *et al.* included an anterior tibialis muscle resection with their tibial periosteum defect in the rat in order to study the inflammatory and cellular response in periosteally mediated bone healing [52] [53]. For the tibial defect, a jeweler's burr was used to create a 0.5 millimeter deep periosteal defect in which the medullary cavity was not exposed. For the muscle defect, 10% of the anterior tibialis adjacent to the bone defect was resected. A composite group included both the tibial and muscle defects. The osteoblast concentration in the inner periosteal layer was increased in the composite injury group as compared to the single-tissue bone and muscle injury groups, but the callus formation did not show a significant difference between the composite injury and the bone injury groups. Early cellular response in the composite model was different as well, despite no permanent change in healing response.

Though these studies showed little difference in bone healing between the composite injury and bone-only injury groups, the muscle injuries in these studies may not have been severe enough to influence bone healing. Utvag *et al.* tested a nailed tibial osteotomy rat model with three levels of soft tissue damage: a control group with intact muscle, a moderate muscle injury group with a muscle crush injury, and a severe muscle injury group with resection of muscles within the anterolateral compartment [54]. At 4 weeks post-injury, the muscle resection group resulted in a significantly lower maximum three-point bending load and a significantly lower callus cross-sectional area as compared to the control group. Surprisingly, the muscle crush injury group did not differ significantly from the control group in these two parameters. It is important to point out that the fibular nerve was also resected, making the animal non-weight bearing. This may add an additional layer of complexity to the model, as this creates an additional nerve tissue defect, and the lack of weight bearing reduces the mechanical stresses that normally guide bone remodeling and homeostasis.

The close anatomical relationship of bones and skeletal muscle lends credence to the idea that muscle contributes to bone healing as a source of blood vessels, growth factors, and progenitor cells. Through careful observation of callus formation after tibial fractures in rats, rabbits, and sheep, Stein *et al.* noted that the callus forms between the fracture and the intact muscle bed adjacent to it [55]. This adjacent muscle acts almost as a “secondary periosteum” that can provide osteoprogenitors, especially when the periosteum itself, normally a good source of osteogenic cells, is damaged [56]. The importance of healthy muscle tissue in bone healing suggests that muscle regeneration in a composite model may aid in bone regeneration as well.

In contrast to most composite injury models that were developed mainly to investigate tissue interactions and regeneration, a study by Pfeifer et al. investigated the systemic inflammatory response that may result from polytrauma. Mice were injected with bone fragments, given a soft tissue injury, or both insults were applied. After 6 hours, systemic inflammatory responses were analyzed, and the composite injury resulted in significantly higher levels of interleukin-6 and interleukin-10 in the blood compared to any single insult [57]. While much research focuses on regenerating tissues, it is important to note that systemic inflammatory effects caused by large traumatic injuries may also play a role in the healing of these injuries.

## **2.3 Current Tissue Engineering Strategies Tested in Pre-Clinical Injury Models**

### **2.3.1 Treatments for Volumetric Muscle Loss**

As the VML field is relatively new, the strategies tested in VML models are currently limited. These strategies can be roughly divided into 2 groups: acellular or devitalized scaffolds (i.e. decellularized extracellular matrix, or ECM), and cell delivery with or without a carrier scaffold. The field of muscle regeneration, which extends past the VML models developed in the last few years, warrants a brief review as well.

#### 2.3.1.1 Decellularized or devitalized scaffolds

Various decellularized or devitalized tissues have been examined as a possible therapeutic for VML injuries. Specifically, research groups have tested decellularized skeletal muscle ECM [47, 58, 59] and porcine small intestine submucosa (SIS-ECM) [44, 60, 61] with some success in functional restoration.

The structure of the skeletal muscle extracellular matrix is linked closely to the function of muscle, specifically in force transmission across the muscle fibers [62]. Thus, it is not unreasonable to postulate that the decellularized ECM of skeletal muscle may aid in muscle regeneration and functional restoration. Ideally, decellularized skeletal muscle ECM could be advantageous over other decellularized matrices by providing a muscle-specific blueprint that could guide the movement of endogenous cells. However, the decellularization of skeletal muscle tissue involves a protocol of various chemical treatments in order to remove or devitalize cells, which also alters the specific structures of the skeletal muscle ECM [63, 64]. Although the implantation of decellularized skeletal muscle ECM resulted in a slight improvement in muscle force (approximately 10% closer to the contralateral uninjured controls), studies have shown that endogenous cells do not migrate into the center of the ECM, and few, if any, muscle fibers are generated within the implanted matrices [47, 59]. Instead, the implanted scaffolds are remodeled within the body into fibrotic scar tissue that no longer resembles the ordered structure of skeletal muscle ECM. These results show that even with a structural scaffold that can guide cellular growth and conduct forces across the defect space, fibrosis still dominates the healing process with little or no regeneration of muscle fibers.

SIS-ECM has been tested as a therapeutic scaffold in a mouse quadriceps VML model [44], two different canine models involving VML in the quadriceps [60, 61], and notably, humans in the clinic [65, 66]. While SIS-ECM is a xenogeneic biologic scaffold due to its porcine origins, it has been found to suppress human T-cell activation *in vitro*, and the cytokine response to this material induced a Th-2 immune response instead of the Th-1 cell-mediated rejection response [67, 68]. In addition to acting as a scaffold, SIS-

ECM has been shown to be degraded by peripheral blood monocytes and drive the invading macrophages down the immunomodulatory and tissue remodeling pathway [69, 70]. In the mouse, the SIS-ECM promotes cellular infiltration, though the scaffold itself still remains at 28 days [44]. Results from the canine model are mixed; while the SIS-ECM resulted in an improvement in muscle function when implanted in the distal gastrocnemius musculotendinous junction, the scaffold caused a strong fibrotic response in the quadriceps [60, 61]. Humans who exhibited a minimum of 25% loss of muscle mass and muscle function were implanted with the SIS-ECM, and 6 months after surgery, 3 out of 5 human subjects showed improved functional outcomes as measured by balance and hop tests [65, 66]. These mixed results warrant further investigations into the full potential of the SIS-ECM in the treatment of VML.

#### 2.3.1.2 Cell delivery

Various combinations of cell types and carriers have been tested for their therapeutic benefit in muscle regeneration in VML models. In VML models, a portion of adult stem cells are removed from the vicinity of the defect due to the amount of muscle tissue that is resected, which mimics the clinical situation. Cell therapies aim to replace these adult stem cells and their roles in muscle regeneration.

Cells in phosphate-buffered saline (PBS) injected locally to a small VML model has been shown to increase skeletal muscle regeneration in the region. Human peripheral blood-derived CD133+ cells and human adipose-derived regenerative cells were injected into the rat tibialis anterior, in which a wedge-shaped defect (6 x 4 x 5 millimeters) was removed [71, 72]. Both cell types demonstrate functional muscle regeneration even as early as 1 week post-injury. The cell-treated group resulted in tissue that included

myofibers with diameters of around 125  $\mu\text{m}$ . However, an injection of PBS in the defect (negative control) resulted in small diameter myofibers (75  $\mu\text{m}$ ) at 4 weeks, indicating that the negative control still exhibited muscle regeneration and myofiber formation. Further research into cell delivery without a biomaterial by this group included bone-marrow-derived mesenchymal stem cells (MSCs) that were delivered in PBS via injection to the injury site. A strong magnet was then placed in proximity to the injury site for ten minutes. The magnetically localized cells resulted in a higher number of capillaries at the defect site as well as increased muscle strength and myofiber diameter compared to cells that were not localized by the magnet [46]. All these cell therapies demonstrate the great potential that cell delivery could have on muscle regeneration.

Porcine bladder acellular matrices (BAM) have been examined as a carrier for muscle progenitor cells (MPCs) for delivery into and for the therapy of VML injuries. This strategy was first tested in a latissimus dorsi (LD) model in which approximately half the muscle was removed. The MPCs were seeded onto the BAM scaffold and pre-cultured in a perfusion bioreactor that stretched the construct cyclically for 7 days *in vitro* to form a tissue-engineered muscle repair construct (TE-MR). At 2 months post-injury, the group treated TE-MR exhibited higher muscle force than the empty defect or scaffold alone when the LD was removed and tested *ex vivo* [73]. Histological analyses showed signs of myofiber, vessel, and neurovascular formations in the TE-MR, though the majority of the TE-MR still comprised of connective tissue. Further studies into TE-MR and the pre-conditioning of the construct showed that a second seeding of MPCs onto the construct after *in vitro* pre-conditioning in differentiation media incrementally improved functional regeneration in the LD model [74]. The implantation of the TE-MR into the rat

TA VML model resulted in higher muscle function compared to untreated or scaffold only control at 4 weeks, with very little functional recovery across time (up to 12 weeks) [75]. Though this strategy delivered a different type of cell (MPCs) compared to previous strategies, the cells again demonstrated potential in aiding muscle regeneration in VML models.

Given the nature of adult muscle progenitors and their propensity to differentiate into muscle cells, various groups have attempted to deliver these cells on different materials. Human muscle progenitor cells were delivered on fibrin microthreads and shown to reduce scar formation and improve muscle function compared to an untreated TA VML defect in a murine model at 90 days post-injury [43]. Freshly isolated satellite cells (or MPCs) were embedded in a hyaluronic acid-photoinitiator complex, delivered directly to the site of injury, then photopolymerized into a hydrogel. The stem cell treated group resulted in an improvement in muscle function as compared to an untreated defect [42]. Rat myoblasts that were cultured to attach to engineered bone anchors were implanted into a rat TA VML and demonstrated functional recovery by 28 days after injury [76]. Signs of small myofibers in histology suggested that the injury is healing despite some fibrotic tissue in the defect site.

Further evidence that a cellular component may be needed in the healing of muscle defects was shown in two separate studies. When human MSCs were delivered into a VML model in the gastrocnemius muscle of the rat on a decellularized muscle ECM, the resulting functional recovery at 42 days post-injury was higher in the ECM-MSc group compared to the ECM only group [77]. This study found a marked effect of a cellular component on muscle regeneration that an acellular therapy did not provide. In

another study, muscle grafts that were either left vital (with live cells) or devitalized (with cells mostly removed as measured by nucleic acid content) were implanted into a rat TA model. The vital graft resulted in higher muscle function as compared to the devitalized graft and the empty untreated control [58]. These studies, as well as the studies involving the TE-MR compared to the BAM scaffold alone, emphasizes the need for a live biological component, in addition to a space-filling scaffold, for improved muscle functional regeneration.

#### 2.3.1.3 Therapies for other muscle injuries

While tissue engineering constructs have been tested in VML models in the recent years, the field of muscle regeneration extends far back and includes a wide array of strategies for repair of muscle injuries that do not involve volumetric muscle loss. Though these other muscle injuries may be smaller in size and different in healing response, the strategies tested for these muscle injuries could lead to insights into muscle regeneration that could be applied to VML.

Literature into tissue engineering strategies for skeletal muscle injuries again confirms the potential of cell therapy for tissue repair [78]. Studies have shown that muscle injury activates and/or recruits a host of different cell types in the body, including satellite cells [79], bone marrow derived myogenic progenitors [80], inflammatory cells such as neutrophils and macrophages [81-83], and fibro/adipogenic progenitors [84]. Other unorthodox cells can also be cultured down the myogenic lineage, including neural stem cells, hematopoietic cells, mesenchymal stem cells, mesangioblasts, endothelial progenitor cells, and adipose-derived stem cells [85]. Thus, there seems to be no

limitation in which types of cells can contribute to muscle regeneration, though the relative regenerative potentials of these cell types may differ.

More recently, studies have focused on the importance of vascularization for survival of grafts in skeletal muscle. Pre-vascularized grafts constructed of a tri-culture of myoblasts, embryonic fibroblasts, and endothelial cells seeded in polymer scaffolds were shown to improve vascularization, perfusion, and survival of muscle tissue when implanted *in vivo* subcutaneously, intramuscularly, and as a graft for an abdominal wall defect [86]. A longer culturing period (3 weeks *in vitro*) that yielded more organized vessels and muscle fibers within the construct exhibited enhanced perfusion and transition of satellite cells to mature fibers compared to constructs with shorter culturing periods (1 day to 2 weeks *in vitro*) [87]. These studies highlight the importance of vascularization for the survival of cells within the construct, and the maturation of satellite cells within these vascularized constructs suggest that there may be an effect of the vascular elements on the myogenic differentiation of muscle progenitor cells. This speculation is further supported by a study in which a vascular endothelial growth factor (VEGF) coated collagen matrix was applied in a soft tissue trauma model and resulted in restoration of muscle force and an increase in muscle fiber count [88]. Other studies in which VEGF and insulin-like growth factor-1 (IGF-1) were delivered in an alginate hydrogel in addition to cultured myoblasts, resulting in increased muscle mass and contractile function after hind limb ischemia [89] and myotoxin damage to the TA of mice [90]. These studies present convincing evidence emphasizing the need for sufficient vasculature for muscular grafts and regeneration.

#### 2.3.1.4 Limitations

While various strategies have been tested in VML injuries, no single treatment has been able to allow for complete functional recovery (back to the strength of an uninjured or contralateral limb) or full recovery of the muscle with little or no fibrosis.

Many treatments allow for partial recovery of function; however, deposition of collagen and scar formation may also contribute to function without functional cells. Additionally, the exact nature and mechanisms behind many of these strategies are not well understood. A prime example of this is evident in SIS-ECM studies. While the potential of SIS-ECM is convincingly demonstrated, its use in larger animals and in humans results in highly variable functional outcomes. All treatments are subject to further investigation in order to more fully understand the mechanisms behind their regenerative potentials.

### **2.3.2 Treatments for Composite Injury Models**

Composite models have been used to test the advantageous effects of muscular flap treatment in pre-clinical models. In a series of canine studies, Richards *et al.* examined blood flow characteristics in a model of devascularized tibial cortex covered on the anterior side with either a local muscle flap or vascularized skin [91, 92]. At 31 days post-injury, the rates of blood flow and osteotomy union were both significantly greater in the muscle flap coverage group as compared to the vascularized skin coverage group. Further study showed that the muscle flap group had increased intracortical blood flow, which correlated with greater cortical porosity, a measure of bone turnover. In a similar study in mice, Harry *et al.* investigated the effect of different soft tissue coverage for open tibial fractures [93]. An inert polymer insert was used for selective tissue exclusion either directly between the bone and the anterior skin/fascia or between the bone and the posterior muscle. At 4 weeks post-injury, the group with muscle coverage (fasciocutaneous separation) was histomorphometrically similar to the fracture control group and performed as well in a four-point bending test. The group with fasciocutaneous coverage (muscle exclusion) demonstrated an impaired healing

response, with a significantly lower load to failure, bone mineral content, bone mineral density, and bone volume compared to the fracture control and muscle coverage groups. All of these pre-clinical studies validate the gold standard treatment of muscular flap coverage for bone regeneration, though no specific mechanisms were elucidated.

Very few composite models have been used for studying additional tissue engineering strategies for treating composite defects. One study tested the use of a biological factor for the treatment of a composite tissue defect. Hamrick *et al.* treated mice given a composite bone and muscle defect with recombinant myostatin propeptide, which effectively inhibits active myostatin [94]. The composite defect consisted of a fibula osteotomy as well as laceration of the lateral compartment muscles. The mice were then treated with myostatin propeptide injections at 20mg/kg at days 0, 5, and 10 post-injury. At 15 days, safranin-O stained histological sections showed an increase in fracture callus in the propeptide-treated group as compared to a saline-treated control group. Masson's trichrome staining on the muscle injury site showed less fibrosis in the propeptide treated group. Micro-CT analyses also showed a significantly higher bridging rate and fracture callus bone volume in the treated group. These results indicate that the myostatin propeptide can be used in a composite defect to benefit both muscle and bone regeneration.

## **2.4 Motivations for Research**

Traumatic injuries to the extremities often result in composite wounds in which bone and muscle tissues are compromised. Composite wounds are more difficult to heal and result in more complications, such as infections and bone nonunion, than single tissue injuries. The main clinical response to composite wounds is to decide between limb

salvage or, if the injury involves a large amount of necrotic tissue or lack of vascular perfusion, amputation of the limb. Though amputation often reduces limb function, especially in the upper extremities, limb salvage has its disadvantages as well. Not only does limb salvage require multiple surgeries and subsequent painful recoveries, patients often experience more complications and do not regain full function, leading to a secondary, late amputation that results in a worse disability than an early amputation and prosthetic. Thus, neither limb salvage nor amputation consistently results in full functional recovery of the limb.

With tissue engineering strategies applied to large composite injuries of the limb for the purpose of restoring limb function, it may be possible to increase the rate of success for limb salvage as well as increase the chance of healing severe extremity injuries. Additionally, composite bone & muscle injury pre-clinical models allow us to study the interactions between the two tissues during healing, which may lead to valuable insights for the tissue engineering field. Thus, the **main motivations** behind this proposal are to **test therapeutic options for treating severe musculoskeletal injuries** as well as to **gain insights to how the muscle and bone tissues interact during healing of a large, complex injury**.

## **CHAPTER 3 Aim 1: Volumetric Muscle Loss Model in the Rat Quadriceps<sup>2</sup>**

### **3.1 Abstract**

Severe injuries to the extremities often result in muscle trauma and, in some cases, significant volumetric muscle loss (VML). These injuries continue to be challenging to treat, with few available clinical options, a high rate of complications, and often persistent loss of limb function. To facilitate the testing of regenerative strategies for skeletal muscle, we developed a novel quadriceps VML model in the rat, specifically addressing functional recovery of the limb. Our outcome measures included muscle contractility measurements to assess muscle function and gait analysis for evaluation of overall limb function. We also investigated treatment with muscle autografts, whole or minced, to promote regeneration of the defect area. Our defect model resulted in a loss of muscle function, with injured legs generating less than 55% of muscle strength from the contralateral uninjured control legs, even at 4 weeks post-injury. The autograft treatments did not result in significant recovery of muscle function. Measures of static and dynamic gait were significantly decreased in the untreated, empty defect group, indicating a decrease in limb function. Histological sections of the affected muscles showed extensive fibrosis, suggesting that this scarring of the muscle may be in part the cause of the loss of muscle function in this VML model. Taken together, these data are consistent with clinical findings of reduced muscle function in large VML injuries. This new model with quantitative functional outcome measures offers a platform on which to evaluate

---

<sup>2</sup> Portions of this chapter were adapted from Li M T A, Willet N J, Uhrig B A, Guldberg R E, Warren G L. Functional analysis of limb recovery following autograft treatment of volumetric muscle loss in the quadriceps femoris. *Journal of Biomechanics* 47(9): 2013-2021. License No. 3503410888108

treatment strategies designed to regenerate muscle tissue volume and restore limb function.

### **3.2 Introduction**

Extremity injuries comprise the majority of combat wounds in recent US conflicts, 53% of which are penetrating soft-tissue wounds involving extensive damage to the muscle, also known as volumetric muscle loss (VML) [1]. Sixty-four percent of all soldiers found unfit for duty are soldiers with extremity injuries, accounting for the majority of the \$170 million in projected disability costs [26]. 12% of civilian patients that had lower extremity trauma experienced VML, and these subsequent treatments resulted in a mean cost of \$65,735 [96, 97]. Despite the high prevalence and societal cost of VML injuries to the extremities, no tissue engineering treatments are currently available.

Coverage of VML wounds with autogenic muscle flaps is known to be critical in reducing early complications to the healing of soft tissue defects and is the current clinical gold standard [98, 99]. Muscle flap type is a significant predictor of short-term complications [100, 101], and muscle coverage aids bone regeneration by increasing bone blood flow [91, 92]. Other treatment options include the use of sophisticated bracing that allows for physical therapy, but no tissue engineering strategies are available in the clinic thus far [13].

The current treatment options do not take into account structural restoration of muscle, and this is evident in the fact that large muscular defects often lead to persistent functional deficits. High-energy trauma to soft tissues were significantly correlated with poor physical Sickness Impact Profile (SIP) scores—a measure of self-reported physical

limitations [102]. Thirty percent of patients with extensive soft tissue injury reported problems with motility and chronic pain 7-10 years post-injury [20, 21]. An increasing number of VML patients requested late amputations due to functional deficits of the limb [103]. This persistence of functional deficits highlights the need for functional tissue engineering of VML injuries as well as animal models to quantitatively evaluate regenerative strategies.

Various preclinical VML models have recently been developed to test tissue engineering strategies, as detailed in the literature review. The associated studies have used a variety of outcome measures; however, standardized and consistent techniques are not established. As we move forward in refining rat VML models, we seek to increase the relevance to clinical outcomes, in which functional biomechanical testing is critical. Further, many of these models utilize relatively small VML defects in a single muscle – an injury that may heal without an intervention. In order to further tissue engineering research in VML and to facilitate the translational aspect of these regenerative strategies, there is a need for preclinical models that mimic the complexity and severity of VML injuries observed in the clinic where there is a significant volume of muscle affected including injury to multiple muscles.

Accordingly, **our objective was to develop a severe skeletal muscle defect model in the rat incorporating quantitative analysis of muscle regeneration and restoration of limb function.** We hypothesized that a full thickness defect through the quadriceps would result in a significant loss of muscle strength and limb function. We further used our model to quantitatively evaluate treatment with muscle autograft, a strategy that has previously been tested in mouse models and shown to improve muscle regeneration by 4 weeks post-injury [41]. Thus, *we hypothesized that an autograft,*

*whether whole or morselized, will significantly increase muscle functional capacity and result in tissue regeneration.* We present a very challenging muscle defect rat model that can be used by the scientific community for two important purposes: 1) to further understanding of VML with quantitative measures of the healing process, and 2) to evaluate the success of different muscle regeneration strategies.

### **3.3 Materials/Methods**

#### *Surgical Procedure*

All surgical procedures were conducted in accordance with guidelines set by the Georgia Tech IACUC (protocol #09039 & #12075). 13-week-old female Sprague-Dawley rats (Charles River) were randomly assigned to three treatment groups: empty untreated defect (n=12), whole autograft (n=12), and morselized autograft (n=12). For all groups, the muscular injury was performed on the left leg while the right leg served as a non-surgical contralateral control. Muscle defects were created in the quadriceps femoris as previously described [104]. Briefly, the full-thickness muscular defect comprised of an 8-mm diameter biopsy punch through the medial anterior portion of the quadriceps, affecting parts of all four muscles (Figure 1A, top). In the whole autograft group, the biopsied muscle (Figure 1B, bottom) was placed back into the defect. In the morselized autograft group, biopsied muscle graft was cut into cubes 2 mm in length. All animals were divided into 2 groups: 2-week (n=6 per group) and 4-week (n=6 per group).

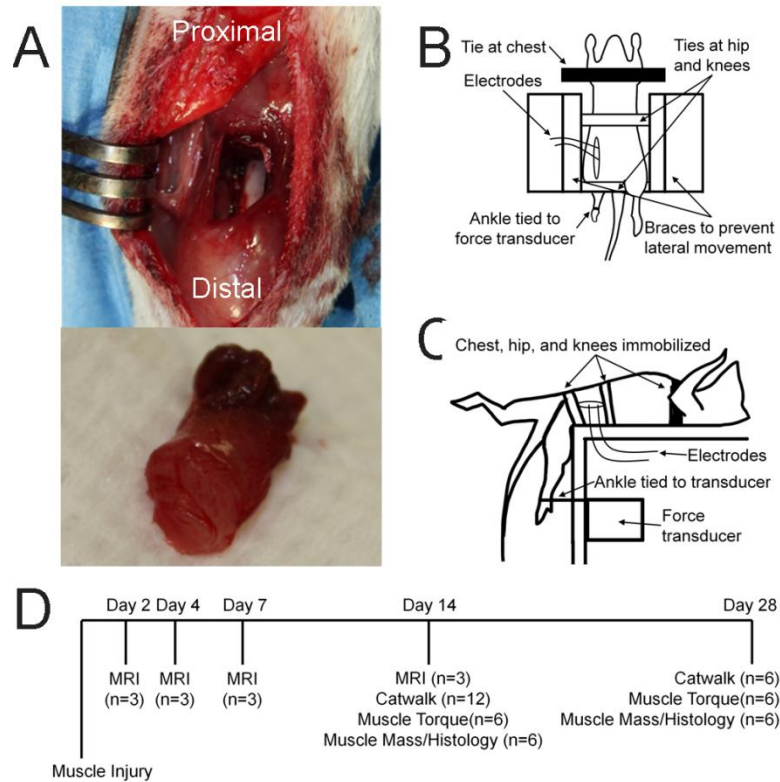


**Figure 1: Methods for Creating and Analysis of the Quadriceps VML Model.** A. Representative images showing the muscle defect surgery (top) and excised 8-mm diameter muscle (bottom). B. Representative diagram of the top-down view of muscle strength measurements. C. Representative diagram of the side view of muscle strength measurements. D. Timeline of longitudinal *in vivo* (MRI, Catwalk) and *ex vivo* (muscle torque, muscle mass, histology) measurements, with sample sizes, for the whole study.

### Gait Analysis

Gait analysis was performed on all animals pre-surgery (baseline) and at 2 weeks post-injury. Only the 4-week recovery group animals were measured at 4 weeks (Figure 1D). Using the CatWalk 7.1 system (Noldus Information Technology, The Netherlands), quantitative gait measurements were collected. The CatWalk system has previously been validated for assessment of functional limb recovery after sciatic nerve injury [105-107] and spinal cord contusion [108]. For each data collection, three uninterrupted runs per rat

were conducted when possible. Runs that traversed at least half the walkway length were analyzed.

### *Magnetic Resonance Imaging (MRI)*

Three additional animals received empty muscle defects and underwent MR imaging at days 2, 4, 7, and 14 post-injury (Figure 1D); no autograft-treated animals underwent MR imaging. MRI has been shown to be useful in characterizing hematoma or edema formation after muscle injuries [109-111]. Images were taken in a 7-tesla MRI system (Pharmascan 7T, Bruker Corp.) and processed in ParaVision 5.1 (BrukerBioSpin, Bruker Corp.). A radiofrequency coil (Doty CP Litzcage coil, 60-mm inner coil diameter) was used for transmitting and receiving signal. T1-weighted images (axial) were taken using a FLASH sequence (TR/TE: 379.5/6.0ms) with 1mm slice thickness. T2-weighted images (axial) were taken using a RARE sequence (TR/TE: 3435.3/52.2ms, rare factor: 6, flip angle: 30 degrees) with 1mm slice thickness. Thirty slices were taken of each leg.

Images were analyzed using ImageJ v1.45 (National Institutes of Health). The volume of interest was determined by using well-defined anatomical structures visible in the T1-weighted images (Figure 2A). VOIs were overlaid on corresponding T2-weighted images (Figure 2B). For uninjured quadriceps femoris muscles, the mean and standard deviation of T2-weighted voxel intensities were used to calculate a threshold value (mean + 2\*SD). T2-weighted images of injured muscle were then thresholded (Figure 2B), and voxels with intensities above the threshold indicated hematoma or edema. The volume (V) of hematoma or edema was determined using the trapezoidal interpolation:  $V = \left( \sum \left( \frac{A_1 + A_2}{2} \right) * h \right)$ , where h is the distance between axial sections and A<sub>1</sub> and A<sub>2</sub> are areas with edema/hematoma of consecutive images.

### *Measurements of Peak Isometric Contraction Torque about the Knee*

At respective recovery time points, 2-week and 4-week rats underwent peak isometric strength measurements, a terminal procedure, to assess the functional capacity of the quadriceps (Figure 1D). An *in vivo* system similar to those used extensively to assess lower leg muscle function was custom fabricated for assessing torque production about the knee [112, 113]. Briefly, a nerve cuff was used to stimulate the femoral nerve as a force transducer was used to measure maximal isometric torque production about the knee. Rat movement was restrained (Figure 1B), and the rat ankle was attached to a force transducer (Figure 1C). The nerve was stimulated with progressively increasing voltages to determine the maximum torque.

To assess the fatigability of the quadriceps femoris muscles, the muscle group was subjected to the standard Burke fatigue protocol [114]. This entailed isometric muscle stimulation with a train consisting of 13 pulses at 25-ms intervals; the train was repeated every second for 2 minutes. The endurance index was calculated as the torque produced at the 1 minute into the protocol divided by the highest torque produced during the protocol. The highest torque was used because varying degrees of potentiation occurred among animals during the first few contractions. Calculation of the endurance index in this manner yielded more reliable values.

### *Histology*

Directly following the measurements of muscle functional capacity, rats were euthanized and underwent perfusion fixation with 10% neutral-buffered formalin (EMD Chemicals, Gibbstown, NJ). The mass of the excised quadriceps was recorded, and the muscle was additionally submersion-fixated in 10% neutral-buffered formalin for 48

hours. Paraffin-processed samples were cut into 5- $\mu$ m sections using a Microm Microtome (Thermo Scientific, Germany). Hematoxylin and eosin (H&E) staining and Masson's trichrome staining were performed on these sections.

#### *Statistical Analyses*

All data are presented as mean  $\pm$  standard error of the mean. Peak isometric muscle torque and muscle mass were analyzed by a two-way ANOVA (3 treatment groups  $\times$  2 time points). Independent t-tests with Bonferroni correction were used to identify within-group differences of recovery time points.

### **3.4 Results**

#### *Characterization of early VML with Magnetic Resonance Imaging*

Magnetic resonance images were taken at days 2, 4, 7, and 14 post-injury to characterize the muscle injury at early time points. Within the first week of injury, the total muscle volume, quantified by axial T1-weighted images, showed no significant difference between the injured left leg and the contralateral control right leg (Figure 2C). Axial T2-weighted images, in which fluid exhibits increased signal intensity, clearly showed edema/hematoma in the left quadriceps at days 2 and 4 (Figure 2E/F/G/H). This fluid volume was quantified and comprised the majority of the muscle volume at day 2 post-injury (Figure 2D). This steadily decreased from day 2 to day 14 (Figure 2D).

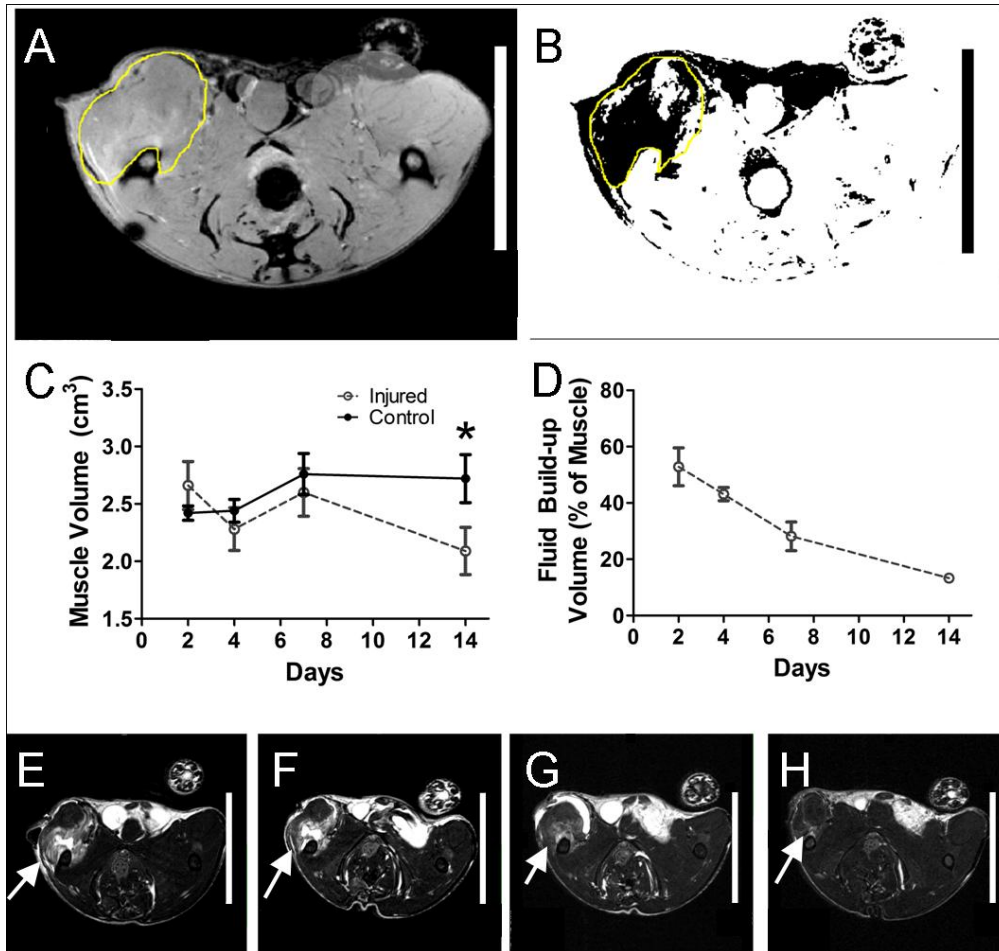


**Figure 2: MRI Visualization of the Extent of Muscle Injury.** A. Representative selection of region of interest using T1-weighted image. B. Representative superposition of ROI on thresholded T2-weighted image. Dark pixels indicate pixels with intensities above threshold. C. Total muscle volume, measured using axial T<sub>1</sub>-weighted MRI images. D. Percentage of the left leg muscle that was inflamed, as determined by edema in the quadriceps area visualized by T<sub>2</sub>-weighted images. E-H. Representative T<sub>2</sub>-weighted images at days 2 (E), 4 (F), 7 (G), and 14 (H) days are shown, with inflamed areas indicated by white arrows. \* $p < 0.05$ ,  $n = 3$ , ANOVA with Bonferroni correction.

### *Measurements of Muscle Functional Capacity*

A representative measurement of muscle isometric tetanic torque about the knee is shown in Figure 3A. In all treatment groups, the maximum tetanic torque about the knee from the injured leg was significantly less than the contralateral uninjured leg strength (Figure 3B). A two-way ANOVA on the ratio of injured muscle torque to that of

uninjured muscle showed no significant differences between treatment groups or time points; there was no significant recovery of muscle strength in any autograft-treated group from 2 to 4 weeks post-injury (Figure 3C).

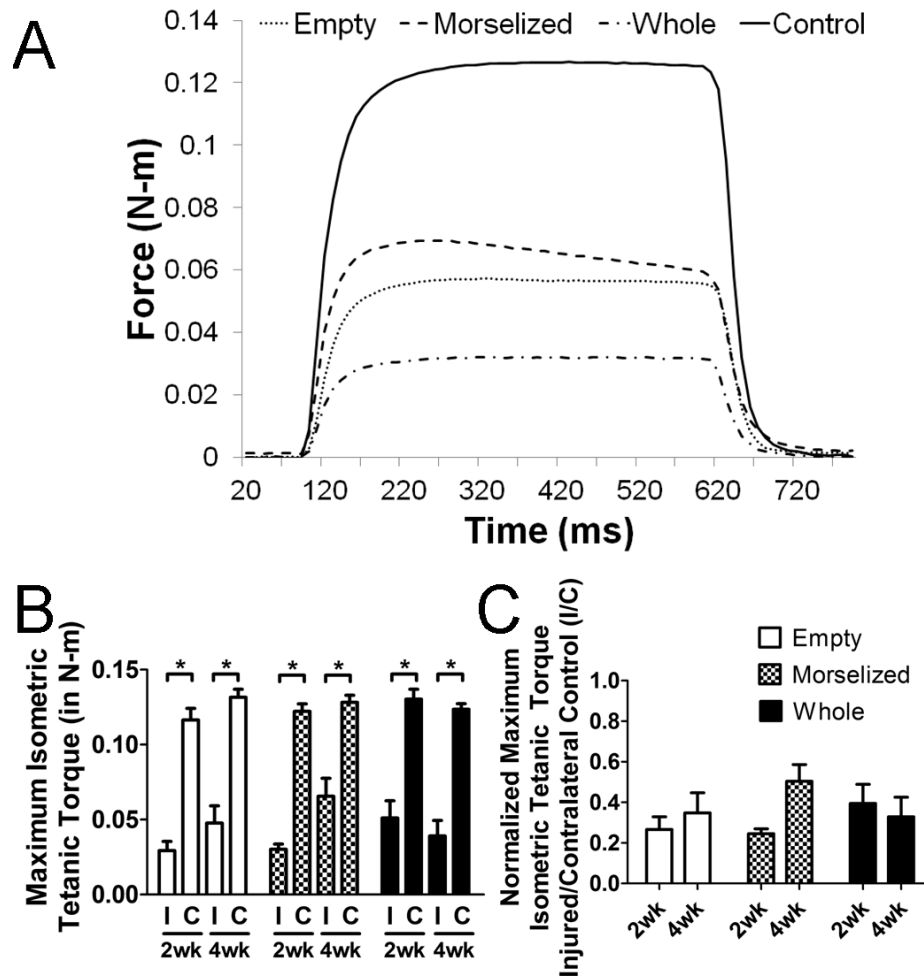


**Figure 3: Quantitative Measures of Muscle Function.** A. Representative graph of tetanic muscle torque measurement for empty defect (dotted), morselized autograft (dash), whole autograft (dash-dot-dash), and unoperated control (solid) groups. B. Maximum isometric tetanic torque of the quadriceps muscle in the injured left leg (I) and contralateral control right leg (C). C. Muscle torque expressed as a ratio of the injured leg to contralateral control (I/C). \* $p < 0.05$ ,  $n = 6$  per group per time point.

Muscle fatigue measurements showed no significant changes in fatigue characteristics between these treatment groups (Figure 4). Endurance indices for 2-week fatigue measurements were  $0.37 \pm 0.08$ ,  $0.28 \pm 0.13$ ,  $0.34 \pm 0.08$ , and  $0.26 \pm 0.11$  for

empty, morselized autograft, whole autograft groups, and contralateral controls respectively while 4-week endurance indices were  $0.32 \pm 0.08$ ,  $0.31 \pm 0.08$ ,  $0.38 \pm 0.04$ , and  $0.29 \pm 0.08$ .

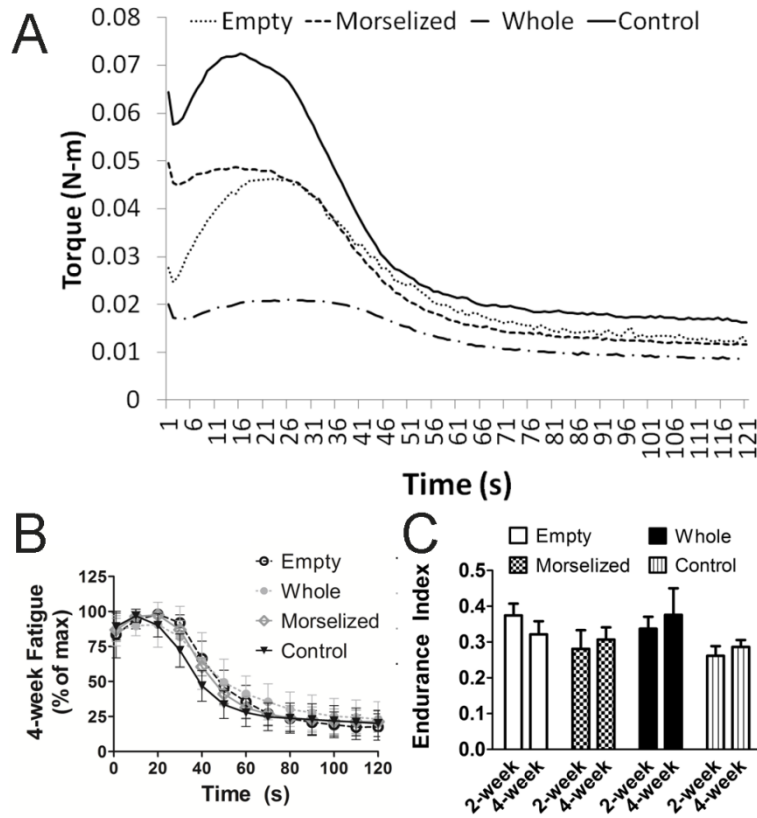


**Figure 4: Quantitative Measures of Muscle Fatigue.** A. Representative raw fatigue measurements for empty defect (dotted), morselized autograft (dashes), whole autograft (dash-dot-dash), and unoperated control (solid) groups. B. Muscle fatigue measured at 4 weeks post injury. C. Endurance index expressed as a ratio of torque produced at one minute into the fatigue protocol to maximum torque produced in protocol.

#### *Muscle Mass Measurements*

Injured muscle from all treatment groups lost a significant amount of muscle mass; the injured muscle had 70-90% of the muscle mass of contralateral controls (Figure 5A). Muscle mass data of injured muscles normalized to contralateral control muscles showed no significant change in muscle mass between the two time points in any treatment groups (Figure 5B). There was no significant difference in muscle mass

between the empty defect group and the treatment groups. Histological cross-sections of muscle tissue at 4 weeks post-injury qualitatively confirmed that injured muscles were similar in size and slightly smaller than a control muscle (Figure 5C). Muscle mass measurements were found to significantly correlate with muscle strength measurements (Figure 6) with a correlation coefficient of 0.52.

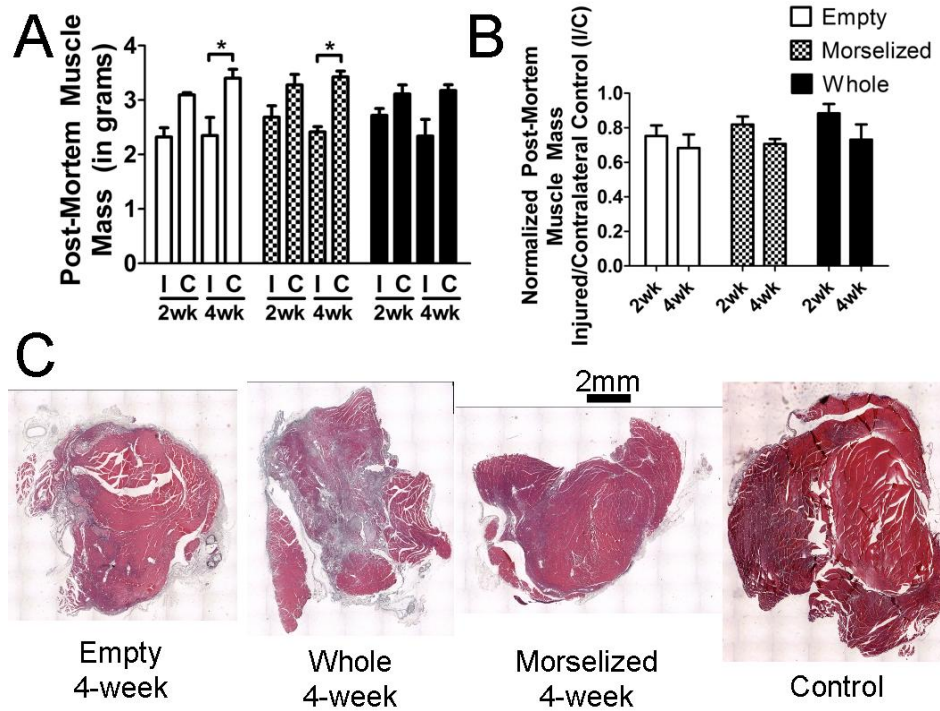


**Figure 5: Muscle Mass and Representative Cross-Sectional Images of Muscle.** A. Post-mortem muscle mass of the quadriceps muscle from the injured left leg (I) and contralateral control right leg (C). B. Post-mortem muscle mass expressed as a ratio of the injured leg to contralateral control (I/C). C. Representative H&E stained transverse (cross-sections) images of muscles from all treatment groups and control. \* $p < 0.05$ ,  $n = 6$  per group per time point.

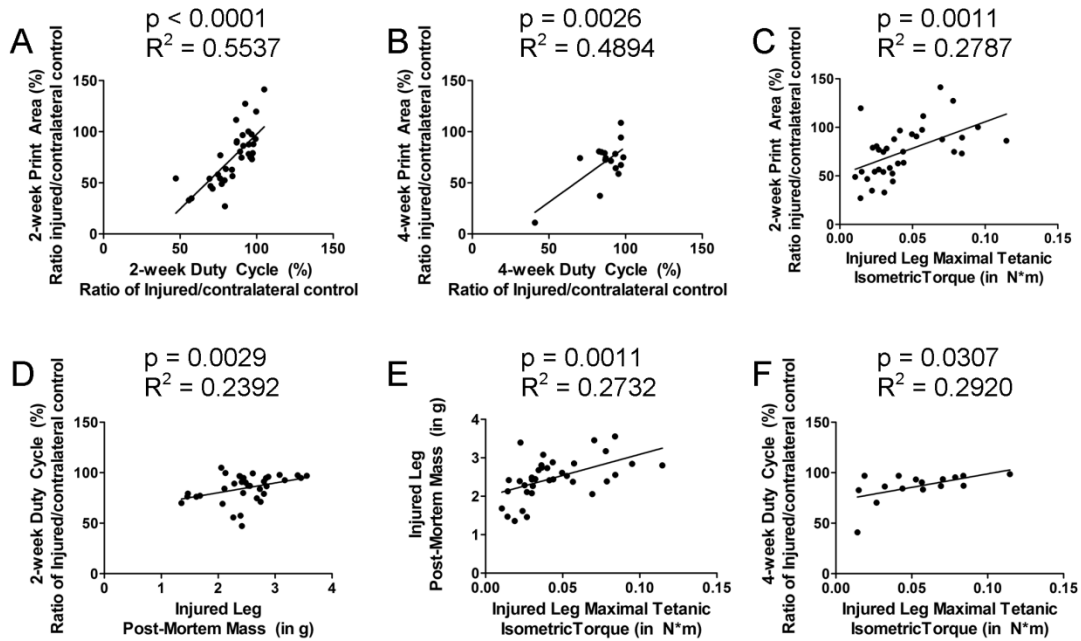


**Figure 6: Correlations between Measurements.** Measured parameters for each individual sample were plotted in order to determine significant correlations between parameters. Significant correlations were found between static and dynamic gait parameters at 2 weeks (A) and 4 weeks (B), injured leg maximal isometric torque with 2-week print area (C) and duty cycle (D), injured leg maximal isometric torque with injured leg mass (E), and injured leg maximal isometric torque with 4-week duty cycle (F). Linear regressions are shown with coefficients of determination.  $p < 0.05$  indicates a significant non-zero slope,  $n=36$ .

### *Measurements of Limb Functionality*

Hind paw print area was measured to quantitatively determine limb function in each treatment group. The empty defect group showed a significant decrease in print area ratio (injured to uninjured) compared to baseline control while autograft-treated groups did not show a significant change (Figure 7A). The duty cycle—measurement of the time a paw is contact with the ground as compared to the stride duration—also decreased significantly at 2 and 4 weeks post-injury compared to baseline control (Figure 7B). The whole autograft treated group had a decreased duty cycle at 2 weeks post-injury, compared to the baseline measurements from the same group. Paw print area and duty

cycle ratios were found to significantly correlate at weeks 2 and 4, with correlation coefficients of 0.74 and 0.70 respectively (Figure 6). 2-week print area and duty cycle ratios and 4-week duty cycle ratios were also found to significantly correlate with the injured leg isometric maximal tetanic torque (Figure 6C, D, F).

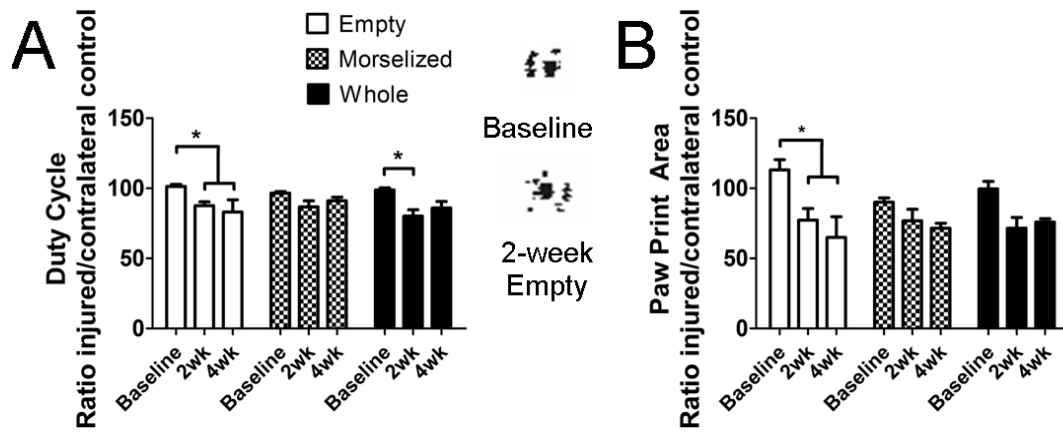


**Figure 7: Quantitative Measures of Gait and Limb Recovery.** A. Print area, a static gait parameter, at baseline (measured prior to surgery), 2 weeks, and 4 weeks post injury. Representative paw prints are shown on the right. B. Duty cycle, a dynamic gait parameter that measures the time a paw is in contact with the ground as compared to stride duration. \*p<0.05, n=12 at 2 weeks, n=6 at 4 weeks.

### *Muscle histology*

Transverse histological sections were taken from all groups and all time points (Figure 8). Sections stained with H&E showed regenerating muscle fibers with centrally-located nuclei at both time points in all groups. However, sections stained with Masson's trichrome showed extensive fibrotic tissue formation (indicated by blue staining of collagen) near or surrounding the regenerating muscle fibers. At 4 weeks, the morselized autograft treated group had dispersed fibrotic tissues in small spaces between muscle cells (stained in blue), compared to the large sections of fibrosis seen in the untreated and whole autograft-treated groups.

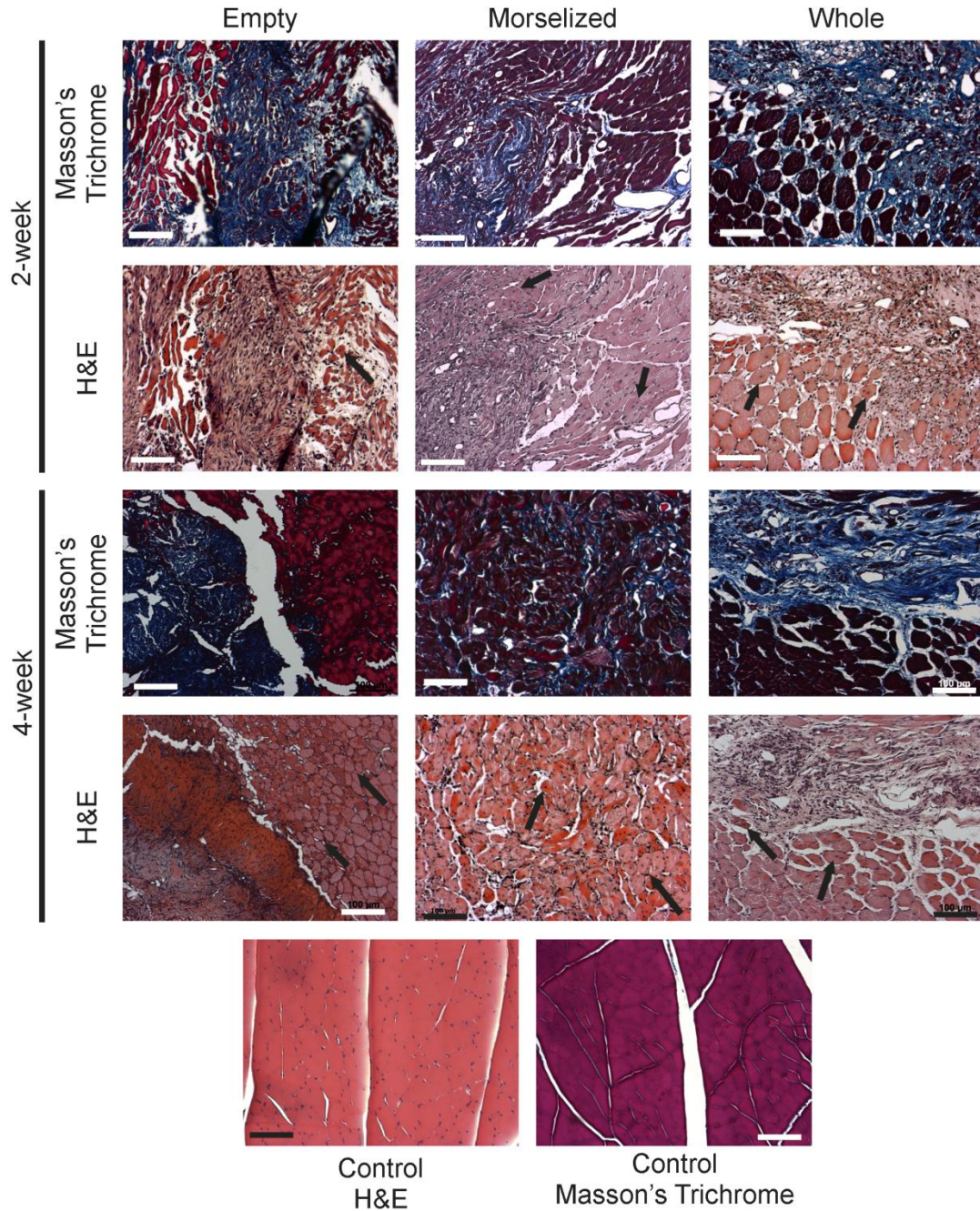


**Figure 8: Fibrosis and regenerating fibers, visualized in histology.** Fibrosis can be seen in Masson's Trichrome stained sections (collagen fibers stain blue). Regenerating muscle fibers, in which nuclei are centrally located, can be seen in H&E stained sections (indicated by black arrows). Images were taken at 10x magnification, scale bars: 100µm.

### 3.5 Discussion

This is, to our knowledge, the first rat model of above-the-knee volumetric skeletal muscle loss. Our model was quantitatively characterized by early analysis of

edema and hematoma in the injured muscle using MRI, peak isometric torque produced by the quadriceps femoris, and functional limb analysis as determined by gait. Given the thorough analyses of functional biomechanical outcomes, our model presents a useful platform in which tissue engineering and regenerative medicine strategies can be tested and quantitatively analyzed for efficacy in muscle regeneration.

Our results showed a large decrease in muscle functional capacity, as hypothesized; however, this decrease in muscle function is not wholly explained by the relatively smaller decrease in muscle mass. One possible explanation is illustrated by Masson's trichrome staining, which showed a large area of blue-stained collagen fibers, indicative of fibrosis of the muscle. Presumably, much of the injured muscle tissue was replaced by fibrotic scar tissue resulting in decreased tissue quality. This non-functional scar tissue in the muscle may account for part of the large functional deficit we see in our model.

Peripheral nerve damage is a likely co-morbidity in our large VML injury. This possible nerve damage further complicates the model and may contribute to the lack of muscle recovery. Denervated muscle flaps have been shown to result in muscle atrophy [115-117]. Our model did not exhibit extensive atrophy, suggesting that although peripheral nerve damage may occur, it does not account for the majority of the functional deficit. Nevertheless, reinnervation of motor nerves may enhance muscle regeneration and function [118] and should be taken into account when developing a treatment strategy for VML.

Clinically, thin muscle flaps that cover large muscle defects are not always effective for functional tissue engineering; thus, we examined the regenerative potential

of autografts, which consist of a higher amount of tissue than a muscle flap. Contrary to our hypothesis that this treatment would improve muscle regeneration and function, our VML model showed little to no improvement with autograft treatment. These results seemingly contradict previous literature; the mouse extensor digitorum longus and the rat triceps surae muscles that had been excised, minced, then placed back into its muscle bed regenerated within 2 weeks with little fibrosis [41] [119]. However, our data showed no significant improvement in muscle function between any treatment groups at any recovery time point. A key difference between the morselized autograft in our model and the minced murine muscle is size. While smaller muscles were able to regenerate with minimal scarring, the larger quadriceps muscle did not reach the same regenerative potential. This is further illustrated in the clinic, where thin muscle flaps are used to cover VML injuries, providing only a small amount of tissue for regeneration with and often resulting in functional deficit.

Another distinct possibility for the lack of functional recovery of the muscle with autograft treatment is related to the muscle extracellular matrix (ECM). In recent years, an increasing number of studies have demonstrated the importance of the ECM in muscle function [62, 120]. The muscle autografts used in our experiments were not specifically aligned with the muscle fibers within the injury bed, and our VML encompasses parts of all four muscles of the quadriceps, further complicating the orientation of our autograft treatment. This juxtaposition of randomly aligned graft ECM on the muscle ECM may have yielded inefficient functional recovery of the muscle. This lack of recovery with misaligned ECM and the importance of muscle ECM on muscle function suggest that

tissue engineering strategies that incorporate structure alignment may result in a more organized tissue and thus a higher chance of functional recovery.

Vascular reconstruction, which is widely used clinically to maintain vascular perfusion in a muscle flap, was not performed in our autograft treatment. The success of muscle flap treatments in the clinic rely heavily on blood supply to the flap. This, again, alludes to the inversely proportional relationship between VML size and the regenerative potential of the muscle. Research investigating muscle flap treatment of open fractures shows that muscle flaps that are constructed too large suffer from ischemia-induced necrosis [121-123]. Additionally, vascularized muscle flaps that have reconstructed nerve connections served as better wound coverage than disconnected flaps, suggesting that vascularization and nerves play a role in survival of the graft [118]. The autografts used in our model may have necrosed from lack of intact vessels, leading to an inflammatory environment that may have deterred any healing response from stem cells or extracellular matrix proteins in the autograft. This suggests that regenerative approaches that facilitate vascular growth may increase the survival rate of implanted or migrated endogenous cells in the center of the VML defect.

As mentioned before, our minced and whole autograft treatments of the VML defect illustrated the importance of differences in mass and nutrient transfer that arise from the size scale of the muscle defect and the animal model. While minced and whole autografts did not result in functional regeneration in our rat quadriceps defect model, another group has demonstrated some success of this therapy in the tibialis anterior muscle of the rat, in which a smaller, single-muscle VML was created [124]. Additionally, while ECM treatment has had moderate success in regenerating muscles in

rodent models, the same treatment used in the dog gastrocnemius muscle resulted in little recovery in the muscle function after 3 months [60, 61]. This, again, highlights the need for a large, challenging regenerative environment in preclinical models to maximize translational potential of therapies.

Various tissue engineering strategies have been tested in preclinical models of VML that have shown promising effects on muscle regeneration. Small intestinal submucosa extracellular matrices (SIS-ECM) have been tested in a mouse quadriceps VML, and host skeletal muscle cells infiltrated the ECM, indicating possible muscle regeneration though no muscle function was tested [44]. Other groups have decellularized the rat gastrocnemius muscle and then recellularized this ECM with mesenchymal stem cells (MSCs). When implanted in a rat gastrocnemius defect, this treatment showed significant functional recovery compared to ECM or injury alone [47, 77]. Other promising interventions have used muscle-derived stem cells or satellite cells seeded on fibrin microthreads or hyaluronic acid hydrogel respectively; both studies showed functional recovery when implanted in a mouse tibialis anterior muscle VML model [42, 43]. These regenerative strategies clearly have potential for the functional healing; however, the VML used to test these treatments were relatively small. Given the size considerations of VML models, it would be beneficial to test strategies such as these in our challenging VML in order to rigorously filter preclinical treatments prior to investigating their potential in even larger animal models or humans.

In conclusion, we have successfully established a novel model of VML in the quadriceps femoris of a rat with quantitative functional outcome metrics. Contrary to our hypothesis, neither minced nor whole autografts resulted in any significant recovery of

muscle function. This is consistent with clinical outcomes, in which autogenic muscle flap treatments of VML injuries often result in functional deficits. While this VML in the quadriceps represents well the major clinical challenges of VML injuries, the possible nerve and vessel damage in this VML model may hinder any tissue engineering strategies that may indeed facilitate muscle regeneration but does not actively support nerve or vessel repair. This is a major limitation to this model that will be addressed in the next chapter of this dissertation.

# **CHAPTER 4 Aim 1: Composite Muscle & Bone Injury Model in the Rat<sup>3</sup>**

## **4.1 Abstract**

Extremity injuries involving large bone defects with concomitant severe muscle damage are a significant clinical challenge often requiring multiple treatment procedures and possible amputation. Even if limb salvage is achieved, patients are typically left with severe short and long-term disabilities. Current pre-clinical animal models do not adequately mimic the severity, complexity, and loss of limb function characteristic of these composite injuries. The objectives of this study were to establish a composite injury model that combines a critically-sized segmental bone defect with an adjacent volumetric muscle loss injury and then use this model to quantitatively assess rhBMP-2 mediated tissue regeneration and restoration of limb function. Surgeries were performed on rats in three experimental groups: muscle injury (8 mm diameter full-thickness defect in the quadriceps), bone injury (8 mm non-healing defect in the femur), or composite injury combining the bone and muscle defects. Bone defects were treated with 2 $\mu$ g of rhBMP-2 delivered in pre-gelled alginate injected into a cylindrical perforated nanofiber mesh. Bone regeneration was quantitatively assessed using  $\mu$ CT, and limb function was assessed using gait analysis and muscle strength measurements. At 12 weeks post-surgery, treated bone defects without volumetric muscle loss were consistently bridged. In contrast, the volume and mechanical strength of regenerated bone were attenuated by

---

<sup>3</sup> Portions of this chapter were adapted from Willet N J, Li M-T A, Uhrig B A, Boerckel J D, Huebsch N, Lundgren T S, Warren G L, Guldberg R E. Attenuated Human Bone Morphogenetic Protein-2-Mediated Bone Regeneration in a Rat Model of Composite Bone and Muscle Injury. *Tissue Engineering Part C* 19(4): 316-325. Reprinted with permission from *TISSUE ENGINEERING Part C: Methods*, 2013, published by Mary Ann Liebert, Inc., New Rochelle, NY

45% and 58%, respectively, in the identically treated composite injury group. At the same time point, normalized muscle strength was reduced by 51% in the composite injury group compared to either single injury group. At two weeks, gait function was impaired in all injury groups compared to baseline with the composite injury group displaying the greatest functional deficit. We conclude that sustained delivery of rhBMP-2 at a dose sufficient to induce bridging of large segmental bone defects failed to promote regeneration when challenged with concomitant muscle injury. This model provides a platform with which to assess bone and muscle interactions during repair and to rigorously test the efficacy of tissue engineering approaches to promote healing in multiple tissues. Such interventions may minimize complications and the number of surgical procedures in limb salvage operations, ultimately improving the clinical outcome.

## **4.2 Introduction**

There is growing appreciation of the profound interactions between skeletal muscle and bone during development, daily function, and healing subsequent to traumatic injury. Clinical studies have reported that composite injuries consisting of both bone fracture and muscle injury significantly complicate fracture healing, often resulting in delayed healing, non-union, infection, re-hospitalization, and additional surgeries [125-129]. Coverage of an open fracture with a muscle flap is the clinical gold standard for intervention and has been shown to improve fracture healing, suggesting that muscle somehow contributes to the bone repair process [54, 130, 131]. Medical advances have made limb salvage common after these severe injuries; however, patients are often left with substantial short-term and long-term disabilities [102, 129]. Though long term function at 2 and 7 years post-injury is approximately equivalent in amputation and limb salvage patients (based on the sickness impact profile scoring system), amputees are at

lower risk for further complications or additional surgeries [102, 129]. Additionally, functional disabilities, pain, neurologic dysfunction, and infection can result in delayed amputations at reported rates of 4-15% in limb salvage cases involving severe bone (grade III) and soft tissue injury (crush or volumetric muscle loss) [132-134]. Though limb salvage techniques have improved, there are substantial advancements still to be made in limb reconstruction and rehabilitation leading to the restoration of normal function. Highlighting this need, composite extremity injuries are the leading battlefield injury faced by returning servicemen [1, 132, 135]. To date, clinical composite injury studies have been mainly observational in nature without offering clear insight into the mechanisms involved.

Potential roles for muscle in bone healing include acting as a source for vascularization, progenitor cells, osteogenic myokines, and also biomechanical stimuli [136, 137]. Studies have shown that muscle surrounding a bone defect contributes to re-establishing the blood supply, a step which is critical to ensure successful bone healing [138-140]. Additionally, muscle cells secrete numerous osteogenic factors (including IGF-1, FGF-2, and TGF- $\beta$ ) under basal conditions, with increased secretion in regenerating muscle [137, 141, 142]. The periosteum, a cellular membrane that separates bone and muscle tissues, expresses receptors for these growth factors suggesting a mechanism of tissue cross talk [137]. These growth factors have also been implicated in the recruitment and differentiation of osteogenic progenitor cells. Muscle progenitor cells have also demonstrated a capability to differentiate into osteogenic cell lineages [143, 144]. A recent study tracked these muscle progenitor cells after an open bone fracture and showed incorporation of these cells in regenerated bone [145]. These studies

have demonstrated potential mechanisms of interaction between bone and muscle during regeneration.

There are currently few models of composite bone-muscle injury in the literature and no models that can be used to assess multi-tissue engineering strategies. The few models in the literature have all been performed in the lower limb and combine a naturally healing fracture or osteotomy with varying degrees of muscle injury (laceration, crush, or resection) [54, 146-148]. Models with severe muscle injury (resection) typically displayed delayed bone healing, while models with less severe muscle injuries commonly displayed no effect on bone healing. A recent consensus recommendation published by experts in the fracture field pointed to the thin soft tissue coverage of the tibia as a reason that it may not be an ideal location to investigate the relation of soft tissue to bone repair [149]. Instead, the femur was recommended due to thick muscle coverage. In addition, a fracture model has limited utility for the investigation of tissue engineered bone constructs, which are typically assessed in critically sized, non-healing defects. To effectively develop and evaluate tissue engineered constructs for multi-tissue limb reconstruction, a more challenging pre-clinical model of traumatic injury is needed as are quantitative functional outcome measures.

In this study, **our objective was to develop a composite injury model consisting of a critically sized segmental bone defect in the femur and an adjacent volumetric muscle injury in the quadriceps.** An established tissue engineered recombinant human bone morphogenetic protein-2 (rhBMP-2) delivery system was tested for the treatment of the bone defect [10, 150, 151]. This system had previously been shown to provide sustained delivery of rhBMP-2 at a dose sufficient to induce bridging of

a bone defect in a single tissue injury model [10, 150, 151]. *It was hypothesized that animals with a composite injury would have attenuated tissue regeneration and impaired limb function despite rhBMP-2 treatment.* Additionally, in order to gain insight into the mechanisms by which muscle and bone interact during regeneration, we further tested whether muscle cells/ECM in the form of an autograft or early revascularization of the limb may play a role in the healing of the bone.

### **4.3 Materials/Methods**

#### *Surgical Procedure for Creation of the Composite Defect*

Thirteen week old female Sprague-Dawley rats (Charles River Labs, Wilmington, MA) were used for this study. Animals were placed in one of three injury groups: bone defect only (n=5), muscle defect only (n=8), or composite bone and muscle defect (n=5). Unilateral bone defects were surgically created in the femora of rats, as previously described [10, 151, 152]. Briefly, an anterior incision was made along the length of the femur and the muscle was then separated using blunt dissection. A modular fixation plate was affixed to the femur using miniature screws (JI Morris Co., Part No. P0090CE250). A full-thickness segmental defect, 8 mm in length, was created in the diaphysis using a miniature oscillating saw. A perforated nanofiber mesh tube made of polycaprolactone (PCL) was then placed over the native bone ends surrounding the defect, and 150  $\mu$ l alginate hydrogel containing 2.0  $\mu$ g rhBMP-2 was then injected into the defect space [10]. This dose had previously been shown to consistently induce bridging of the bone defect [150]. Non-treated controls were not used in this study as previous studies have demonstrated that in the absence of rhBMP-2, the defect contains very little bone formation [150, 152]. Muscle defects were created through the full thickness of the

quadriceps down to the femur using an 8 mm diameter biopsy punch (Figure 9A). The defect encompassed regions of the rectus femoris, vastus lateralis, vastus medialis, and vastus intermedius. The muscle defect was untreated in this study and left empty. In composite injury animals, the bone defect was made first, then, once the incised muscles had been closed with 4-0 suture, the muscle defect was created. Animals were given buprenorphine post-surgery to manage pain (0.03 mg/kg 3x daily for the first 48 hours, then 0.01 mg/kg 3x for the next 24 hours). All procedures were approved by the Georgia Institute of Technology Institutional Animal Care and Use Committee (protocol #A09039).

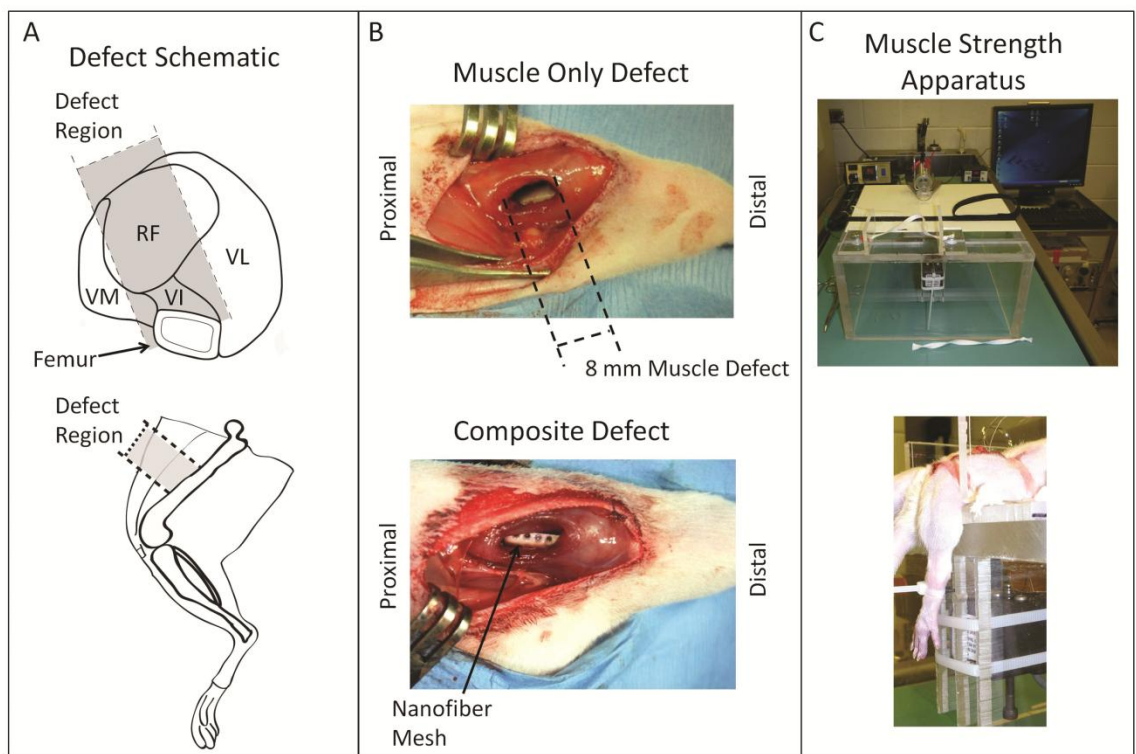


**Figure 9: Representative Methods Images.** Panel A shows schematics illustrations of the anatomical injury location including a cross section through the quadriceps (top) and a side view of the hindlimb (bottom). Panel B shows images from the muscle defect only surgery (top) and the composite bone and muscle defect surgery (bottom). Panel C shows

representative images of the muscle strength-measuring apparatus (top) and positioning of a rat limb in the apparatus (bottom). The animal was secured at the hips and the knee by a strap, and then the ankle was fastened to a force transducer. VM – Vastus Medialis; RF – Rectus Femoris; VI – Vastus Intermedius; VL – Vastus Lateralis

### *Functional Gait Analysis*

Hind limb function was assessed after injury using the CatWalk system (CatWalk 7.1, Noldus Inc., Leesburg, VA) at baseline (1 week prior to surgery) and at 2, 4, 8, and 12 weeks post-injury. The system consisted of an illuminated platform, an enclosed walkway and a digital camera mounted below the platform. The rats were placed at the open end of the track and allowed to ambulate freely to the other end. Illuminated paw prints were recorded and paw print area and duty cycle were assessed for each group. Paw print area is a static parameter that measures the area of contact that the paw makes with the glass walkway during the stance phase. Duty cycle is a dynamic parameter indicative of limb use during ambulation, and is represented as the ratio of the stance duration to the sum of the stance and swing duration (stride duration).

### *Muscle Isometric Tetanic Torque Assessment*

Isometric tetanic torque production about the knee by the knee extensor muscles was measured at 12 weeks post-surgery using a custom built apparatus based on a previous design used for assessment of lower leg muscle function (Figure 9B) [113]. All measurements were made under isoflurane anesthesia during a terminal procedure immediately prior to euthanasia. A 2-cm long incision was made through the skin exposing the femoral triangle in the upper thigh. The posterior branch of the femoral nerve was carefully isolated and a nerve cuff was positioned surrounding that branch.

The rat was then carefully secured to the platform of the apparatus. The animal was positioned so that the knee angle was at 90° and the ankle was secured to a force transducer (Isometric Transducer Model No. 60-2996, Harvard Apparatus). The knee extensor muscles were stimulated using a stimulator (GRASS S11 Stimulator, Grass Technologies) and the nerve cuff implanted on the femoral nerve. Stimulator pulse duration, frequency, and train duration were set to 0.5 ms, 175 Hz, and 500 ms, respectively; these settings elicited maximal isometric tetanic torque as determined in a pilot study. Measurements of injured muscles were normalized to contralateral intact muscle for each animal. A fatigue protocol was run using 60 Hz stimulation for 330 ms every second for two minutes. Fatigue was calculated as the ratio of the force produced at the end of the two minute protocol compared to the highest force, which typically occurred in the first few seconds of the protocol.

#### *Faxitron X-Ray Analysis*

Digital radiographs (Faxitron MX-20 Digital; Faxitron X-ray Corp.) of the defect region in the femur were performed at an exposure time of 15 s and a voltage of 25 kV. Animals received X-ray imaging at 2, 4, 8 and 12 weeks post-surgery. Blinded analysis of bridging rates at 12 weeks was performed by three researchers.

#### *MicroCT Analysis*

MicroCT scans (VivaCT 40, Scanco Medical) were performed at 38.0  $\mu\text{m}$  voxel size at a voltage of 55 kVp and a current of 109  $\mu\text{A}$ . Scans were taken at 4 and 12 weeks post-surgery. Bone tissue was segmented by application of a global threshold corresponding to 386 mg hydroxyapatite/ $\text{cm}^3$  (roughly 50% of the native cortical bone density), and a low-pass Gaussian filter (sigma = 1.2, support=1) was used to suppress

noise. Samples were contoured and evaluated over 141 slices taken from a central region within the defect in order to normalize between samples without including cortical bone. *Ex-vivo* analysis over the entirety of the defect region was also performed and showed the same differences among the groups as the *in vivo* data at 12 weeks.

### *Biomechanical Analysis*

Animals were euthanized by CO<sub>2</sub> inhalation 12 weeks post-surgery. This time point was chosen based on previous publications demonstrating that bone apposition reaches a plateau by this time [150]. Torsional testing was performed on extracted femurs. The femurs were cleaned of soft tissue and the ends potted in mounting blocks using Wood's metal (Alfa Aesar, Wood Hill, MA). After removal of the fixation plate, the specimens were tested (ELF 3200, Bose ElectroForce Systems Group, Minnetonka, MN) at a rotational rate of 3° per second. Maximum torque was measured at the failure point from the torque-rotation data. Torsional stiffness was calculated by fitting a straight line to the linear portion of the curve before failure.

### *Histology*

Histological analysis was performed at 12 weeks post-surgery on extracted quadriceps muscles and femurs. Samples were perfusion fixed then immersion fixed for 48 h at 4 °C with 10% neutral buffered formalin. Following paraffin processing, 5 µm-thick cross-sections were cut and stained with hematoxylin and eosin (H&E), 0.5% Safranin-O (for bone), or Masson's Trichrome (for muscle). Bright-field images were obtained with the Axio Observer.Z1 microscope (Carl Zeiss, Thornwood, NY). Images were taken at 4x and 10x magnification using the AxioVision software (Carl Zeiss, Thornwood, NY).

### *Surgical Procedure and Analyses for Testing Muscle Autografts in the Composite Defect*

Thirteen week old female Sprague-Dawley rats (Charles River Labs, Wilmington, MA) were used for this study. The composite bone and muscle defect was applied to all animals as previously described, with 2.0  $\mu\text{g}$  rhBMP-2 delivered in RGD-functionalized 2% alginate injected into a PCL perforated nanofiber mesh tube. Animals were placed in one of three muscle treatment groups: empty quadriceps defect (n=8), whole autograft (n=7), and morselized autograft (n=8). The autografts were applied as previously described in Section 3.1.3. Longitudinal micro-CT measurements and faxitron x-ray images were taken at 4, 8, and 12 weeks post-injury. At 12 weeks post-injury, muscle force measurements were performed as previously described.

### *Surgical Procedure and Analyses for Determining Revascularization of the Limb*

Thirteen week old female Sprague-Dawley rats (Charles River Labs, Wilmington, MA) were used for this study. The animals were placed in one of two injury groups: composite bone and muscle defect, or bone defect alone. All animals received 2.0  $\mu\text{g}$  rhBMP-2 delivered in RGD-functionalized 2% alginate injected into a PCL perforated nanofiber mesh tube for the treatment of the bone. For evaluation of early revascularization, animals were euthanized at day 3 (n=3-6), 7 (n=7), and 14 (n=9) post-injury.

### *$\mu\text{CT}$ Angiography*

For all samples in the study determining revascularization of the limb post-composite defect, contrast agent-enhanced micro-CT angiography was performed terminally at the designated time points (day 3, 7, or 14). The technique has been previously described in detail [153-155]. Briefly, 0.9% salt solution (physiological saline)

containing 0.4% papaverine hydrochloride (Sigma-Aldrich) was perfused through the vasculature to clear the blood vessels. The vasculature was then perfusion fixed with 10% neutral buffered formalin, rinsed with physiological saline, and injected with lead chromate-based radioopaque contrast agent (2 parts microfil MV-22: 1 part diluent, Flow Tech). Samples were stored at 4°C overnight to allow for polymerization of the contrast agent. Hind limbs from the hip to the knee were excised. For day 3 and day 7 samples, the assumption was made that minimal bone was formed by that point, and limbs were scanned immediately. For day 14 samples, the samples were immersed in decalcification solution (Cal-Ex II, Fisher Scientific) for a period of 2-3 weeks under gentle agitation with solution changes every 1-3 days.

Excised samples were oriented with the femur along the z-axis for micro-CT scanning (vivaCT 40, Scanco Medical). Two sets of scans and volumes of interest (VOIs) were used to analyze within the bone defect only or within the thigh (including both muscle and bone). Scans were performed at 21µm voxel size for vessels within the bone defect region and 38µm voxel size for vessels within the thigh (muscle and bone). All scans were performed with an applied electroc potential of 55 kVp and a current of 109 µA. The VOI analyzing the bone region consisted of a cylindrical volume 5mm in diameter that spanned the center 7mm of the bone defect. A global threshold was applied for segmentation of vasculature, and a Gaussian low-pass filter was used to suppress noise ( $\sigma = 0.8$ , support = 1).

### *Statistical Analysis*

All data are presented as mean +/- standard error of the mean (SEM). Differences between multiple groups were assessed by analysis of variance (ANOVA) or for analyses

with only two groups a student t-test or Mann-Whitney test were used. A Tukey post hoc comparison was performed on the muscle and bone regeneration data, while the gait data was assessed with a Bonferroni post hoc test with pairwise comparisons within groups across time points or within time points across groups. A p-value less than 0.05 was considered significant. GraphPad Prism 5 (GraphPad Software, Inc., La Jolla, CA) was used to perform the statistical analysis. One sample was removed from the control bone defect group as an outlier. Bone volume, stiffness, and failure strength from this sample were over two standard deviations from the mean for the group (and from historical values for over 20 samples) [150].

#### 4.4 Results

##### *Bone Regeneration*

Faxitron X-ray radiographs were taken at 2, 4, 8, and 12 weeks post-surgery and illustrated the progression of bone formation in each group (Figure 10). Blinded analysis of bridging rates showed that the defect was bridged at 12 weeks in all animals with bone only defects while only three of six animals in the composite group showed bridging of the defect.

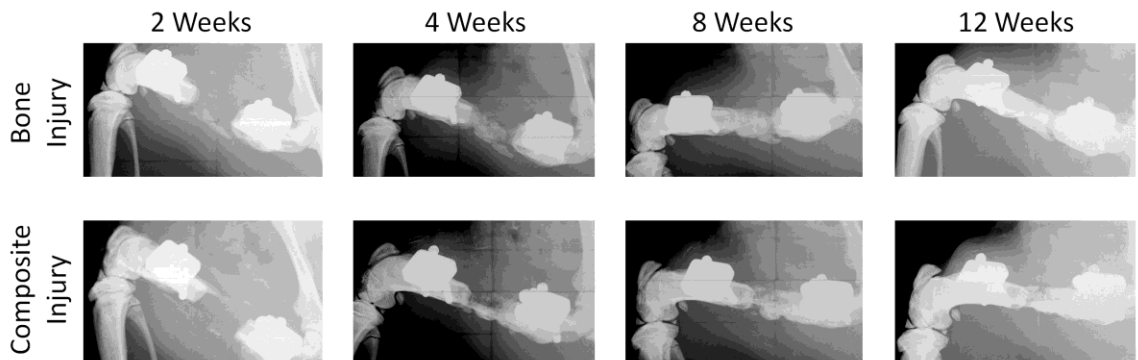


**Figure 10: Femur Radiographs.** Representative radiographs of the femurs from bone defect and composite defect animals at time points 2, 4, 8, and 12 weeks.

Micro-CT quantification of bone formation was performed at 4 and 12 weeks post-surgery (Figure 11A-B). At week 4, there were no significant differences between the groups though there was a trend for attenuated bone formation in the composite injury group. Animals in both groups had a significant increase in bone formation in the defect region between 4 and 12 weeks. By week 12, the composite injury animals had 45% less bone volume formed in the defect region as compared to animals in the bone injury-only group, a significantly lower value.

The degree of functional restoration in the regenerated bone tissue was measured using torsional testing to failure (Figure 11C). The composite injury group had significantly lower failure torque (59% lower) and stiffness (87% lower) as compared to the bone from animals in the bone-only injury group.

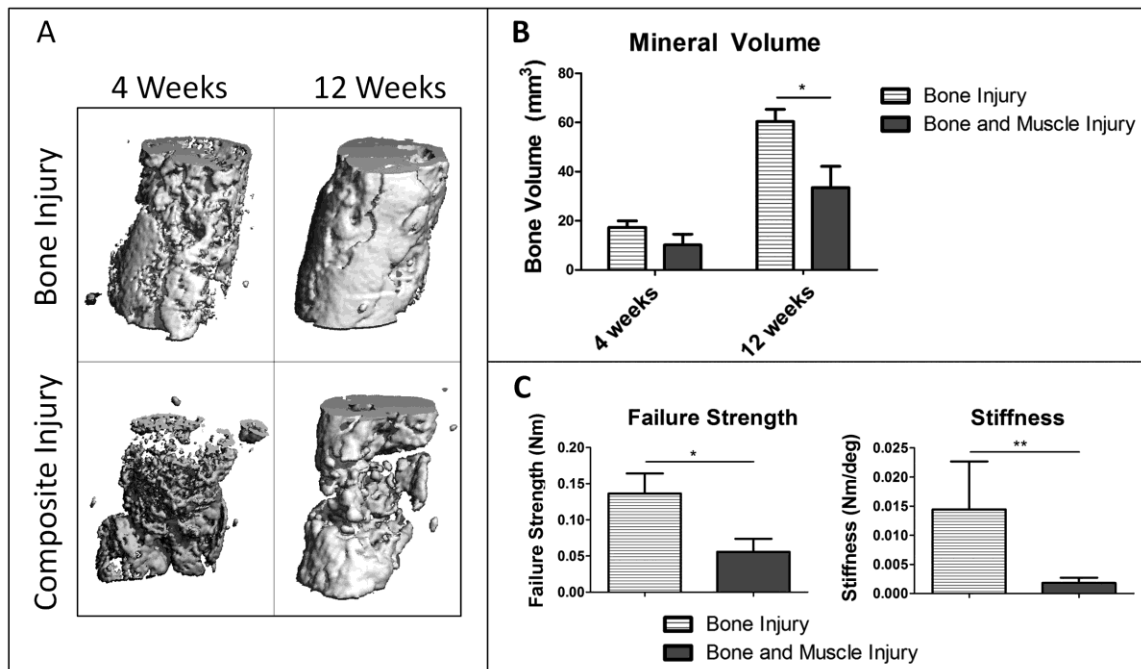


**Figure 11: Bone Regeneration.** Panel A shows representative  $\mu$ CT reconstructions at 12 weeks from the defect regions of bone defect and composite defect animals. Quantitative measurements of mineral volume in the defect region are presented in panel B. Mechanical data showing failure strength and stiffness acquired from torsional testing to failure are presented in panel C. \*  $p < 0.05$ ; \*\*  $p < 0.05$  using a Mann-Whitney test,  $n = 5-8$ .

Histological assessment of bone quality and composition was performed using H&E and Safranin-O staining (Figure 12). Bone injury animals showed areas of bone formation and endochondral ossification with larger well defined pockets of alginate when present. Composite injury animals showed some bone formation, though endochondral ossification was not observed. Alginate was present throughout the bone defect region in smaller pockets integrated within the regenerated bone.

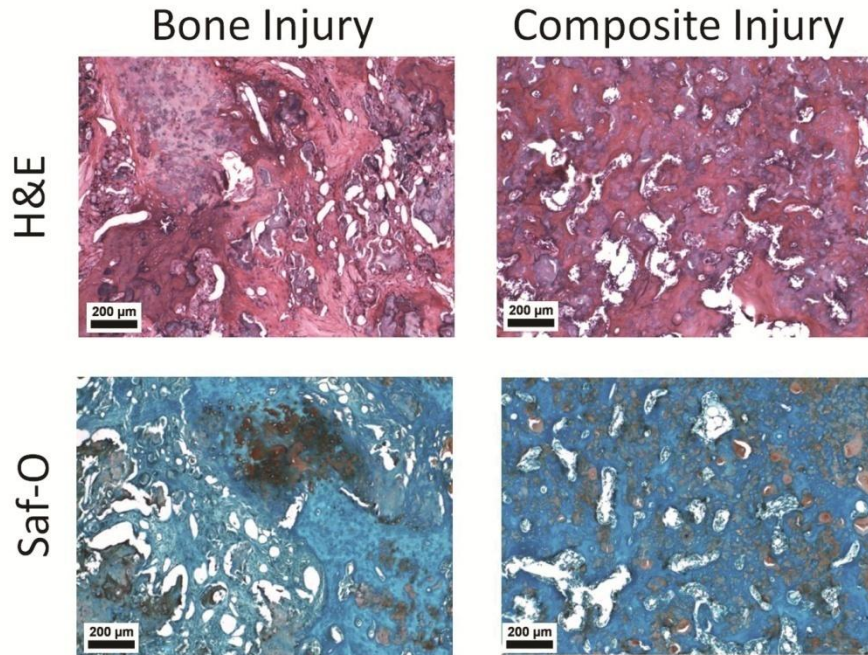


**Figure 12: Bone Histology.** Representative H&E and Safranin-O images are presented from within the bone defect region. Bone injury animals showed pockets of hypertrophic chondrocytes indicative of endochondral ossification from Saf-O staining and few larger isolated pockets of alginate. Composite injury animals had smaller pockets of alginate dispersed throughout the defect region as identified in both Saf-O (glossy light pink) and H&E (glossy purple) staining. All images were from 12 weeks post-surgery.

### *Muscle Regeneration*

Muscle regeneration was assessed histologically using H&E and Masson's Trichrome staining. Masson's Trichrome stain from the composite injury group showed fibrosis surrounding individual muscle fibers and fat nodules, indicating poorly regenerated muscle (Figure 13B). Animals from the muscle injury only group showed a band of fibrosis through the central region while fibrosis was not apparent in the bone only injury group. Animals in all three groups primarily showed peripherally located nuclei in muscle fibers throughout the H&E stained tissue cross sections, indicating that most muscle fibers were mature and not regenerating 12 weeks post-injury (Figure 13A).

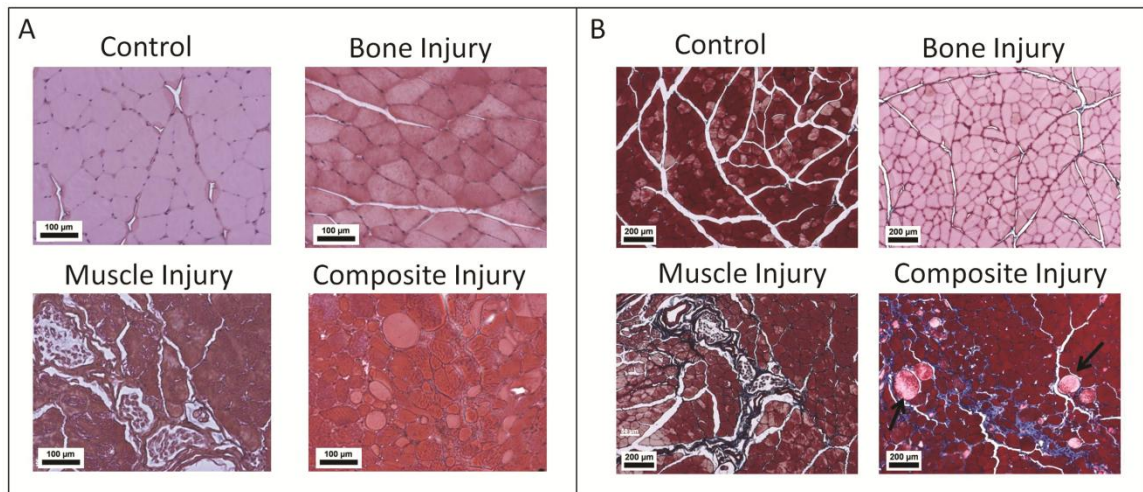


**Figure 13: Muscle Histology.** Panel A shows representative H&E images from quadriceps muscle sections taken from control, bone injury, muscle injury or composite injury animals. Most muscle fibers showed peripherally located nuclei indicating mature fibers and minimal muscle regeneration at this time point. Panel B shows representative Masson's trichrome images from sections adjacent to the images in Panel A. Blue staining shows fibrosis and the black arrows point to lipid deposits. Both fibrosis and lipid deposits were observed in the composite injury animals indicating poorly regenerated muscle. All images shown were from 12 weeks post-surgery.

Muscle function was assessed by measuring isometric torque produced around the knee, which is a direct measure of quadriceps strength (Figure 14A). Representative force-time tracings during femoral nerve stimulation are presented. All groups showed a significant decrease in muscle strength as compared to the contralateral control limb, 12 weeks post-injury. Strength in the injured limbs was 38 %, 38 %, and 18 % of the contralateral control in the bone only defect group, muscle only group, and composite group respectively. Normalizing the strength of the injured limb by that of the contralateral control limb showed that animals with a composite injury had a significantly greater deficit in muscle strength as compared to animals with a single tissue injury (51% greater deficit). Fatigue waveforms showed normal profiles with a peak in force produced shortly after initial stimulation then slowly dropping off (Figure 14B). Compared to contralateral controls, muscle fatigue was significantly decreased in animals with muscle only injuries, but not the bone only or composite injury groups.

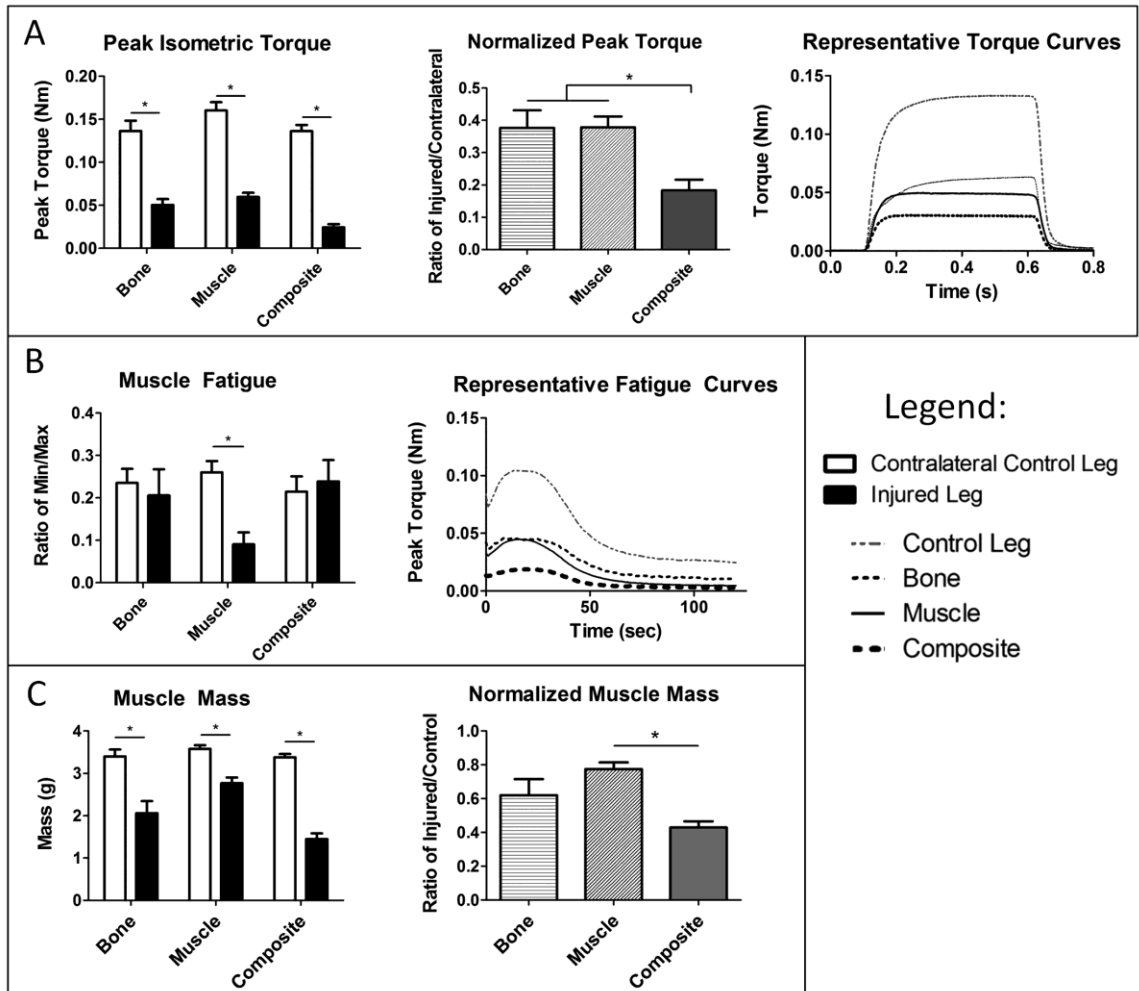


**Figure 14: Muscle Functional Capacity.** Panel A presents peak torque data from animals in all groups at 12 weeks post-surgery including: peak isometric torque (left) in injured and contralateral non-operated control limb. Normalized torque (center) as the ratio of the peak torque in the injured limb compared to the peak torque in the contralateral non-operated limb, and representative torque curves (right). Panel B shows representative fatigue curves (right) and muscle fatigue data (left) Muscle fatigue was measured for each animal as the ratio of the minimum peak torque compared to the maximum peak torque for each limb. Panel C shows the wet muscle mass from the quadriceps immediately after euthanasia. Mass (left) and normalized mass are presented (right). \* -  $p < 0.05$ ,  $n = 5-8$

Mass of the knee extensor muscle group was measured immediately after euthanizing the animals. All three groups showed a significant reduction in muscle mass in the injured limb as compared to the contralateral control limb (Figure 14C).

Normalized muscle mass (ratio of the mass of the injured limb to that of the contralateral control limb) in the composite injury animals was significantly lower compared to the muscle injury group but not the bone injury.

### *Limb Function*

Limb function was quantitatively evaluated by measuring two gait parameters: paw print area and duty cycle (Figure 15). All groups, including bone injury, muscle injury, and composite injury, showed a significant deficit in paw print area at two weeks post-surgery compared to baseline values. The print area deficit observed at 2 weeks was significantly worse in composite injury animals compared to the single tissue injury animals. The composite injury animals showed a steady recovery in print area between 2 and 12 weeks, reaching a comparable level to the deficit observed in the single tissue injury animals. Similarly, the composite injury animals had a deficit in duty cycle at 2 weeks compared to baseline values and compared to single tissue injury animals at the same time point. By 4 weeks, duty cycle showed no significant differences among any of the groups.

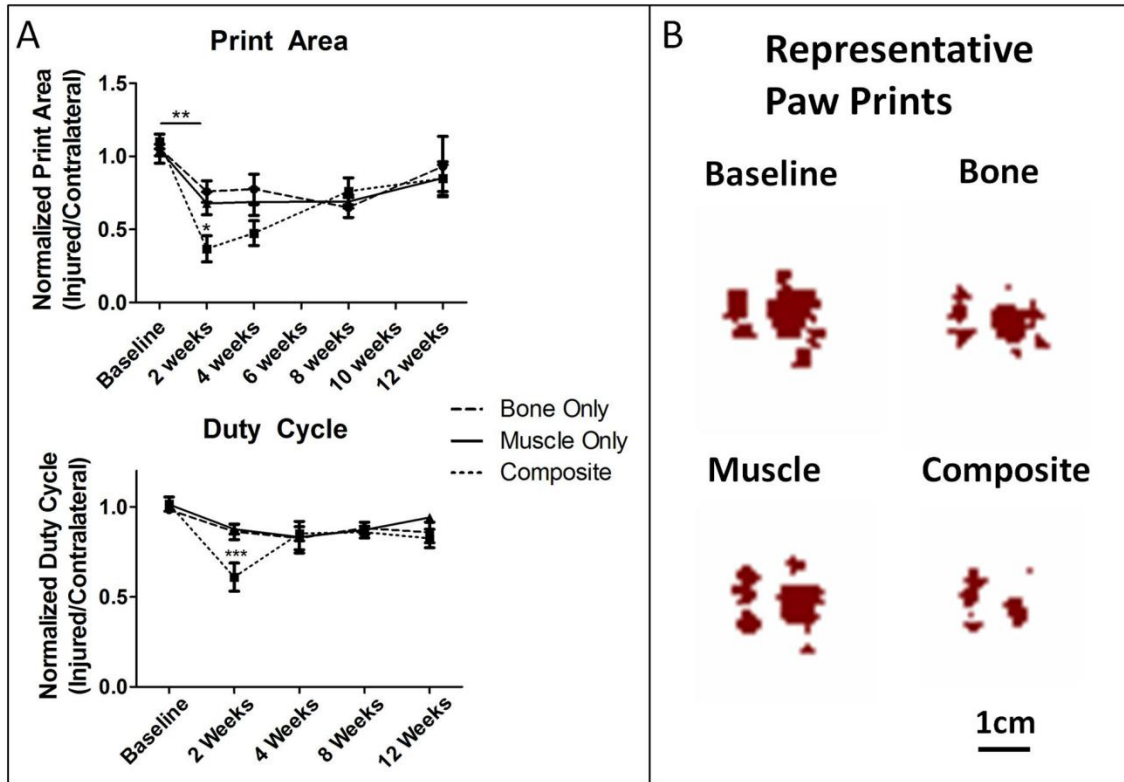


**Figure 15: Limb Function.** Measurements of gait were made using the Noldus Catwalk system. Print area and duty cycle (ratio of the stance duration to the sum of the stance and swing duration) at 2 week intervals from animals in all groups are presented in panel A. Data is presented as the ratio of the injured limb to the contralateral non-injured control limb. Panel B shows representative paw prints, corresponding to the paw print area from the injured limb of animals 2 weeks post-surgery. \* -  $p < 0.05$  between groups within time point, \*\* -  $p < 0.05$  between time points within group, \*\*\* -  $p < 0.05$  compared to baseline within group and within time point between groups,  $n = 5-8$

#### *Treatment with Muscle Autografts*

To determine if the removal of a large amount of cells/ECM is the main reason behind the attenuated bone regeneration, muscle autografts (whole or morselized) were implanted into the quadriceps defect and compared to the empty defect. Longitudinal faxitron images showed no significant differences between the three treatment groups (empty, whole, and morselized autograft) (Figure 16A), and  $\mu$ CT quantification of mineral volume confirmed this finding (Figure 16B). 12-week analysis of muscle

strengths showed significantly decreased muscle strengths in the injured legs compared to the uninjured contralateral controls (Figure 17A). No significant differences were found in normalized muscle forces between the three treatment groups (Figure 17B). Wet muscle mass was also lower in the injured legs compared to uninjured controls, with no differences in the normalized data between the three treatment groups (Figure 17C,D).

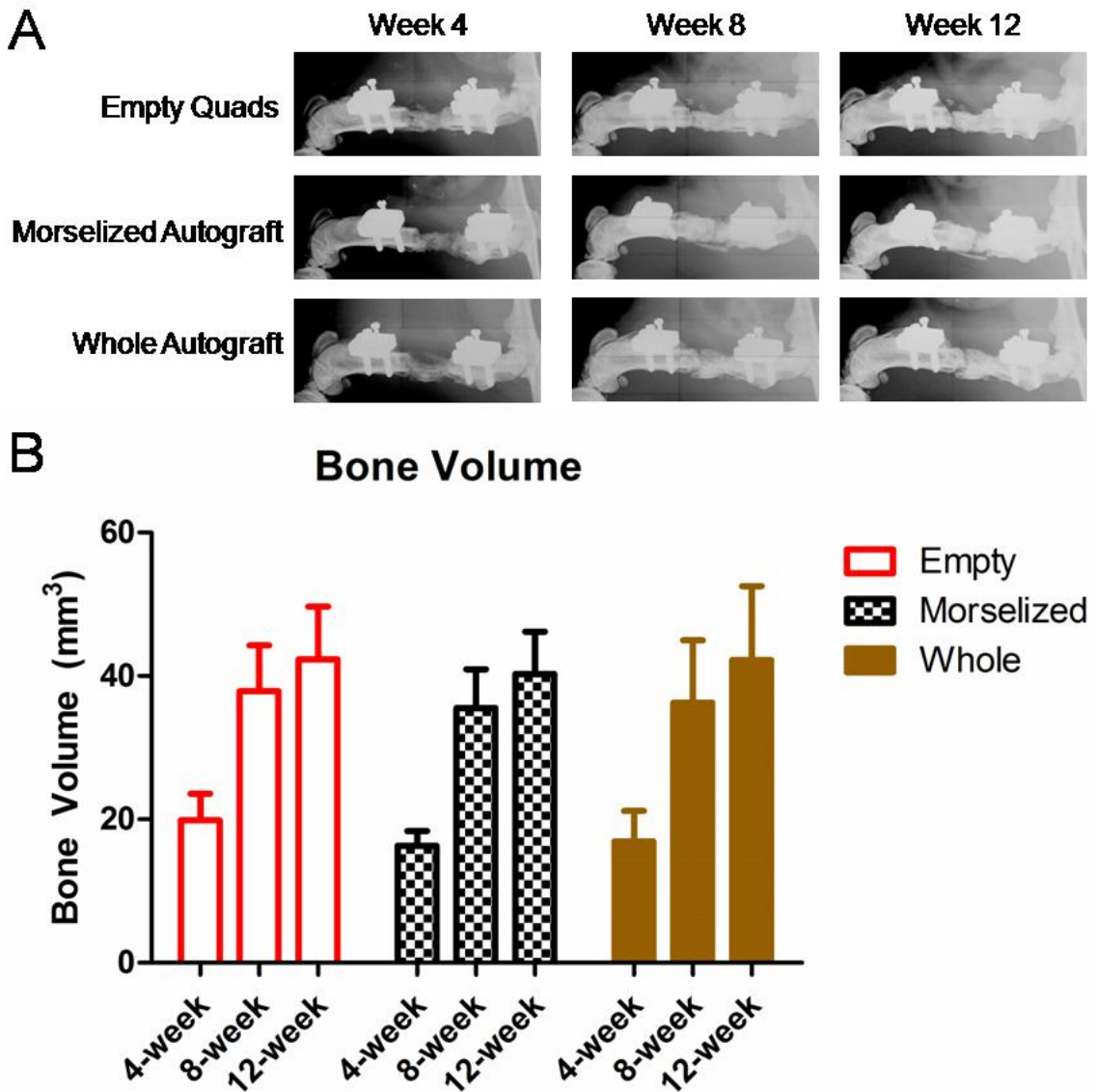


**Figure 16: Bone Volume after Treatment with Muscle Autografts.** Bone regeneration was monitored at 4, 8, and 12 weeks post-surgery. Panel A shows no visual differences between the three treatment groups at any time point. Panel B confirms this finding with

$\mu$ CT analysis of mineral volume in the defect region. No differences were found between the three treatment groups at any time point. Empty n=8; morselized n=8; whole n=7.

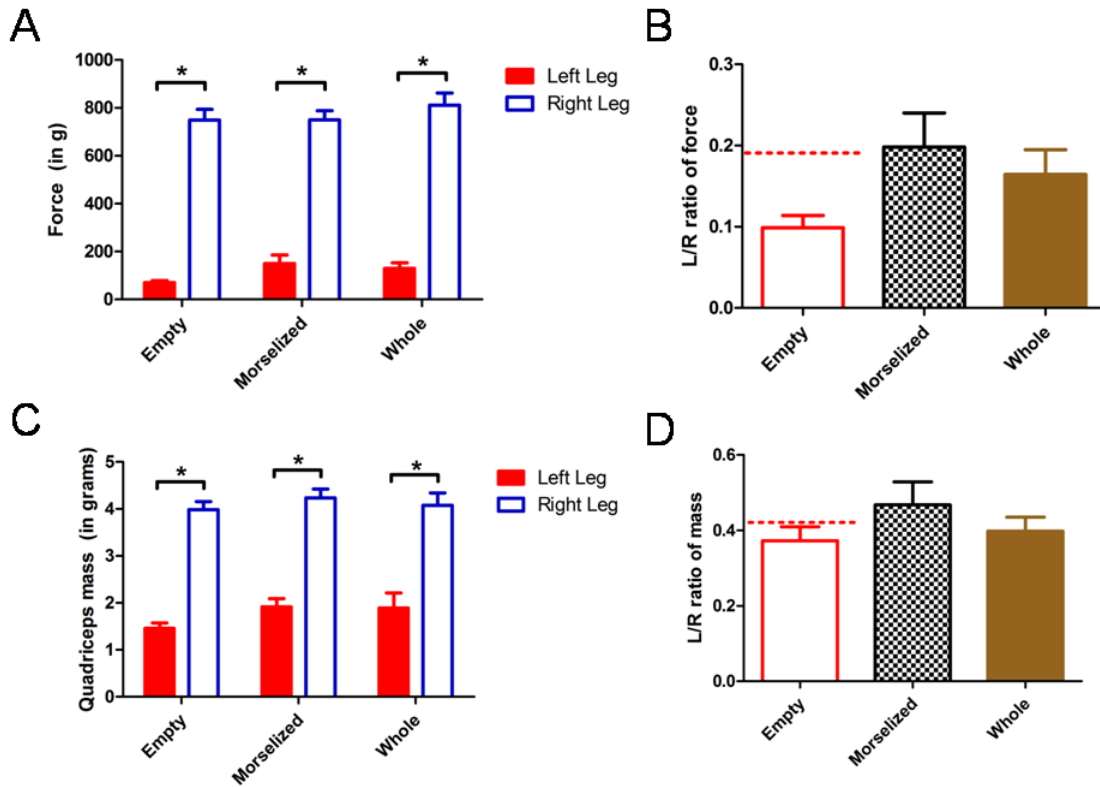


**Figure 17: Muscle Regeneration after Treatment with Muscle Autografts.** Maximal isometric force of the quadriceps was measured at 12 weeks post-injury in a terminal procedure. Panel A shows the maximal force produced by each leg in each group while panel B shows the same data with the left (injured) leg force normalized to the right (contralateral uninjured control) leg force. Panel C shows the wet muscle mass from the quadriceps immediately after euthanasia. Panel D shows the same muscle mass data with the left leg normalized to the right. In Panels B and D, the dotted red line indicates the level of muscle recovery from the initial composite injury study (from **Figure 14**) for comparison. \*  $p < 0.001$  between the indicated groups; empty n=8, morselized n=8, whole n=7.

#### *Early Revascularization of the Composite Defect*

Early revascularization of the defect areas was analyzed using  $\mu$ CT angiography at days 3, 7, and 14 days post-injury. Because this analysis method is terminal, these measurements are not longitudinal and represent results from different animals at

different time points. The bone injury group had a higher thigh vascular volume early on at days 3 and 7 compared to contralateral control whereas the composite group was not significantly different from control. By day 14, vascular volume in both injury groups had increased from day 7 and were both significantly greater than the contralateral control leg (Figure 18A). Representative images of the vasculature in the thigh (within the defect area) show this difference is mainly from the surrounding muscle rather than in the bone defect itself (Figure 18B).

By examining the number of voxels within each diameter bin, we can determine the vessel size profile in either the thigh or the bone (Figure 19). At days 3 and 7, we see that the bone defect only group has more voxel counts in smaller diameter bins in the thigh compared to the composite groups, though there are no significant differences between the two groups. At day 7, there seems to be more smaller sized vessels (<400 $\mu$ m) in the bone defect group (not significant). Representative images of the vessels within the bone defect in both groups clearly shows that vessels do not grow through the PCL nanofiber mesh, as there is a clear empty space where the mesh resides (Figure 20). However, at distinct points in the mesh, vessels are seen to cross the mesh and link the bone defect region to the surrounding muscle. These points likely correspond to the 1-mm macropores present on the mesh.

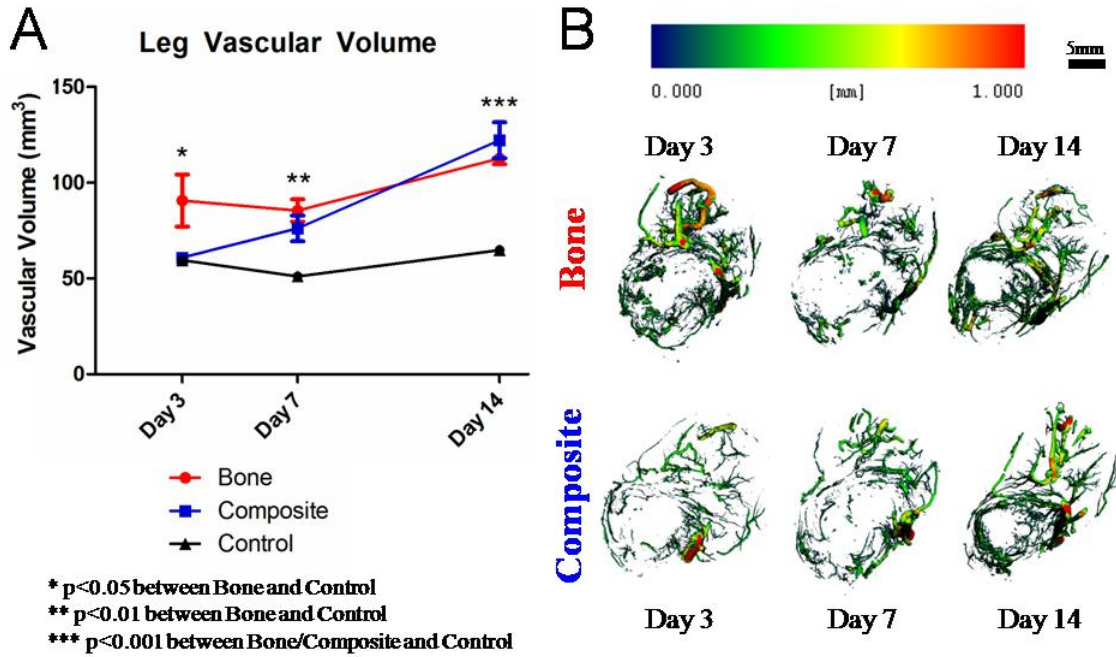


**Figure 18: Early revascularization of the Thigh within the Defect Areas.**  $\mu$ CT angiography analysis showed that the bone only group had a significantly higher leg (thigh) vascular volume compared to contralateral uninjured control while the composite group was not significantly different from control (Panel A). Panel B shows representative images of the vasculature. Heat map represents vessel diameter. \*  $p < 0.05$  between Bone and Control. \*\*  $p < 0.01$  between Bone and Control. \*\*\*  $p < 0.001$  between Bone/Composite and Control.

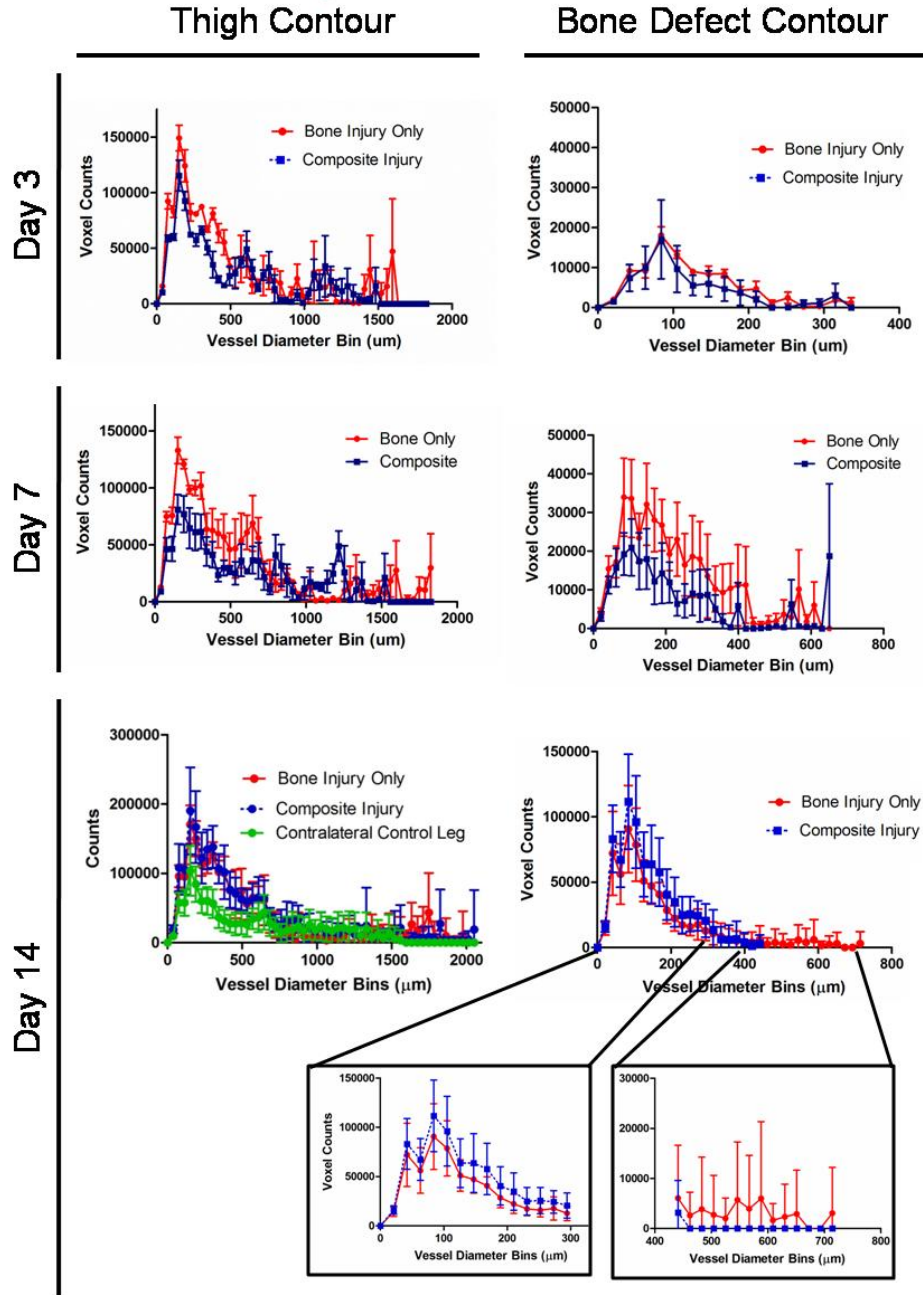


**Figure 19: Vessel Diameter Distribution at Days 3, 7, and 14.** Vessel diameter distributions at day 3 were similar between the two groups in the thigh and bone defect regions. However, by day 7, the bone injury group had more small blood vessels in both thigh and bone defect area as compared to the composite injury group. At 14 days, the composite injury group did not have any blood vessels within the bone defect area with diameters greater than 450 microns whereas the bone injury group had vessels up to 700 microns in diameter (see insets).

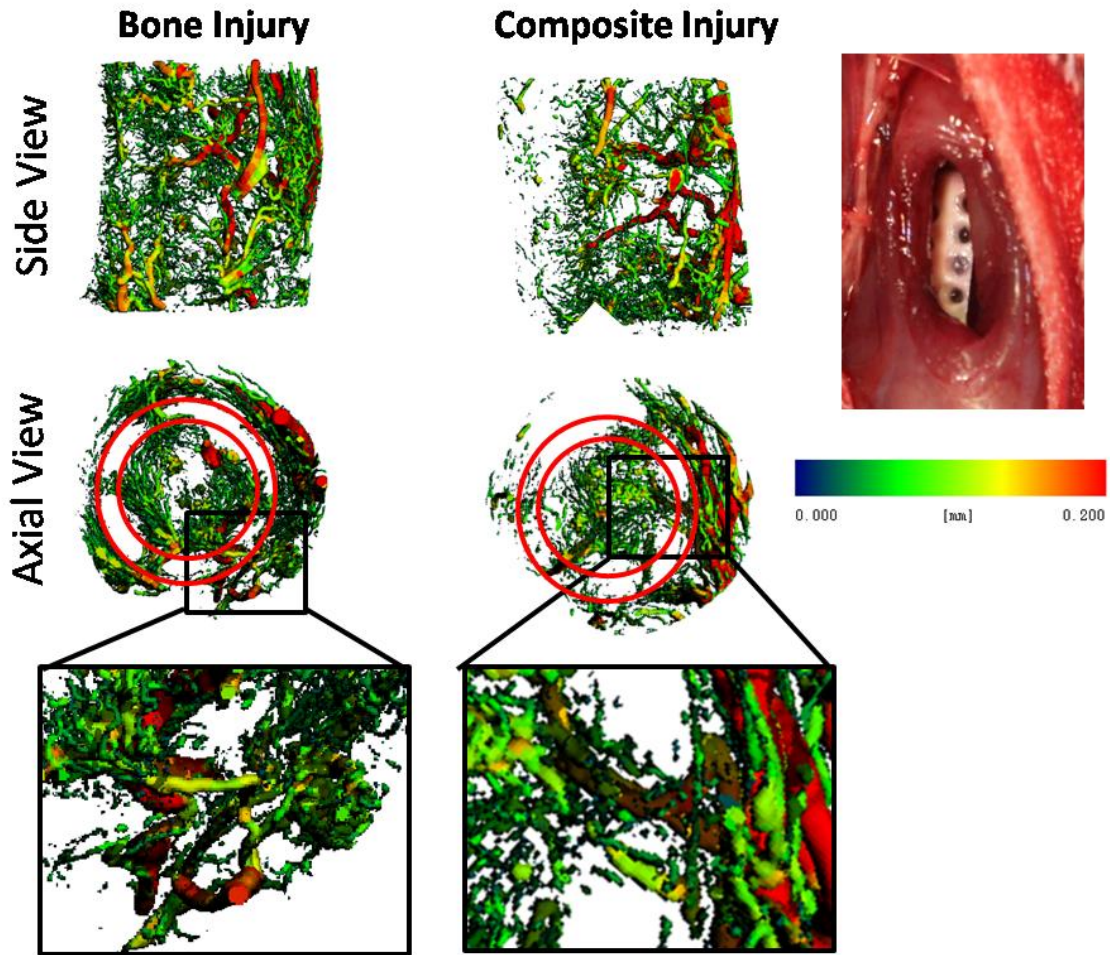


**Figure 20: Representative Vessel Images within the Bone Defect Area at Day 14.** The location of the mesh is shown by the red concentric circles in the axial view of both injury groups. Insets show vessels crossing the mesh itself at very specific points, which correspond to the 1-mm macropores present on the mesh, as seen in the surgical image (top right). Heat map represents vessel diameter.

#### 4.5 Discussion

Traumatic injuries that create large bone defects often include damage to the surrounding soft tissues. Modern clinical techniques have improved the rates of success in limb salvage; however, patients still require repeated hospitalizations for multiple surgeries and complications during the healing process, such as non-union or infection, are common [126, 127, 129]. Even when limb salvage is successful, patients are often left with large functional deficits. The complexity, severity, and loss of limb function

associated with these injuries are not represented by current pre-clinical animal models limiting the utility of these models to test the efficacy of tissue engineered interventions. In this study, we developed a challenging rat model of composite bone and muscle injury by combining a critically sized segmental bone defect model with an adjacent volumetric muscle defect. We then tested the efficacy of a hybrid rhBMP-2 delivery system to regenerate bone and restore limb function.

Pre-clinical animal models of composite injury have previously been limited to lower limb tibial fractures and thus have lacked the capability to assess tissue engineering interventions for multi-tissue limb reconstruction. In this study, we incorporated a well-established, larger than critically sized, segmental bone defect in the femur of a rat. The 8 mm defect used in this model is 60% larger than the necessary critical size, 5 mm, and provides a more challenging regenerative environment; smaller defects could also be combined with an adjacent volumetric muscle injury, and would provide valuable information on the relative importance of defect size (surface area in contact between the bone and muscle) and insight into potential mechanisms of interaction. We have previously demonstrated the efficacy of a sustained release, hybrid rhBMP-2 delivery system, showing consistent bridging of the bone defect with doses of rhBMP-2 as low as 1.0  $\mu\text{g}$  [150]. This system previously outperformed the clinical gold standard for rhBMP-2 delivery, absorbable collagen sponge. Furthermore, the dose used was at the low end of doses commonly reported in similar rat models, which typically range from 2  $\mu\text{g}$  to 20  $\mu\text{g}$  [10, 150-152, 156-160]. Consistent with previously published data, the current study showed that the hybrid rhBMP-2 delivery system promoted consistent bone bridging in the bone-only injury model [150]. At 12 weeks, animals in the composite injury group

had significantly attenuated rhBMP-2 mediated bone regeneration compared to the bone injury only group, both in terms of mineralized matrix volume and mechanical strength. In this new composite injury model, which utilizes a segmental bone defect, it was demonstrated that a healing dose of rhBMP-2 sufficient to bridge a large bone defect, failed to promote regeneration when challenged with a concomitant volumetric muscle injury.

The surrounding soft tissue may be expected to play a larger role in the healing of a femoral segmental bone defect compared to the previously used tibial fracture. This may simply be due to the relative distance of the defect region to the muscle as opposed to the periosteum. Fractures primarily heal through endochondral bone repair, a process largely directed by the periosteum [161-164]. The contribution of muscle derived cells to fracture healing was recently demonstrated by tracking muscle derived cells (MyoD-Cre<sup>+</sup>) [145]. After a closed fracture very few muscle derived cells were present in the fracture callus, however, after an open fracture with the adjacent periosteum denuded, there was a substantial population of muscle derived cells in the callus, fracture gap and pericortical bone [145]. This study speculated that the periosteum is sufficient for fracture healing, and when present, other sources for osteoprogenitor cells are not necessary. In critically sized segmental defects, the periosteum is not sufficient to direct healing and the natural healing progression will instead cap off the cortical bone ends. During rhBMP-2 mediated healing of segmental defects the relative contribution of various cell sources is unknown; however, new models, like the one presented in this study, will provide tools to address these gaps in the current understanding of bone regeneration.

The deleterious effects of concomitant muscle injury on bone regeneration may be attributable to numerous potential mechanisms which have not yet been fully elucidated. One potential mechanism may be a diminished blood supply, which has been shown to be a risk factor for successful healing of a bone defect[165]. The large volumetric muscle defect was from a highly vascularized region of tissue. Beyond, simply a loss in normal blood supply, there may be hyperemia through the collateral network immediately following the bone defect injury. This altered blood supply (whether normal or hyperemic)in the muscle defect animals may produce changes in nutrient and waste exchange, inflammation, circulating stem cell recruitment, and ultimately revascularization of the defect. Another potential mechanism may be that the loss of muscle volume removes a source for resident muscle stem cells and myokines (including IGF-1, FGF-2, or TGF- $\beta$ ) which may contribute locally to bone regeneration. While these factors and cells are key components to muscle regeneration they have also been shown to have osteogenic capabilities [137, 142-144].There is also an increasing body of literature that suggests that muscle may act systemically on other organs, potentially through neural feedback or endocrine type mechanisms[166, 167]. Studies on injury, hindlimb unloading, and paralysis implicate both systemic and local roles for muscle in bone homeostasis, though the exact mechanisms are still unclear[166, 168, 169]. Restoration of a vascular supply, muscle derived stem cells, or growth factors all may be targets for tissue engineering interventions of composite injuries. An improved understanding of the mechanisms and timing of bone, muscle, and vasculature interactions involved in tissue regeneration will be valuable to inform the development of multi-tissue interventions.

Composite injury animals had impaired muscle regeneration in addition to the impaired bone regeneration. These animals showed decreased muscle mass and impaired muscle function compared to single tissue injury animals. The decrease in mass may be attributable to a loss in volume from the defect as well as potential muscle atrophy. In the bone defect only animals there is a significant decrease in muscle mass potentially as a result of decreased limb function or the presence and volume of the fixation plate. The decreased muscle mass may account for some of the decreased function; however, in all three groups, the relative proportion of muscle mass lost was less than the relative decrease in muscle strength. This suggests that there is also a loss of functional capacity which may be due to poor muscle structure. Histology of muscle from the composite injury animals showed poorly regenerated tissue with fibrosis and lipid deposits. The local fibrotic response in the muscle tissue can result in increased local concentrations of fibrotic factors, such as TGF- $\beta$ , tissue inhibitor of matrix metalloproteinase (TIMP), and chemokine ligand 17 [47, 170]. These factors may reach the bone defect region and could direct a fibrotic response instead of bone regeneration [170]. Additionally, the impaired muscle function may have an effect on the bone regeneration as muscle atrophy and wasting are both associated with negative changes in bone structure and osteoporosis [166, 171, 172]. The bone defect itself, however, is largely stress shielded by fixation hardware, precluding a direct mechanical loading effect.

Composite injury animals showed functional gait deficits in injured limbs compared with single tissue injury animals at 2 weeks. By 4 weeks, composite injury animals had deficits that were comparable to single tissue injury deficits. These functional deficits could have a direct effect on limb usage and ultimately tissue

regeneration. A limitation of this technique is that these measurements assess functional gait ability (i.e. how well the animal can walk) at a given time but are not necessarily indicative of daily limb usage. It is, however, a quantitative functional metric with clear clinical relevance. No established model has yet proven to be an effective predictor for clinical translation of multi-tissue interventional strategies; however, this composite injury model provides a challenging regenerative environment, rigorous and quantitative analytical methods, and clinically relevant functional deficits. This model, therefore, has unique potential to discriminate between new technologies.

There is currently no accepted standard for treatment of composite injuries, though debridement of necrotic tissue, prevention of infection, muscle flap coverage, and bone grafting are most common [130, 173, 174]. While initial assessment of healing using a muscle autograft will be important, additional strategies could utilize novel grafting materials such as decellularized muscle tissue, which could be combined with controlled spatiotemporal growth factor delivery or progenitor cell delivery. A key component to the long term clinical treatment of composite injuries is rehabilitation and physical loading (physical therapy); however, this is often neglected in animal models. Recently, we demonstrated that properly applied mechanical loading to a bone defect could stimulate vascular remodeling and enhance bone regeneration [153, 175]. The muscle atrophy and functional deficits observed in this study suggest that a properly timed intervention providing physical stimulus to the injured limb may have an effect on revascularization and tissue regeneration.

In order to further characterize the regenerative cross-talk between the muscle and the bone, cells/ECM was analyzed to determine its role in the healing of this model. We

delivered an autograft, either whole or morselized, into the quadriceps defect site in the composite defect. Previously, it has been shown the morselized autograft could aid in the healing of the VML, possibly due to the cells, ECM, and factors present in the graft [41, 124]. However, in our quadriceps VML model, the morselized autograft did not significantly influence the functional outcome [176]. Similarly, our treatment of the quadriceps in the composite model did not result in a functional improvement at 12 weeks post-injury. Because the autograft was delivered immediately into the defect space after isolation, it was not possible to characterize the types of cells and ECM present in the autograft. This limitation in the autograft treatment prevents a detailed scrutiny of what may or may not be present in the graft that could aid in the healing of the defect. Though the presence of adult muscle stem cells has been demonstrated to aid in muscle regeneration [177, 178], it is difficult to assess exactly how many stem cells were present in the autograft and if they survived the transplantation. Additionally, because microsurgery was not performed to ensure perfusion of the autograft tissue, it is possible that this graft was not viable after implantation. While the autograft tissue may contain multipotent progenitors that could aid in healing as previously shown [179], damaged and devitalized muscle tissue is usually debrided in order to prevent infection and minimize ectopic bone formation in the traumatized muscle [180, 181]. Leaving dying tissue in the body may result in a heightened inflammatory response by the body that may preclude any positive regenerative effects that the autograft may have [182, 183]. Thus, our autograft treatment may have not had a therapeutic effect and therefore did not positively influence the bone healing.

Our investigation into the early revascularization of the defect space yielded interesting results that may have implications in the treatment of composite defects. Vascularity is known to play a large role in bone repair [184], and vascularized muscle flap coverage is often used in the clinic to cover bony defects in order to reduce infection rates as well as provide a vascular supply for bone healing [185-188]. Our early revascularization data support these claims that vascularization from the muscle is important for vascularization of the bone by demonstrating the lack of larger blood vessels within the bone defect region in the composite injury group that had reduced vasculature from the surrounding muscle. Our results suggest that if we can provide early revascularization within the composite defect, we can improve bone regeneration. This specific strategy will be investigated in Chapter 5 of this dissertation.

This pre-clinical model uniquely combined a segmental bone defect with a volumetric muscle injury. The results showed that the increased challenge of concomitant muscle injury impaired rhBMP-2 mediated bone regeneration. Impaired limb and muscle function were also found, which are similar to clinical observations after severe composite tissue injury. We used this model to investigate some possible causes for the attenuated bone healing and found that early revascularization may play a role. This composite injury animal model provides a platform with which to analyze the mechanistic relationship of regeneration between tissues as well as test the efficacy of tissue engineering approaches to promote healing in multiple tissues. Such interventions may minimize complications and the number of surgical procedures needed for limb salvage operations, ultimately improving clinical outcomes.

## **CHAPTER 5 Aim 2: Development and Characterization of the Hamstrings VML Model**

### **5.1 Abstract**

Volumetric muscle loss injuries are a challenge to treat in the clinic; treatment options are limited, and pain and disability are reported a decade after injury. We have previously established a VML in the quadriceps of a rat in which a large portion of muscle was resected; however, possible nerve or vessel damage and damage to four distinct muscles complicate this model and may deter tissue engineering strategies. For this study, we aimed to develop a large VML model (>100mg muscle damage) that can be used to test therapeutics for their muscle regenerative potential quickly and efficiently. We created a 12-mm full-thickness defect in the biceps femoris of a rat and left the defect empty (negative control) or treated with an aligned autograft (positive control). We tracked muscle regeneration with muscle function, biochemical assays of enzymatic activity, and histology up to 8 weeks. Histologically, the negative and positive controls differed greatly in appearance, with a very thin fibrotic tissue forming in the empty defect and a thick tissue with myofibers in the autograft-treated defect. However, muscle force did not show a significant difference in function between the two groups, highlighting limitations of muscle function based on the chosen muscle of interest. Micro-CT angiography showed significant differences in vascular response between the negative and positive controls for muscle regeneration. This model serves as a platform for testing tissue engineering strategies and provides insights about the different healing responses of varying degrees of muscle regeneration.

### **5.2 Introduction**

Penetrating soft-tissue wounds, the most prevalent of combat extremity injuries, often involve extensive loss of skeletal muscle, also known as volumetric muscle loss

(VML). These large injuries are first irrigated and debrided to remove necrotic tissues and reduce infections, after which a muscle flap can be used to cover the wound in order to increase blood flow in the region as well as to reduce the likelihood of further infections [17]. Even with treatment of the wound, VML injuries are associated with poor long-term outcomes, including motor disability and pain [22, 102]. In light of poor functional outcomes, the field of tissue engineering of VML in preclinical models has come to fruition in the last decade.

Various VML models have been developed within the last half decade in order to test different therapeutics [43-46, 72]. While these strategies have contributed some success to the healing of muscle, the muscle defects themselves tend to be small (10-20% of whole muscle weight) and are not a full-thickness defect that further complicates the healing response. In order to capture the severity of clinical VML, our lab has previously developed a VML model in the quadriceps of the rat in which an autograft treatment does not contribute to functional recovery [176]. This model recapitulates complications in the clinic in which muscle flaps, the gold standard treatment for large defects in the muscle, may necrotize and require a second reconstructive surgery.

Though our quadriceps VML is a large defect that emulates clinical VML challenges and can be consistently produced, this model has limitations in its use as a tissue engineering test bed. First, the severity and size of the defect and hematomas in the days after the surgery suggest that major damage was done to nerves or vasculature in this model. While this may emulate the damage seen in the clinic, these injuries add a level of complexity to the healing of the defect. Tissue engineering strategies that have potential to regenerate muscle may not be able to overcome these other injuries to

nervous and vascular tissues. A second limitation lies in the fact that this injury is a full-thickness injury that spans all four muscles in the quadriceps. Each of these four muscles are aligned differently, which makes the creation of a structured construct more challenging. Additionally, the quadriceps muscle itself folds in on itself during healing, and the defect space itself is hard to discern within a week after injury.

Because of these complications in our quadriceps VML model for testing tissue engineering strategies, **our objective was to develop a simpler VML model that can be used to test therapeutics for their muscle regenerative potential quickly and efficiently.** To do this, we decided to set the following design criteria. First, the muscle defect must not damage any major nerves or vessels so that the model will not be complicated by injury to these other tissues. Second, the muscle defect should ideally be a full-thickness defect created in one muscle in which the myofibers are approximately parallel. We posit that this will allow for ease of alignment should the therapeutic aim to reproduce muscle structure. Third, the empty defect should allow for minimal muscle regeneration while the autograft-treated defect should result in some muscle regeneration. This would allow for the empty defect to serve as a negative control for muscle regeneration and the autograft-treated defect to serve as a positive control.

The muscle we decided to choose for this VML model was the biceps femoris, a muscle group that spans from the hip to the tibia in the rat. The biceps femoris is a muscle that is part of the hamstrings, which also includes the semitendinosus and semimembranosus muscles and serves as a knee flexor. This muscle meets the first criterion, where we can confirm that the nearby major nerve (tibial nerve) is not damaged upon defect formation. Additionally, we did not note a high rate of hematoma formation

when the defect was created. This muscle meets the second criterion in that the defect would be in one muscle, and the muscle fibers are mostly parallel despite their fanning out from the hip inserts to the tibial insert that spans the entire length of the tibia. The muscle is distinctly separate from the surrounding muscles, and a full-thickness defect can be created in the biceps femoris easily. Additionally, the biceps femoris offer the advantage of being superficial, allowing the creation of the defect with very little damage to any other muscles. The biceps femoris is also a thin muscle, ranging from 1 to 5 millimeters thickness, depending on the location of the tissue. This reduces the complexity of the defect, and flatter constructs can be tested in this model prior to scaling the construct into a more three-dimensional structure, which has its own challenges such as perfusion for survival at the construct center.

It remains to be seen whether the biceps femoris will satisfy the third criterion, in which the empty defect and autograft-treated defect could serve as the negative and positive controls respectively. Thus, the question in this study is to determine the muscle regeneration in empty and autograft-treated biceps femoris VML. The *hypothesis is that the empty treated biceps femoris will result in minimal muscle regeneration while the autograft-treated biceps femoris would result in regenerated muscle with little fibrosis.*

### **5.3 Materials/Methods**

#### *Surgical Procedure*

Bilateral surgeries were performed on 13-week female Sprague-Dawley rats. To create the defect, a plastic spatula was inserted between the biceps femoris and the deeper hamstrings muscles after blunt dissection, carefully avoiding the sciatic nerve. A 12-mm biopsy punch was used to create a full-thickness muscle defect with the plastic spatula serving as a firm base for the biopsy punch and to protect underlying tissue. The defect

was either left empty (with 4 suture markers placed near the defect margins) or treated with an autograft (with the cut tissue attached back on the defect with 8 sutures). Animals were euthanized at 2, 4, 6, and 8 weeks post-injury.

#### *Muscle Force Measurements*

A custom muscle force apparatus was used to measure the hamstrings force *in vivo* at 2 and 4 weeks post-injury. All measurements were made under isoflurane anesthesia during a terminal procedure immediately prior to euthanasia. A 1-cm long incision was made through the skin exposing the anterior biceps femoris and gluteus maximus. The tibial branch of the sciatic nerve was carefully isolated, and a nerve cuff was placed securely on this nerve branch. The knee was stabilized with a needle passed through the distal femur, anchoring it to a cork board platform onto which the animal was securely fixed for the duration of these tests. The animal was placed in a prone position, and the knee and base of the tail were securely anchored into the cork board with needles. The ankle was secured to a force transducer (Isometric Transducer Model No. 60-2996, Harvard Apparatus) using a suture. A nerve cuff implanted on the tibial branch of the sciatic nerve allowed electrical stimulation and subsequent contraction of the hamstrings muscle with the use a stimulator (GRASS S11 Stimulator, Grass Technologies). Stimulator pulse duration, frequency, and train duration were set to 0.5 ms, 200 Hz, and 500 ms, respectively; these settings elicited maximal isometric tetanic force as determined in a pilot study. Hamstrings muscle torque was determined by multiplying the maximal isometric tetanic force by the moment arm length.

#### *Micro-CT Angiography*

At 2 and 4 weeks post-injury, contrast agent-enhanced micro-CT angiography was performed terminally on animals from both groups (n=6). The technique has been previously described in detail [153-155]. Briefly, 0.9% salt solution (physiological saline) containing 0.4% papaverine hydrochloride (Sigma-Aldrich) was perfused through the vasculature to clear the blood vessels. The vasculature was then perfusion fixed with 10% neutral buffered formalin, rinsed with physiological saline, and injected with lead chromate-based radioopaque contrast agent (2 parts microfil MV-22: 1 part diluent, Flow Tech). Samples were stored at 4°C overnight to allow for polymerization of the contrast agent. The biceps femoris was excised, and the defect region (marked with sutures) was isolated. For contralateral control legs, a 12-mm biopsy punch was used to remove a similarly-sized piece of uninjured muscle.

Excised samples were further fixed for 48 hours then stored in PBS. Samples were scanned in the micro-CT (vivaCT 40, Scanco Medical) with a resolution of 21 $\mu$ m voxel size. All scans were performed with an applied electroc potential of 55 kVp and a current of 109  $\mu$ A. The VOI consisted of a cylindrical volume 14.7mm in diameter that spanned the full thickness of the biceps femoris. A global threshold was applied for segmentation of vasculature, and a Gaussian low-pass filter was used to suppress noise ( $\sigma = 0.8$ , support = 1).

### *Muscle Homogenization*

At 2, 4, 6, and 8 weeks, animals were euthanized (n=6 per time point per group), and the defect area was harvested using a 12-mm biopsy punch as during the initial surgery. The harvested tissue was immediately weighed, flash-frozen in liquid nitrogen, and stored at -80°C until homogenization.

For homogenization, tissues were removed from -80°C, cut with a razor blade into small pieces, then manually homogenized with a tissue grinder (Dual<sup>TM</sup> tissue grinders, Kimble-Chase Kontes). Samples were homogenized in 100mM potassium phosphate buffer (pH 7.4) at a ratio of 400µL of buffer for every 50mg of tissue. The homogenate was then separated into 5 equal volumes for analysis of creatine kinase activity, citrate synthase activity, and quantification of myosin/actin, triglycerides (fat), and hydroxyproline (collagen) content. Homogenates were frozen and stored at -80°C.

#### *Creatine Kinase (CK) Activity*

The activity of creatine kinase, a metabolic enzyme that is specifically present in tissues with high consumption of energy such as skeletal muscle, was measured to determine the extent of skeletal muscle regeneration. A creatine kinase activity assay kit was used (Cat# MAK116, Sigma-Aldrich). Homogenate samples were centrifuged at 10,000 x g for 15 minutes, and the cleared supernatant was used for the assay. For each assay, reagent consisting of 100 µL assay buffer, 10 µL substrate solution, and 1 µL of enzyme mix were used with 10 µL of sample. Blank (110 µL of water) and calibrator (100 µL water with 10 µL calibrator) wells were used per plate. Samples were mixed with the assay reagent in a UV-96-well plate and incubated at 37°C for 20 minutes. After 20 minutes, the initial absorbance was read at 340nm. The plate was further incubated at 37°C for an additional 20 minutes after which a final absorbance measure was read at 340nm.

#### *Citrate Synthase Activity*

Muscle homogenates were freeze-thawed 3 times and diluted (1:7) in 100mM Tris buffer (pH 8.0) prior to running the assay. 5.18µL of the diluted sample was added to the

143.59  $\mu\text{L}$  of 100mM Tris buffer, 20.5  $\mu\text{L}$  1.0mM 5,5'-dithio-bis(2-nitrobenzoic acid) (DTNB) in 100mM Tris buffer, and 10.25  $\mu\text{L}$  3mM acetyl CoA in 100mM Tris buffer. The assay reaction was started by adding 20.5  $\mu\text{L}$  of 5mM oxaloacetic acid in 100mM Tris buffer. Solutions were warmed up to 30°C prior to the assay, and the assay was carried out at 30°C. The spectrophotometer (BioTek PowerWave XS) was programmed to delay for 2 minutes prior to running a kinetic program to take OD readings at 412nm every 15 seconds for 3 minutes. The CS activity was calculated using the following equation:

$$\text{Units} \left( \frac{\frac{\mu\text{mol}}{\text{min}}}{\text{g wet wt}} \right) = \frac{\frac{\Delta A}{\text{min}} * V_{\text{rxn}} * \text{dil}}{\varepsilon * L * V_{\text{sample}}} * \frac{(V_{\text{buffer}} + \frac{\text{wt}_{\text{muscle}}}{\delta})}{\text{wt}_{\text{muscle}}}$$

where  $\Delta A/\text{min}$  is the change in absorbance,  $V_{\text{rxn}}$  is the volume of the assay reaction (0.2mL), dil is the dilution factor (7),  $\varepsilon$  is the extinction coefficient ( $13.6 \text{ mmol}^{-1}\text{cm}^{-1}$ ), L is the light path length (0.552cm for 0.2mL in a 96-well plate),  $V_{\text{sample}}$  is the volume of the sample used in the assay,  $V_{\text{buffer}}$  is the volume of homogenizing buffer,  $\text{wt}_{\text{muscle}}$  is the weight of the homogenized muscle in g, and  $\delta$  is the density of muscle (1.06g/mL).

#### *MHC/Actin Quantification*

Samples were centrifuged at 5,000 x g for 15 minutes, and the supernatant was removed. The pellets were resuspended in 400 $\mu\text{L}$  of 100mM potassium chloride and 20mM imidazole (pH 7.0). 10 $\mu\text{g}$  of the sample was run in a NuPAGE 4-12% Bis-Tris precast gel (Life Technologies), and the gels were dyed in a Coomassie Blue solution for 1 hour. Gels were destained overnight and imaged with Bio-Rad Gel Doc XR.

#### *Histology*

Transverse muscle sections taken approximately from the middle of the muscle defect were stained with H&E and Masson's trichrome for morphological analysis. Representative histology was performed at 2, 4, 6, and 8 weeks post-injury.

### *Statistics*

As none of the measurements were longitudinal (i.e. made from the same animal across time), the independent samples were tested for statistically significant differences with two-way ANOVAs (time x treatment) with consequent pair-wise comparisons using the Šídák method.

## **5.4 Results**

### *Enzyme Activities*

Creatine kinase (CK) and citrate synthase (CS) activities were determined as a measure of metabolic activity. While creatine kinase is an enzyme that is predominantly present in skeletal muscle, citrate synthase is an important enzyme within the citric acid cycle and is present within all cells, though activity will be higher in tissues with higher metabolic activity. Creatine kinase activity was measured to be at a consistent level for control right legs, and both injured groups (autograft-treated and empty) resulted in a significant decrease of CK activity (Figure 21). On the other hand, citrate synthase activity was significantly lower in both injured groups only at 2 weeks post-injury. At 4, 6, and 8 weeks post-injury, the autograft-treated group had a significantly higher citrate synthase activity compared to the empty defect group and comparable CS activity as the uninjured control group.

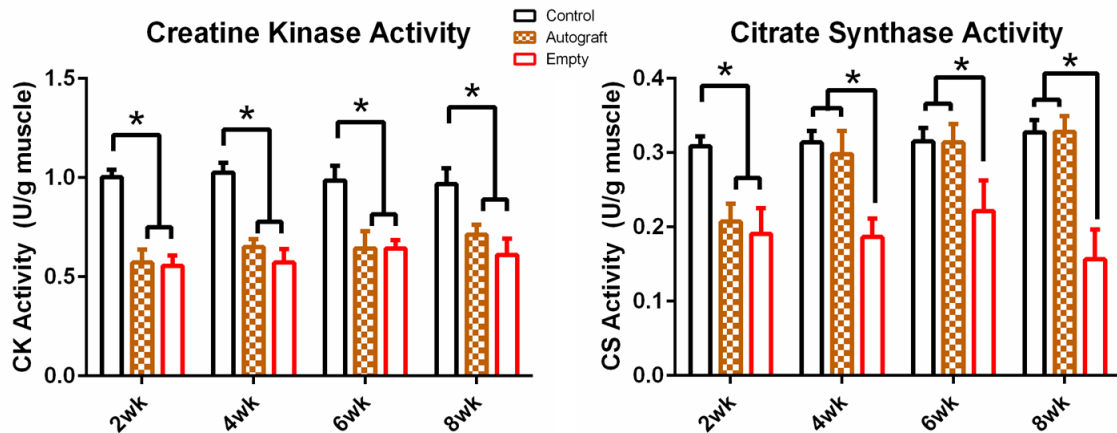


**Figure 21: Enzyme Activities of Defect Tissue after Biceps Femoris VML.** Creatine kinase activity of the defect area was consistent among the right leg controls, and the autograft-treated and empty defect groups had significant lower CK activity than the right leg controls. Citrate synthase activity was also consistent among the right leg controls. Both the empty defect and autograft-treated group had significantly lower CS activities compared to uninjured controls at 2 weeks post-injury. The autograft-treated group had an increased CS activity from 4 weeks post-injury onwards, with significantly higher CS activity compared to empty defects. \* $p < 0.05$ ,  $n = 6$  for autograft-treated and empty groups,  $n = 12$  for contralateral controls.

### *Muscle Functional Outcome*

At 2 and 4 weeks post-injury, the hamstrings muscle maximal tetanic torque was significantly lower in the injured groups (both empty and autograft-treated) as compared to the contralateral control muscles (Figure 22A). Examining the spread of the data, the range of the measured muscle forces from the injured groups spanned about 100 to 150 gram-force (Figure 22B). The uninjured hamstrings muscle produced an average of 250 gram-force. Representative torque curves of the hamstrings functional testing show tetanic stimulation was achieved (Figure 22C & D).

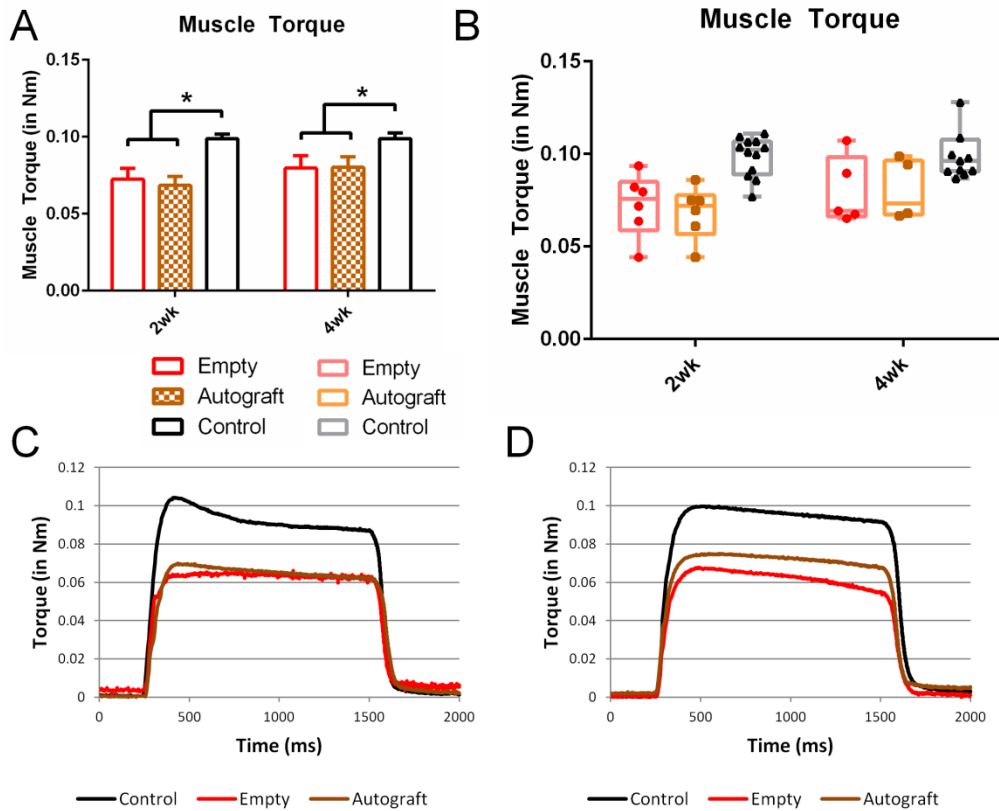


**Figure 22: Hamstrings Muscle Function.** Panel A shows hamstrings torque in the empty and autograft-treated groups were significantly lower than the torque produced by the uninjured contralateral control at 2 weeks post-injury. Panel B shows the spread of the muscle force data (same data as Panel A). Panels C and D show representative torque curves at 2 and 4 weeks post-injury respectively.  $p < 0.05$ ,  $n = 5-6$  per injured group per time point,  $n = 21$  for contralateral controls.

### *Biceps Femoris Revascularization*

Defect site revascularization was found to be significantly higher in both injured groups compared to the uninjured contralateral control (Figure 23). The autograft-treated groups had a significantly higher vascular volume at 2 and 4 weeks post-injury compared to the empty defect group. Representative images show the autograft-treated group had more smaller vessels and slightly thicker large vessels compared to the empty group.

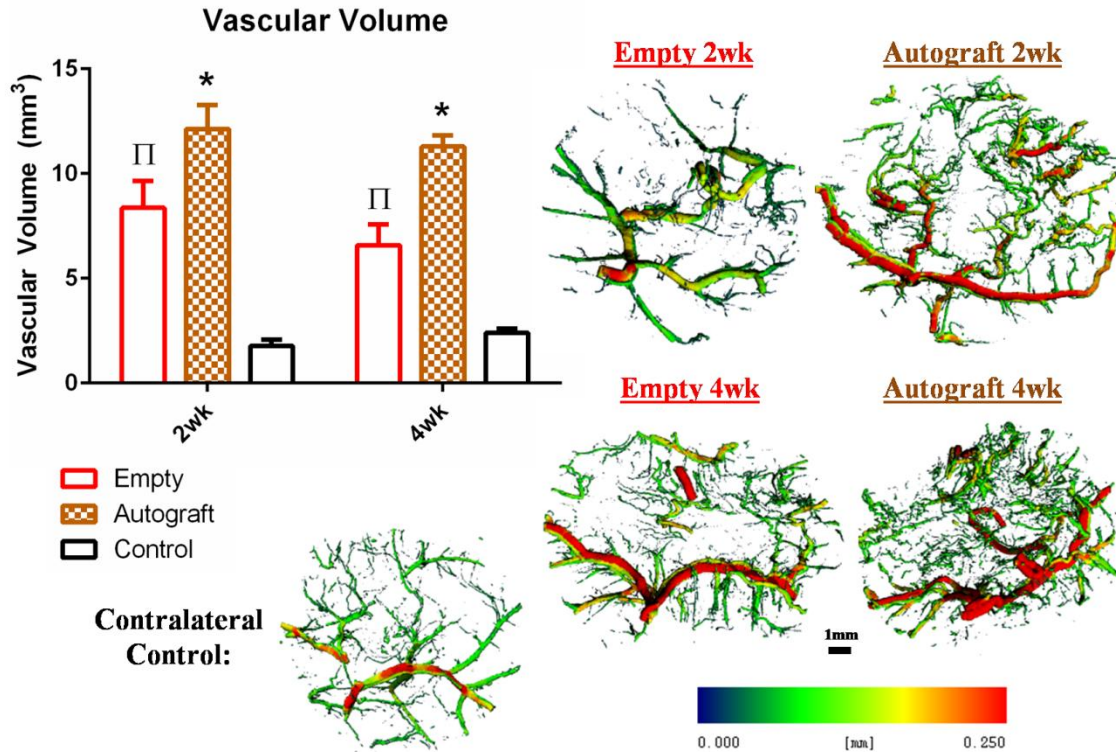


**Figure 23: Defect Revascularization 2 and 4 weeks post-injury.** The revascularization of the defect site in the biceps femoris was determined by micro-CT angiography at 2 and 4 weeks post-injury. The vascular volume was significantly higher in the autograft-treated group compared to the empty defect group at both 2 and 4 weeks post-injury. All injured groups at all time points had a significantly higher vascular volume compared to the uninjured contralateral controls. Representative images of defect vasculature are shown with heat maps showing vessel diameter. \* $p < 0.05$  compared to empty and control. □  $p < 0.05$  compared to control.  $n = 6$  per injured group per time point,  $n = 24$  for contralateral controls.

### *Muscle Histology*

H&E and Masson's trichrome stained sections showed very different healing responses by the empty defect and autograft-treated defect. In the empty defect, a thin connective tissue was left within the defect space with no myofibers present at the center of the defect at 2 weeks post-injury (Figure 24A-D & Figure 25A-D). This minimal regeneration in the empty defect group persisted through to 4 weeks post-injury, in which the tissue at the center of the defect consisted of vascularized fibrotic tissue (Figure 26 A-

D & Figure 27 A-D). At 6 weeks post-injury, the empty defect group was infiltrated by fatty tissue (Figure 28A-D), and at 8 weeks post-injury, the defect area was thin with sparse areas of myofibers (Figure 29A-D). On the other hand, the autograft-treated group had thick tissue at the defect site, with distinct connective tissue deposition around the autograft site at 2-weeks post-injury (Figure 24 E-H & Figure 25 E-H). By 4 weeks post-injury, the autograft-treated group had very little fibrosis and was mostly populated by myofibers (Figure 26 E-H & Figure 27 E-H). At 6 weeks post-injury, the representative autograft-treated section had some fatty infiltrate (Figure 28 E-H), though by 8 weeks, there was no sign of muscle injury in the autograft-treated muscle (Figure 29 E-H).

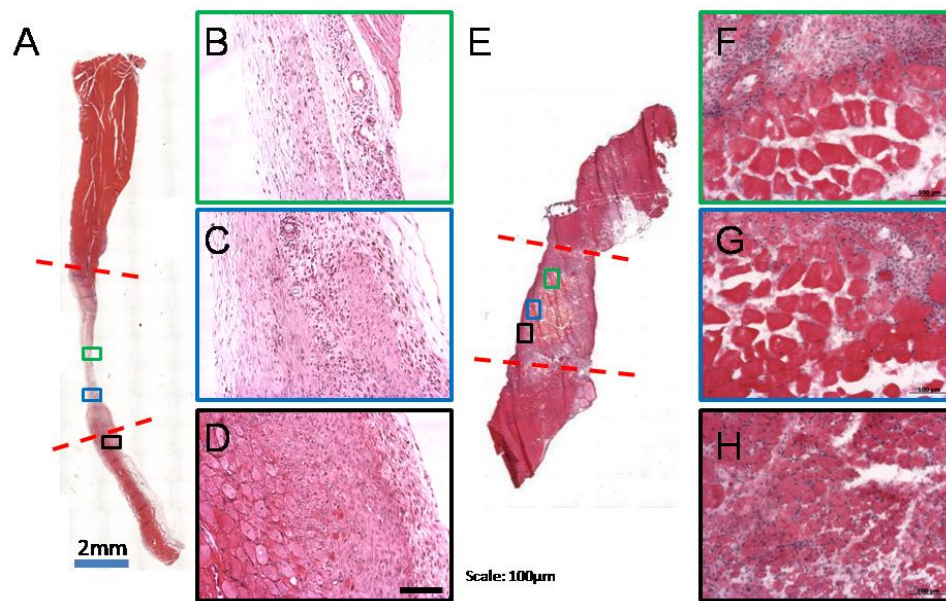


**Figure 24: H&E Histology at 2 weeks post-injury.** Cross-sections of the entire biceps femoris show a thin defect space in the empty defect group (A) and a thick defect area in the autograft-treated group (E). Panels B, C, and D are enlarged images that correspond to the colored blocks in Panel A. Panels F, G, and H are enlarged images that correspond to the colored blocks in Panel E. Red-dotted lines show approximate location of the defect space.

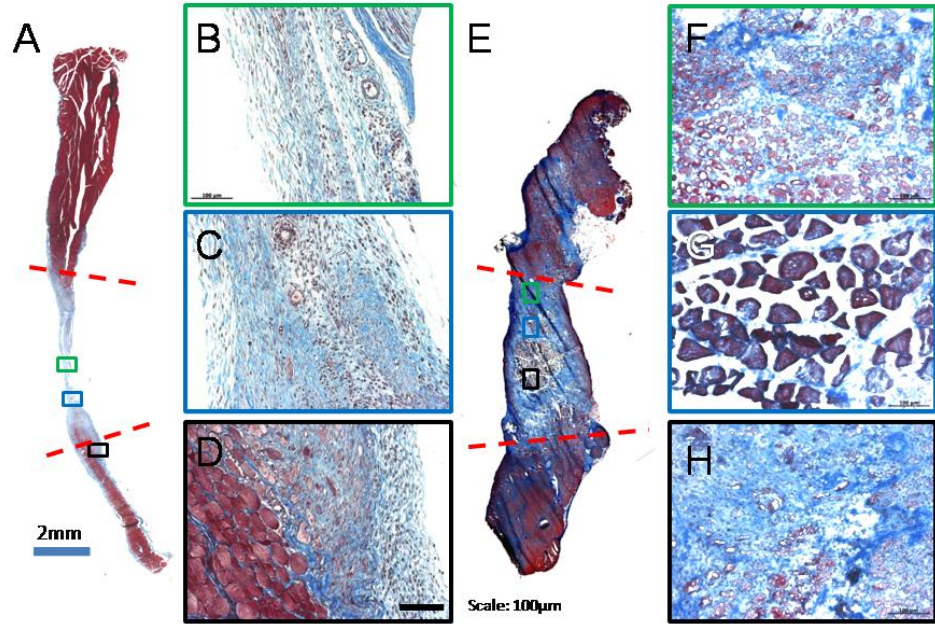


**Figure 25: Masson's Trichrome Histology at 2 weeks post-injury.** Blue staining shows connective tissue (i.e. fibrosis, collagen) while red staining shows muscle cells. A representative muscle from the empty defect group showed mostly connective tissue filling the defect space (A). Panels B, C, and D are enlarged images that correspond to the colored blocks in Panel A. The autograft-treated group showed connective tissue surrounding the autograft (E). Panels F, G, and H are enlarged images that correspond to the colored blocks in Panel E. Red-dotted lines show approximate location of the defect space.

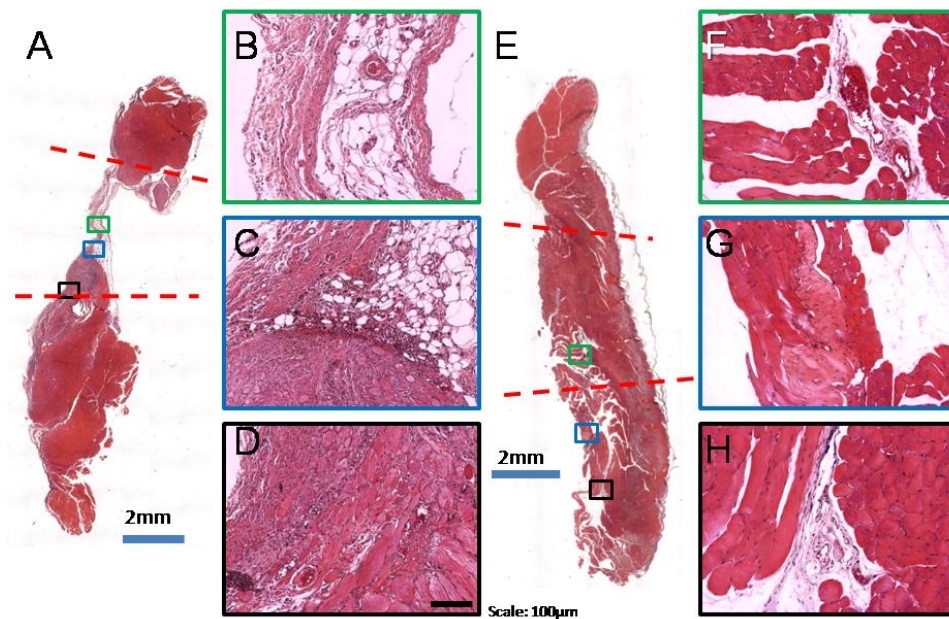


**Figure 26: H&E Histology at 4 weeks post-injury.** The empty defect group showed very little muscle regeneration, with a thin tissue lacking in muscle cells in the center of the defect (A). Panels B, C, and D are enlarged images that correspond to the colored blocks in Panel A. The autograft-treated group showed predominantly regenerated muscle at 4 weeks post-injury (E). Panels F, G, and H are enlarged images that correspond to the colored blocks in Panel E. Red-dotted lines show approximate location of the defect space.

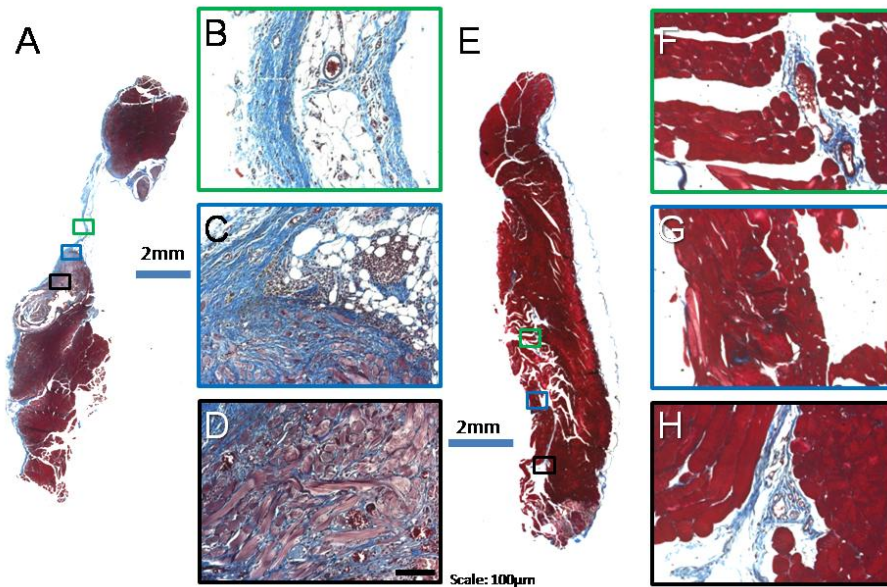


**Figure 27: Masson's Trichrome Histology at 4 weeks post-injury.** Only a thin connective tissue stretched across the defect in the empty defect group, with no signs of muscle fibers in the center (A). Panels B, C, and D are enlarged images that correspond to the colored blocks in Panel A. The autograft-treated group showed very little fibrosis and connective tissue at 4 weeks post-injury (E). Panels F, G, and H are enlarged images that correspond to the colored blocks in Panel E. Red-dotted lines show approximate location of the defect space.

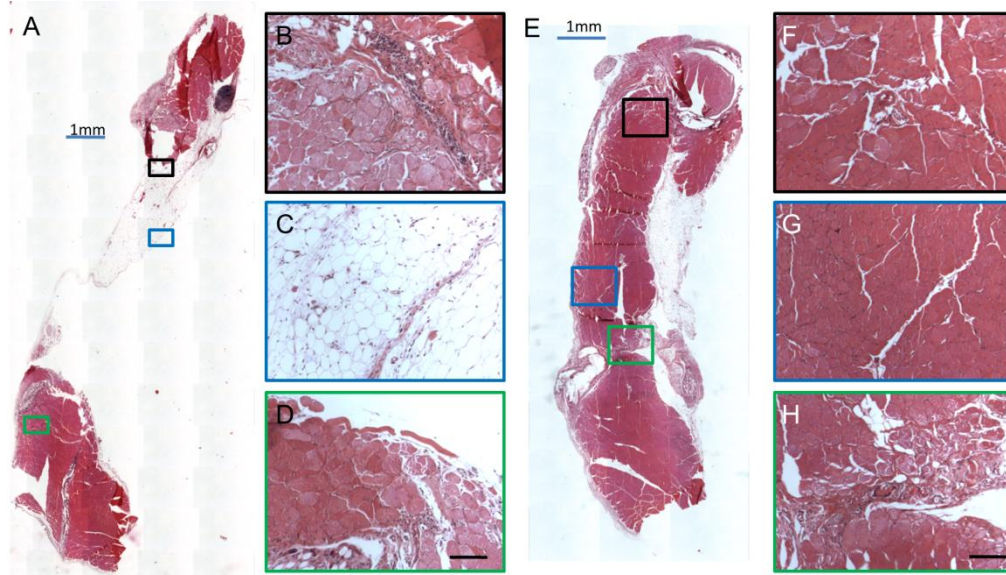


**Figure 28: H&E Histology of Biceps Femoris at 6 weeks post-injury.** The middle of the empty defect at 6 week post-injury was thin with some fatty infiltrate (A). Panels B, C, and D are enlarged images that correspond to the colored blocks in Panel A. The autograft-treated group showed very little fibrosis, with a little bit of fatty infiltrate. (E). Panels F, G, and H are enlarged images that correspond to the colored blocks in Panel E. Red-dotted lines show approximate location of the defect space.

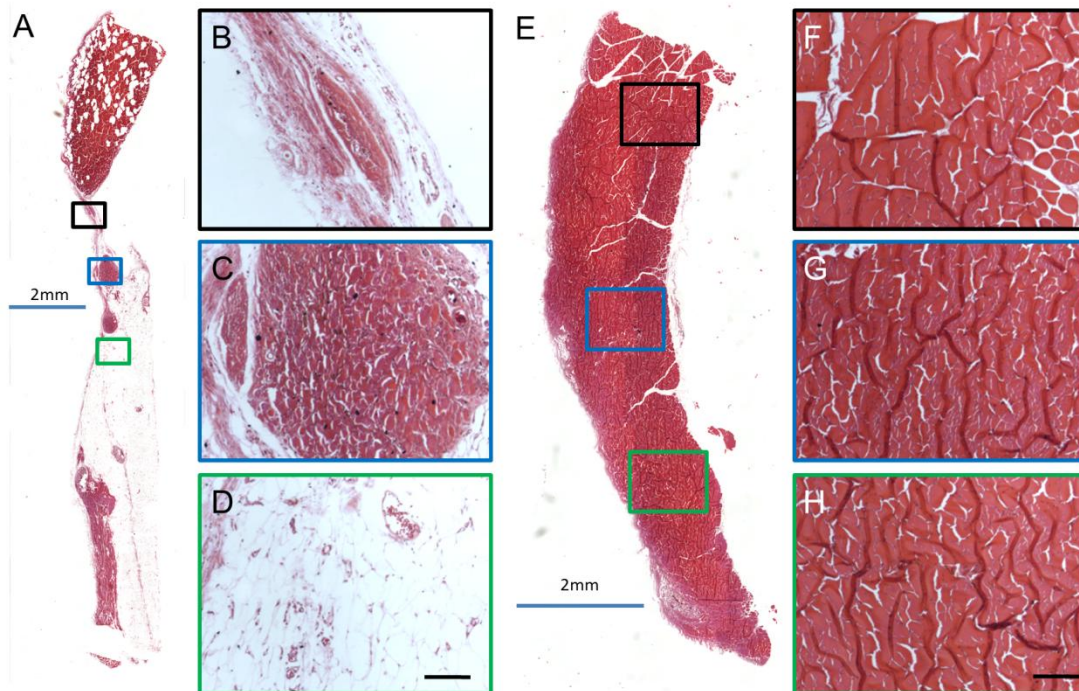


**Figure 29: H&E Histology of Biceps Femoris at 8 weeks post-injury.** The empty defect group had mostly connective and fatty tissue in the center of the defect except for a small area of myofibers in the center (A). Panels B, C, and D are enlarged images that

correspond to the colored blocks in Panel A. The autograft-treated group had no signs of injury at 8 weeks post-injury (E). Panels F, G, and H are enlarged images that correspond to the colored blocks in Panel E. Red-dotted lines show approximate location of the defect space.

## 5.5 Discussion

We have developed the first volumetric muscle loss model in the rat biceps femoris. In this model, the empty defect resulted in a thin connective tissue filling the defect space up to 8 weeks post-injury, serving as a good negative control for muscle regeneration. An autograft-treated defect resulted in thick tissue at the defect site with myofibers and very little fibrosis, serving as a good positive control for muscle regeneration based on histology. Additionally, this model has the added benefits of ease of access to the muscle defect site and the ability to test thinner constructs, as this defect, though full-thickness, is within a 1-5mm thick muscle. We present this model as a good test bed for tissue engineering strategies focused on muscle regeneration.

This empty VML defect is unique in that it has a distinct lack of muscle regeneration in the center of the defect. Many VML models involve damage to only half a muscle or a full-thickness defect in one muscle in a muscle group. In both cases, the muscle defect is in close contact to other muscles that can contribute cells or factors directly to the defect site. In this biceps femoris defect, on the other hand, the defect itself is a full-thickness defect in the muscle with no closely linked muscles surrounding it. Because of this, the thickness of the tissue at the center of the empty defect was consistent and was a good indication of muscle regeneration or lack thereof.

This is the first VML model in which a positive control of muscle regeneration is presented, with a large difference in healing response between the negative and positive controls. This positive control treatment is reminiscent of the clinical gold standard

treatment of VML; however, there are distinct differences between this autograft treatment presented here and clinical treatments. In this positive control, the defect was sutured directly into the defect site with relatively aligned myofibers. This represents the ideal case for an autograft treatment and is obviously not possible in traumatic VML injuries in humans. Clinically, a large muscle defect would be treated with coverage of the area with a local or free muscle flap with different alignment and fiber density from the injured muscle [14]. Vascular reconstruction typically accompanies this muscle flap therapy to maintain perfusion in the flap. This type of microsurgical capability would be very difficult to achieve in a rodent model and was not performed in this study. Additionally, muscle flaps are used to cover the defect site, not to necessarily replace the empty defect site with tissue, and are limited in availability and restricted in applicability. The autograft treatment was specifically sutured into the empty space left by the defect and meant to directly replace the cells and structural proteins within the defect space, minimizing the distance stem cells would need to traverse to reach the injured area. Though the autograft treatment was similar to the muscle flaps used for human VML, the differences in the application of the muscle tissue between these two treatments suggest that the mechanisms by which they aid in muscle regeneration may differ as well.

It was observed in this study that despite the lack of vascular reconstruction to re-connect the defect autograft tissue to the surrounding muscle, the autograft treatment still induced a vascular response that is greater than that of an empty defect. Clinically, it is well known that vascularization plays a role in maintaining muscle flap viability, as demonstrated by the movement towards using perforator-based flaps to maintain perfusion within flaps [189-191]. Preclinical studies have also shown the importance of

vascularization for the integration and successful implantation of graft materials [86, 87]. The high vascularity seen in the autograft-treated group may have increased the likelihood of the autograft survival within the hamstrings defect. While this study did not delve into specific mechanisms by which vascularization may play a role in muscle regeneration, this difference in vascular response between empty and autograft groups may have implications on how much tissue can regenerate and maintain viability within the defect space. In addition to maintaining the viability of the graft and defect area, the higher vascularization in the autograft-treated group may increase nutrient and waste transport, allow access to the defect site for circulating cells, and facilitate graft innervation [11]. Studies that deliver a vascular supply to the defect space may help determine if and how the increased vascularization may aid in muscle regeneration in this model.

In contrast to the difference in vasculature in the two groups, the muscle function was similar in both groups at 2 and 4 weeks post-injury. This was a surprising result given the stark differences in tissue appearance as well as the histological differences between the two tissues at each time point. While the autograft-treated defect appeared to be regenerated by 4 weeks based on histology images, there is still a large difference between the function of this tissue from the contralateral uninjured control. More importantly, while the empty defect appeared to have very little tissue at the defect area with no signs of regenerating myofibers at the center of the defect, hamstrings stimulations still generated comparable force to the autograft-treated group. One possible explanation for this is the effect of the defect on the physiological cross-sectional area (PCSA) of the stimulated muscles. The PCSA is closely related to the maximum muscle

tetanic force, and the PCSA can be used to accurately estimate the maximum tension a muscle can create [192]. The tibial branch of the sciatic nerve stimulates the biceps femoris and the semimembranosus, both of which would affect the readings in the force measurements. Though the defect volume and mass may be large in the biceps femoris defect, the cross-sectional area of the defect space is actually relatively small due to the thinness of the biceps femoris. Combined with the semimembranosus PCSA, the reduction in the PCSA by the defect may not be a large enough one to detect in functional force measurements. Moreover, the semimembranosus muscle may act as both a flexor and extensor in different conditions, which could potentially complicate the force readings [193].

The hamstrings force measurements were vastly different from the quadriceps force measurements, in which the 8-mm full thickness defect resulted in a drastic reduction of muscle force. The uninjured quadriceps muscle produced a force about twice the maximal force produced by the hamstrings muscle. This is because of the anatomical differences between these muscles. The quadriceps muscles have large PCSAs and shorter fibers, allowing for the generation of greater forces. The hamstrings muscles, on the other hand, have intermediate PCSAs and longer fibers, allowing for larger excursions [194, 195]. Thus, while both the hamstrings and quadriceps muscle force measurements have a comparable amount of variability, the quadriceps model has a large enough range to allow for the detection of force differences between treatments. The hamstrings stimulations, on the other hand, would require a much larger sample size to find a significant difference between the negative and positive controls for muscle regeneration.

In order to fully characterize the healing of the muscle defect, this study made use of biochemically analyzing enzyme activity and protein content from the tissue within the injured area to determine the degree of muscle regeneration at the defect site. Creatine kinase (CK) is an enzyme that catalyzes the reaction in which adenosine triphosphate (ATP) is used to convert creatine into phosphocreatine. This enzyme is found in highly metabolic tissues, especially skeletal muscle. CK has been traditionally measured in serum as a sign of myocardial infarction or muscular dystrophy [196, 197]. However, it has been used to characterize muscle regeneration in a minced muscle model in the rat tibialis muscle [198]. Although there is an initial decrease in CK activity within the first week of surgery, the activity increases as regeneration occurs through the next five weeks. While our study did not include early readings that would be required to see the initial decrease, CK activity was seen to increase slowly over time in the autograft-treated group, as expected of healing muscles after injury. The CK activity for the empty defect group rose slightly up to 6 weeks and decreased slightly at 8 weeks. Notably, the empty defect group and the autograft treated group did not have significantly different CK activity at 2, 4, 6, or 8 weeks post-injury. This is in agreement with our muscle function data in which the two groups also did not differ in maximal tetanic torque at 2 and 4 weeks post-injury.

On the other hand, citrate synthase activity, which is an indication of the metabolic activity of the tissue, showed a different result, with the autograft-treated group improving to the level of uninjured controls by 4 weeks post-injury. Citrate synthase (CS) is a protein within the citric acid cycle that is necessary for cell metabolism and is present in all cells. However, tissues with higher metabolic activity will have a higher citrate

synthase activity. This CS activity matches the muscle histology much more closely than the CK activity, which may be due to the amount of tissue within the defect area. Even though both are indicative of muscle bioenergetics, studies have shown that the phosphocreatine utilization in skeletal muscle, which is usually catalyzed by creatine kinase, is still present in CK-deficient mice [199]. This suggests that muscle can still have a relatively high metabolic activity through the phosphocreatine system even without CK. This could help explain the differences between CS and CK activity in the autograft-treated group; while CK activity was lower in the autograft-treated group, the muscle metabolic activity may still be high, accounting for the high CS activity.

In summary, this work established a new VML model in the biceps femoris of the rat that shows stark differences in tissue make-up histologically. While this model is limited in its ability to measure differences in muscle function *in vivo* across the different treatment groups, histology can easily be used to determine myofiber or fibrosis formation within the defect area. With the disparity in appearance between the negative (empty defect) and positive (autograft treatment) controls for muscle regeneration, the muscle regeneration of a treatment can be determined by comparing its thickness and cellular make-up with the two controls. Additionally, by comparing the negative and positive controls, insights into the differing healing responses may be elucidated. In this study, we found that revascularization of the defect site was different between the two groups, indicating that this may be one of the reasons behind the dissimilar regenerative responses. Further work is needed to fully determine the effect of revascularization on the healing of the biceps femoris defect, and this work will be outlined in part 2 of this chapter.

## **CHAPTER 6 Aim 2: Treatment of the Biceps Femoris VML Model with Microvessels**

### **6.1 Abstract**

Large skeletal muscle injuries, such as volumetric muscle loss, result in a large defect space devoid of vasculature and cells. Vascularization is thought to play a crucial role in muscle regeneration in maintaining graft viability and eventual integration. Microvascular constructs have been shown to form vascular networks *in vitro* that can be facilitated by co-culture with myoblasts. This study aimed to evaluate the ability of these microvascular constructs, with or without myoblasts, to induce early revascularization of the defect space and to regenerate muscle. When grown *in vitro*, the microvessels co-cultured with myoblasts resulted in faster sprouting of vessels and fuller networks than microvessels alone. When implanted, the two groups resulted in similar vascular volumes, though the microvessels with myoblasts group had a significantly higher vascular volume compared to an empty defect. Despite the increased vascular volume, both groups resulted in very little tissue in the defect space at 8 weeks post-injury. At 2 and 4 weeks post-injury, the defect spaces in both the microvessels and microvessels + myoblasts groups were partially occupied with fat. While vascularization may play a role in muscle regeneration, the findings of this study suggest that other factors that influence muscle regeneration may have a larger effect than vascularization alone.

### **6.2 Introduction**

The majority of extremity injuries are penetrating soft-tissue wounds involving extensive damage to the muscle, also known as volumetric muscle loss (VML). In VML injuries, a large section of muscle is damaged and debrided, resulting in a large volume of space devoid of vasculature and stem cells. The gold standard for VML injuries is coverage of the damaged area with local vascularized muscle flaps; however, these flaps

tend to be thin and are not always readily available . With a large VML, it would be difficult to find a sufficient amount of viable, vascularized muscle near the defect to serve as a local muscle flap. Additionally, a muscle flap is only a coverage strategy; there is currently no means of replacing injured muscle with a functional unit that can maintain or restore normal function [30].

In a large defect like VML, vascularization is of great importance. Intact skeletal muscle is highly vascularized, with capillary to muscle fiber ratios of around 1.5 [200, 201]. Studies have shown that delayed angiogenesis and VEGF production impairs skeletal muscle regeneration after cardiotoxin damage [202]. For skeletal muscle to be regenerated, a vascular source must be present early in the healing stages in order to provide nutrients, cells, and guidance to the center of the defect site. In trying to develop tissue engineering strategies towards repairing VML, a major challenge that arises is the issue of transport to the center of the scaffold, where the lack of vascularization and nutrient/waste transport will likely lead to necrosis and poor survival of delivered cells or tissues [11]. Recent research into vascularized muscle constructs highlights the benefits of early vascularization for survival and eventual functional integration of the graft to skeletal muscle [86, 87].

One promising strategy of creating vascular networks *in vitro* that are readily implantable involves microvascular constructs (MVC) in which intact microvessel segments are isolated and suspended in collagen type I gel. Adipose-derived microvessels (or microvascular fragments) can be grown in a collagen gel *in vitro*, and within 7-12 days of culture, the freshly isolated microvessels grow into vascular networks within the collagen [203]. When implanted into a mouse subcutaneous model, these constructs have

integrated with the tissue and produced viable perfusion-capable blood vessels within a week of implantation [204]. Freshly isolated microvascular fragments have been transplanted into a VML in the TA of a rat and were shown to increase perfusion in the defect site over an empty and cellular control [205]. Though freshly isolated fragments have the advantages of immediate transplantation and maintenance of tissue phenotype with no time in culture, there may be advantages in growing the microvascular networks *in vitro* as well. Studies have shown that pre-existing microvascular networks facilitate revascularization due to inosculation of host vessels to the preformed vascular network and the network's angiogenic effect on the surrounding tissue [206]. Thus, there may be a benefit of implanting microvessels that are grown *in vitro* to form networks that can then inosculate *in vivo*.

While microvascular constructs hold potential in regenerative medicine, its effects could be compounded by the addition of satellite cells. Satellite cells, also known as myoblasts when cultured *in vitro*, are adult muscle precursor cells that reside adjacent to skeletal muscle fibers [207]. Rhoads et al. showed that microvascular constructs (i.e. microvascular fragments in collagen gel) cultured over a rat myoblast monolayer resulted in greater sprout numbers and lengths than a fibroblast monolayer control after 5 days in culture [208]. In the same study, by culturing microvessels in media pre-conditioned by myoblasts, it was found that the effect that the myoblasts had on the microvascular fragments was due to a paracrine effect. Additionally, by adding VEGF receptors that directly competed for and blocked VEGF activity, the myoblast-mediated angiogenic effects were reduced, suggesting that VEGF may play a large role in the growth of the microvessels.

Not only would the addition of myoblasts be beneficial to the growth and networking of microvascular fragments, the myoblasts themselves could play a role in muscle regeneration. In fact, recent studies have shown that Pax-7+ satellite cells are crucial for muscle regeneration after a cardiotoxin injury. Conditional depletion of Pax-7+ satellite cells in a transgenic model resulted in failure to regenerate muscle, which were replaced with inflammatory cells and adipocytes [209, 210]. This reduced muscle regeneration was rescued after transplantation of Pax-7+ satellite cells. Satellite cell implantation for Duchenne muscular dystrophy resulted in fusion of the implanted cells with host fibers. However, the attempt at translating this treatment failed due to poor survival and migration of donor cells after transplantation [85]. Implantation of the myoblasts with the rapidly inosculation microvascular networks could also benefit the myoblasts by aiding in the survival and migration, especially when used as a therapy for a large defect like VML.

While microvascular fragments have been implanted subcutaneously as well as in a VML model with success with inosculation with host vessels, it is unclear if vascularization is indeed a road block for effective muscle regeneration. Additionally, microvascular constructs with myoblasts may increase the vascular response as well as provide vital muscle stem cells to the defect area but have yet to be tested for its regenerative potential in large muscle injuries. Thus, our **objective** was to determine the effects of a pre-formed microvascular construct with myoblasts on the revascularization and muscle regeneration of a VML defect. We *hypothesized* that treatment of the VML defect with these constructs will yield a higher revascularization in the muscle defect at early time points and will result in improved muscle regeneration.

### 6.3 Materials/Methods

#### *Myoblast Isolation*

Myoblasts were isolated from GFP-transgenic Sprague Dawley rats. The soleus muscle was carefully isolated from each leg, weighed, and placed in a small volume of sterile PBS. The tissue was washed in sterile PBS and placed into 0.2% collagenase XI (6mL for every 2 muscles). The tissue was minced manually using two sterile razor blades for 5 minutes and transferred into a 15mL conical tube. The tube was incubated in a 37°C water bath and incubated for 60 minutes, mixing once halfway through the incubation. Collagenase was then removed, and the homogenate was incubated in 6mL/2 muscles of dispase (2.4U/mL) at 37°C for 45 minutes. The dispase was then removed, and the cells were resuspended in growth medium (F10, 20% FBS, 1% penicillin/streptavidin, and 2.5ng/mL bFGF). The cells were then passed through a 100µm strainer (Steriflip, Millipore) and pre-plated for 30minutes to obtain a myoblast-enriched population.

#### *Microvessel Isolation*

Epididymal fat was isolated from Sprague-Dawley retired breeder rats. The fat was minced and digested with collagenase, after which vessels smaller than 500 microns and larger than 20 microns were isolated through filters. The microvessels were then suspended in a collagen gel (3mg/mL, 150,000 microvessels/mL  $\pm$  10<sup>6</sup> myoblasts/mL) around a polycaprolactone nanofiber mesh and cultured *in vitro* in serum-free media for 4 days prior to implantation (Figure 30C & D).

#### *Surgical Procedure*

Unilateral biceps femoris defect surgeries were performed on 13-week-old female Sprague-Dawley rats. A plastic spatula was inserted next to the medial aspect of the

biceps femoris, providing a hard surface on which a 12-mm diameter biopsy punch was applied to the muscle's lateral aspect to create the full-thickness circular defect (Figure 30B). The defect was left empty (negative healing control), treated with an autograft (gold standard control), treated with a microvessel construct (microvessels group), or treated with a microvessel construct with myoblasts (microvessels + myoblasts group).

#### *μCT Angiography*

At 2 weeks post-injury, contrast agent-enhanced micro-CT angiography was performed terminally on animals from the microvessels and the microvessels + myoblasts groups (n=5-6). The technique has been previously described in detail [153-155]. Briefly, 0.9% salt solution (physiological saline) containing 0.4% papaverine hydrochloride (Sigma-Aldrich) was perfused through the vasculature to clear the blood vessels. The vasculature was then perfusion fixed with 10% neutral buffered formalin, rinsed with physiological saline, and injected with lead chromate-based radioopaque contrast agent (2 parts microfil MV-22: 1 part diluent, Flow Tech). Samples were stored at 4°C overnight to allow for polymerization of the contrast agent. The biceps femoris was excised, and the defect region (marked with sutures) was isolated. For contralateral control legs, a 12-mm biopsy punch was used to remove a similarly-sized piece of uninjured muscle.

Excised samples were further fixed for 48 hours then stored in PBS. Samples were scanned in the micro-CT (vivaCT 40, Scanco Medical) at 21μm voxel size. All scans were performed with an applied electroc potential of 55 kVp and a current of 109 μA. The VOI consisted of a cylindrical volume 14.7mm in diameter that spanned the full thickness of the biceps femoris. A global threshold was applied for segmentation of

vasculature, and a Gaussian low-pass filter was used to suppress noise ( $\sigma = 0.8$ , support = 1).

### *Muscle Homogenization*

At 2, 4, 6, and 8 weeks, animals were euthanized (n=6 per time point per group), and the defect area was harvested using a 12-mm biopsy punch. This defect area tissue was measured to obtain a wet weight, flash-frozen in liquid nitrogen, and stored at  $-80^{\circ}\text{C}$  until homogenization.

For homogenization, tissues were removed from  $-80^{\circ}\text{C}$ , cut with a razor blade into small pieces, then hand-homogenized with a tissue grinder (Duell™ tissue grinders, Kimble-Chase Kontes). Samples were homogenized in 100mM potassium phosphate buffer (pH 7.4) at a ratio of 400 $\mu\text{L}$  of buffer for every 50mg of tissue. The homogenate was then separated into 5 equal volumes for analysis of creatine kinase activity, citrate synthase activity, and quantification of myosin/actin, triglycerides (fat), and hydroxyproline (collagen) content. Homogenates were frozen and stored at  $-80^{\circ}\text{C}$ .

### *Citrate Synthase Activity*

Muscle homogenates were freeze-thawed 3 times and diluted (1:7) in 100mM Tris buffer (pH 8.0) prior to running the assay. 5.18 $\mu\text{L}$  of the diluted sample was added to the 143.59  $\mu\text{L}$  of 100mM Tris buffer, 20.5  $\mu\text{L}$  1.0mM 5,5'-dithio-bis(2-nitrobenzoic acid) (DTNB) in 100mM Tris buffer, and 10.25  $\mu\text{L}$  3mM acetyl CoA in 100mM Tris buffer. The assay reaction was started by adding 20.5  $\mu\text{L}$  of 5mM oxaloacetic acid in 100mM Tris buffer. Solutions were warmed up to  $30^{\circ}\text{C}$  prior to the assay, and the assay was carried out at  $30^{\circ}\text{C}$ . The spectrophotometer (BioTek PowerWave XS) was programmed to delay for 2 minutes prior to running a kinetic program to take OD readings at 412nm

every 15 seconds for 3 minutes. The citrate synthase (CS) activity was calculated using the following equation:

$$\text{Units} \left( \frac{\frac{\mu\text{mol}}{\text{min}}}{\text{g wet wt}} \right) = \frac{\Delta A}{\text{min}} * V_{\text{rxn}} * \text{dil}}{\varepsilon * L * V_{\text{sample}}} * \frac{(V_{\text{buffer}} + \frac{\text{wt}_{\text{muscle}}}{\delta})}{\text{wt}_{\text{muscle}}}$$

where  $\Delta A/\text{min}$  is the change in absorbance,  $V_{\text{rxn}}$  is the volume of the assay reaction (0.2mL), dil is the dilution factor (7),  $\varepsilon$  is the extinction coefficient ( $13.6 \text{ mmol}^{-1}\text{cm}^{-1}$ ),  $L$  is the light path length (0.552cm for 0.2mL in a 96-well plate),  $V_{\text{sample}}$  is the volume of the sample used in the assay,  $V_{\text{buffer}}$  is the volume of homogenizing buffer,  $\text{wt}_{\text{muscle}}$  is the weight of the homogenized muscle in g, and  $\delta$  is the density of muscle (1.06g/mL).

#### *MHC/Actin Quantification*

Samples were centrifuged at 5,000 x g for 15 minutes, and the supernatant was removed. The pellets were resuspended in 400 $\mu$ L of 100mM potassium chloride and 20mM imidazole (pH 7.0). 10 $\mu$ g of the sample was run in a NuPAGE 4-12% Bis-Tris precast gel (Life Technologies), and the gels were dyed in a Coomassie Blue solution for 1 hour. Gels were destained overnight and imaged with Bio-Rad Gel Doc XR.

#### *Histology*

Transverse muscle sections taken approximately from the middle of the muscle defect were stained with H&E for morphological analysis.

## **6.4 Results**

#### *In vitro growth of microvessels*

Microvascular constructs grown with myoblasts resulted in expedited sprouting of vessels at day 2 and denser networks with more branches of vessels at day 5 in culture (Figure 30A).

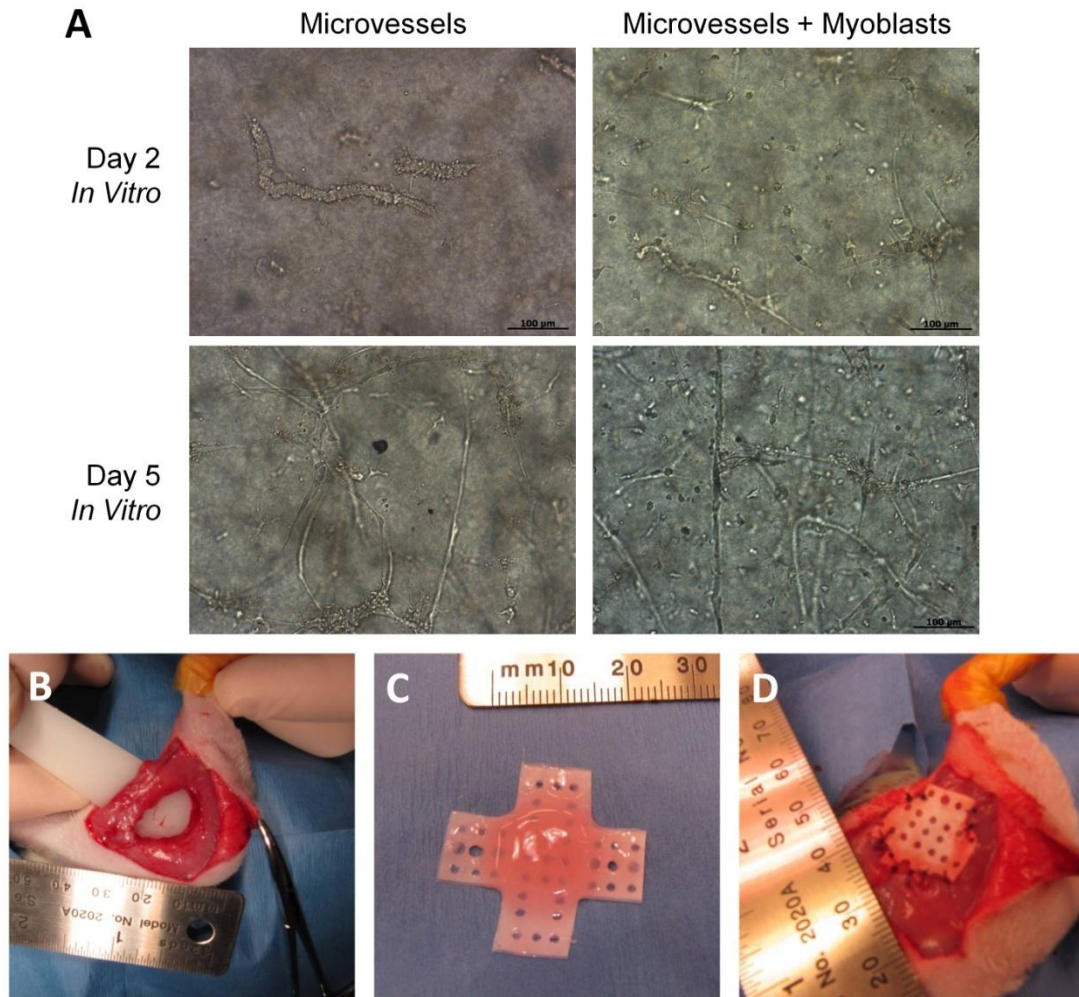


**Figure 30: Microvessel Culture, Construct, and Surgery.** (A) Microvessels grown *in vitro* with or without myoblasts. At days 2 and 5 in culture, the microvessels + myoblasts group showed more robust and faster growth than microvessels alone. (B) A 12-mm defect was created in the biceps femoris. (C) The microvessels were gelled around a nanofiber mesh. (D) The mesh was placed with microvessels face down into the defect and sutured.

#### *Early Revascularization of Muscle Defect with Microvessels*

At 2 weeks post-injury, the vascular volume in the defect area of the microvessels and microvessels + myoblasts groups were significantly higher than the contralateral control. When compared to the vascular volumes of the empty and autograft-treated groups from the previous hamstrings characterization study, the microvessels +

myoblasts group had a significantly higher vascular volume compared to the empty defect group. Representative images of the vasculature from each group shows that all groups have comparably sized vasculature. The microvessels and microvessels + myoblasts group seemed to have more smaller vasculature that contributed to their vascular volumes.

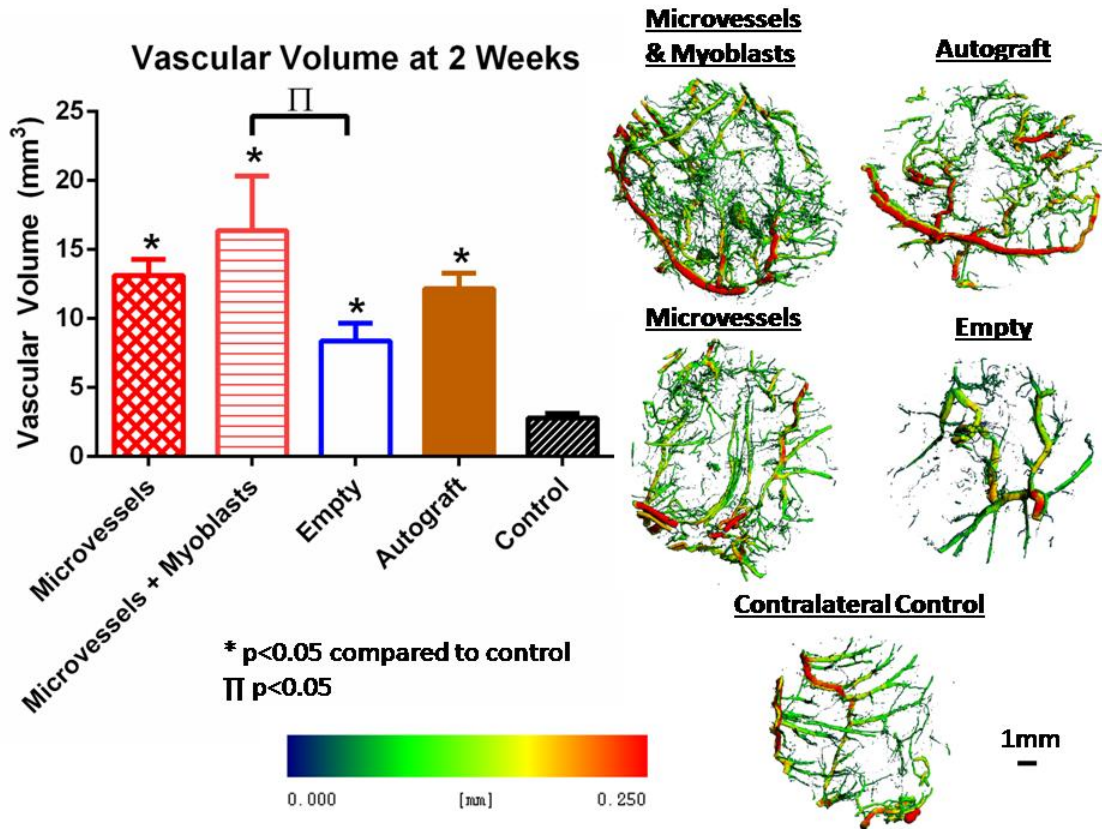


**Figure 31: Vascular Volume in Microvessel-Treated Biceps Femoris.** At 2 weeks post-injury, all injured groups had a higher vascular volume compared to the contralateral uninjured control. The microvessels + myoblasts group had a higher vascular volume than the empty defect group. Representative images of the vasculature in each group show that the microvascular groups have comparable vascular volume to the autograft group. Vessels colors represent vessel thicknesses. n=5-8 for injured groups, n=24 for contralateral controls.

*4-week microvessel histology*

At 4 weeks post-injury, both the microvessel and microvessels + myoblasts group had regenerating fibers close to the defect site (Figure 32 B,H) as well as fat deposits (Figure 32 C, G). While the microvessels only group exhibited areas of fibrotic tissue (Figure 32D), the microvessels + myoblasts group had a small island of muscle in the center of the defect (Figure 32G).

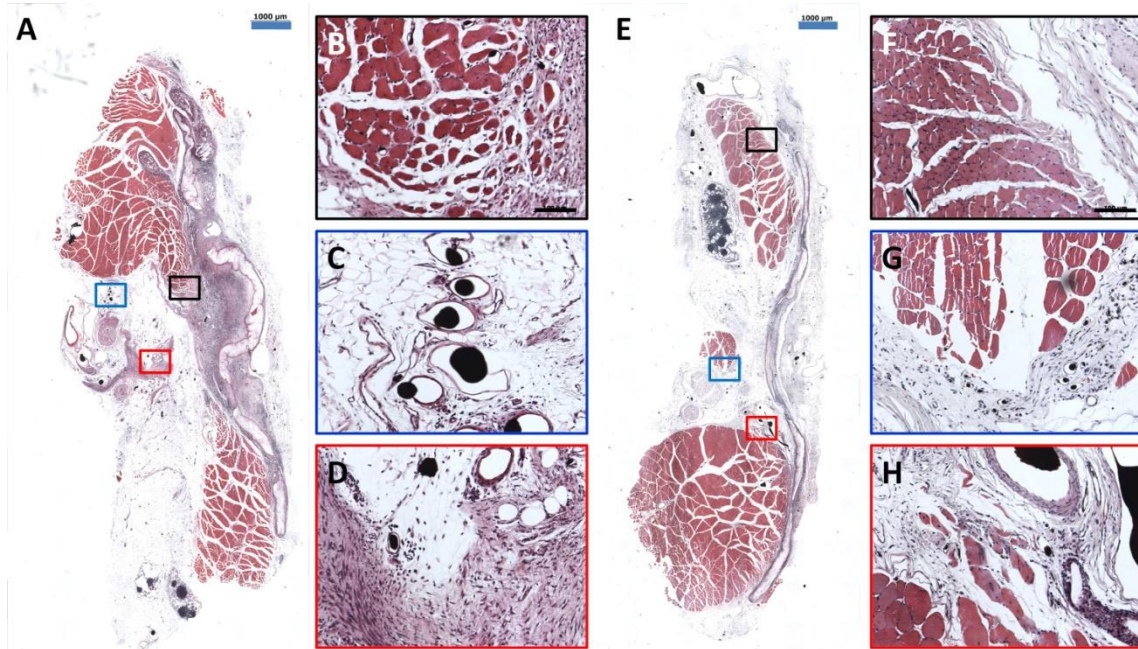


**Figure 32: Histology of Microvessel and Microvessels+Myoblasts groups at 4 weeks Post-Injury.** (A) Transverse H&E stained section of microvessels-treated biceps femoris 4 weeks after Injury. (B), (C), and (D) are 10x zoomed-in images with locations shown by colored squares in (A). (E) Transverse H&E stained section of microvessels + myoblasts-treated biceps femoris 4 weeks after injury. (F), (G), and (H) are 10x zoomed-in images, with locations shown by colored squares in (E). Blue scale bars: 1000μm. Black scale bars: 100μm.

#### *8-week CS Activity*

While citrate synthase activity was significantly lower in the empty defect compared to the contralateral uninjured controls at 8 weeks post-injury, the autograft, microvessels, and microvessels + myoblasts groups had relatively similar citrate synthase activity as the control (Figure 33).

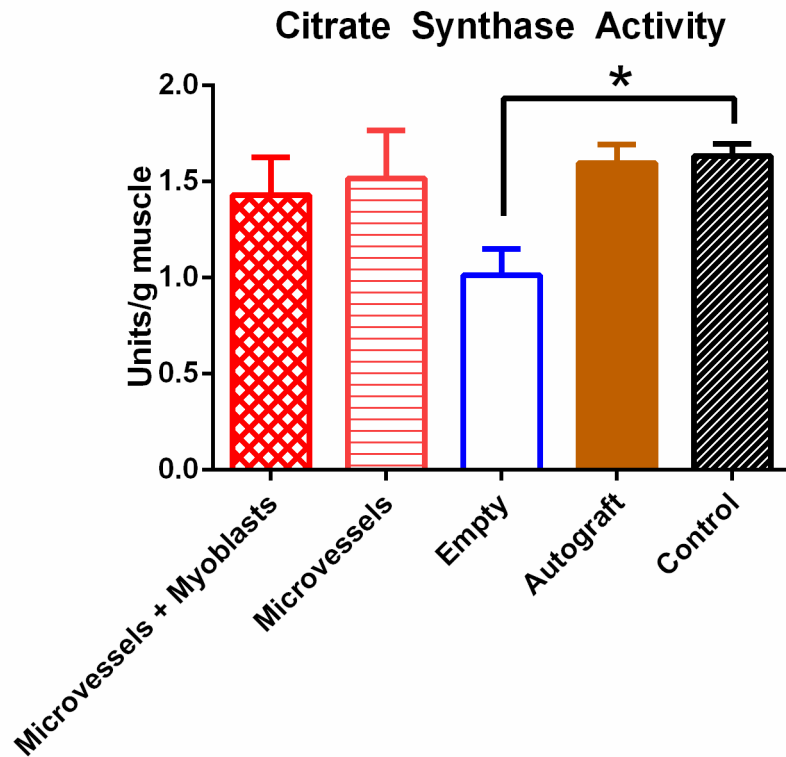


**Figure 33: Citrate Synthase Activity 8 weeks post-injury.** Citrate synthase activity, expressed as units (mmol/min) per gram muscle wet mass, was significantly lower in the empty defect group compared to the uninjured contralateral control. n=6 for empty, n=27 for controls,  $p < 0.05$ .

#### *8-week histology*

By 8 weeks post-injury, both the microvessels group and the microvessels + myoblasts group resulted in thin fibrous tissue within the center of the defect, with some fatty infiltration (Figure 33). The defect area was occupied either only with the mesh or with the mesh and some fibrotic tissue.

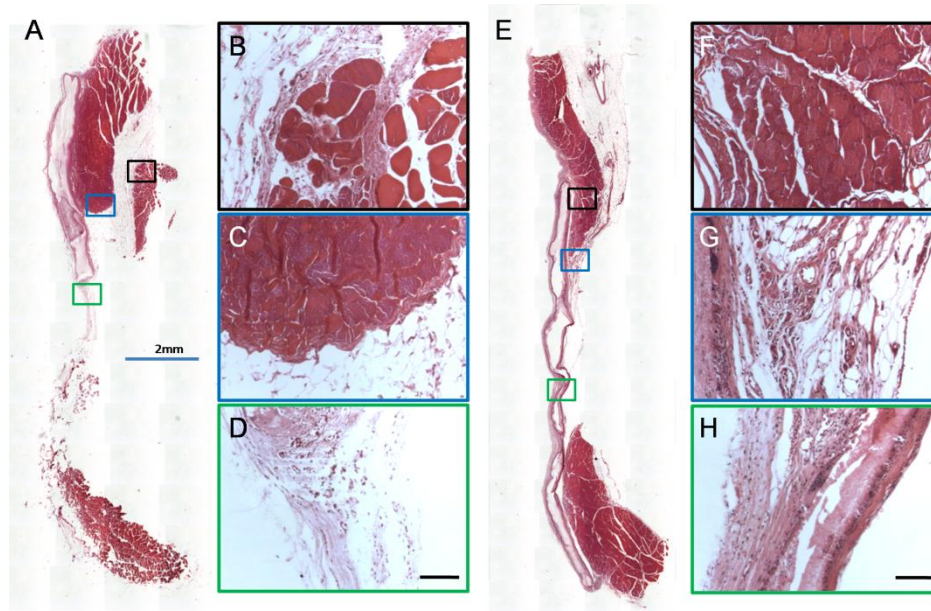


**Figure 34: Histology of Microvessel and Microvessels+Myoblasts groups at 8 weeks Post-Injury.** (A) Transverse H&E stained section of microvessels-treated biceps femoris 8 weeks after Injury. (B), (C), and (D) are 10x zoomed-in images with locations shown by colored squares in (A). (E) Transverse H&E stained section of microvessels + myoblasts-treated biceps femoris 8 weeks after injury. (F), (G), and (H) are 10x zoomed-in images with locations shown by colored squares in (E). Blue scale bar: 2000µm. Black scale bar: 100 µm.

## 6.5 Discussion

We tested the ability of microvascular constructs with or without myoblasts for their abilities to quickly re-vascularize a large empty defect in the muscle and to regenerate the muscle. As was hypothesized, the microvascular constructs with myoblasts had a higher vascular volume compared to the empty defect group, indicating that this construct facilitated re-vascularization of the VML defect. However, contrary to our hypothesis, both the microvascular constructs alone and with added myoblasts resulted in very little muscle regenerated in the center of the defect space at 8 weeks post-injury.

According to previous research, the addition of myoblasts to microvascular constructs aid in the formation of vascular networks through a paracrine effect *in vitro* [208]. Thus, we expected the microvessels + myoblasts group to result in a higher re-

vascularization in the biceps femoris defect compared to the microvessels group. While we did see an effect of the myoblast addition in culture *in vitro*, analysis of the implanted vascular network 2 weeks post-injury showed no significant difference between the microvessels group and the microvessels + myoblasts group. The reason for this may be due to the time point at which the vascular volume was taken. We decided on determining vascular volume at 2 weeks in order to give the vasculature enough time to inosculate but prior to its complete remodeling within the body. According to literature, perfusion of microvessels within implanted constructs increased through day 28 [211]. From the same study, microvessels that were implanted subcutaneously still showed an irregular morphology at day 14, and by day 28, the vessels had remodeled to a typical, smooth vascular tree with larger diameter vessels. This data indicated that analyzing the vasculature at an intermediate time point such as day 14 would be ideal for determining implant vascularization though the microvessels may be in the process of remodeling at day 14.

Despite no differences between the microvessels versus the microvessels + myoblasts group in early revascularization, both groups had vasculatures within the defect area that were more similar to the autograft treated group compared to the empty defect group. However, even with the early vasculature, neither the microvessels nor the microvessels + myoblasts groups had muscle myofibers within the defect space by 8 weeks after injury. These data suggest that the role of vasculature in tissue regeneration in this model was overpowered by other factors within the regenerative process.

Deposits of fat that were apparent in the defect space at 2 and 4 weeks post-injury in the microvessels and microvessels + myoblasts treated groups, which seemed to be

remodeled away to leave a thinner tissue at week 8 post-injury. Though mesenchymal progenitors isolated from skeletal muscle and satellite cells have been shown to be capable of differentiating down the adipogenic pathway given the right conditions [212-214], there is no sign within literature that microvessels would induce such fat formation [204, 215]. Fat deposition is associated with muscle disorders and incomplete muscle regeneration [48, 49]. Increased fat accumulation that impairs muscle regeneration are typically dispersed between muscle fibers or fibrotic tissue [216, 217]. In our study, the adipocytes formed a large continuous portion of the tissue cross-section rather than intermuscularly, as has been seen in the untreated empty biceps femoris defect previously. More studies are needed to determine the mechanism by which the fat was created at the defect site and how it may influence muscle regeneration.

Despite very little muscle regeneration at the center of the defect, the microvessels and microvessels + myoblasts groups showed slight improvements in citrate synthase activity compared to the empty defect group. Citrate synthase exists in most cells as it is the enzyme that catalyzes the first step in the citric acid cycle. It is commonly used as a metabolic marker to assess oxidative capacity and can be used to determine skeletal muscle oxidative capacity [218, 219]. However, because it is ubiquitous to all cells, differences in citrate synthase activity only characterizes the metabolic activity of the tissues involved. Thus, even though the microvessels and microvessels + myoblasts groups had similar creatine kinase activities compared to the control and autograft-treated groups at 8 weeks, this is not necessarily an indication of muscle regeneration. Creatine kinase, on the other hand, is an enzyme that is more specific to skeletal muscle and is also linked to the energy usage of the tissue [198]. The

creatine kinase activity was slightly higher, though not significant, in the microvessels and microvessels + myoblasts treated groups compared to the empty defect. This indicates that there may be some differences in the amount of myofibers or myofiber activity within the defect area. These differences were likely at the edges of the defect rather than in the center, as the histology clearly showed no or few myofibers in the center of the defect in any group other than the autograft-treated group.

It is important to note that certain controls were not included in this study because they do not contribute greatly to the objective of this study, which was to determine the effects of early revascularization on muscle regeneration. Controls that include just the collagen alone or myoblasts delivered without microvessels were not crucial for this study because both of these groups have been shown to not improve vascularization [205, 220]. Additionally, delivery of myoblasts alone have been shown to be futile due to the lack of graft viability without surrounding vasculature, particularly in a large empty defect [11]. While microvessels with a non-myoblast cell would have been an interesting control if the study focused mainly on the differences between the microvessels and microvessels + myoblasts group, *in vitro* studies have already shown that these constructs grown with fibroblasts do not induce the same vascular response as constructs grown with myoblasts [208].

Several limitations exist in the testing of microvascular constructs in the biceps femoris model. First, the microvessels and myoblasts are both derived from Sprague-Dawley rats and implanted into Sprague-Dawley rats, which are not purely inbred. Due to this allogeneic nature of the implants, there may be a concern with rejection of the tissue or cells, which would affect its ability to regenerate muscle or promote revascularization.

There are no signs of immune rejection in histology at 14 days, and CD-4 staining for T-cells indicated no differences between the autograft and microvessel-treated groups, suggesting that there was no chronic rejection (data not shown). Acute or hyperacute rejection may still occur and would be difficult to determine in this model although proper perfusion and histology support the lack of complete immune rejection. Second, the myoblasts used in this study were isolated from a GFP transgenic rat, which could have implications on its functionality. From our *in vitro* co-cultures of myoblasts with microvessels, no differences were apparent between myoblasts isolated from wild-type Sprague-Dawley rats compared to myoblasts isolated from GFP-transgenic Sprague-Dawley rats. Though minor differences may exist between GFP- and non-GFP-myoblasts, these differences did not deter the paracrine effects of myoblasts on microvessel growth. Third, the micro-CT angiography performed in this study was limited by a resolution of 21 $\mu$ m voxels, which did not allow for the detection of smaller vessels in the capillary range which are prominent in muscles. Additionally, the contrast agent is perfused through the vasculature with applied pressure and is not indicative of the natural perfusion of the body. Though laser doppler perfusion imaging was considered as potential indicator of perfusion, the nanofiber mesh in the microvessel constructs block the laser and prevent accurate measurements.

In this study, we have evaluated the effects of microvascular constructs with or without myoblasts on the revascularization and muscle regeneration of the biceps femoris muscle after a VML. While the microvascular construct with myoblasts did induce higher revascularization compared to an empty defect, the microvessels with or without myoblasts did not result in the recovery of myofibers within the defect space. Instead, the

defect space was occupied with fat cells within 14 days post-injury, and by 8 weeks post-injury, the defect area was occupied by a thin fibrous tissue. More studies are needed to determine the exact effects of the microvessels on the surrounding skeletal muscle, though current data suggest the recovery of vascular supply in the defect space did not induce a large regenerative effect.

## **CHAPTER 7 Aim 3: Effects of Microvascular Constructs on the Healing of Composite Muscle & Bone Injuries**

### **7.1 Abstract**

Large extremity injuries, such as open fractures in which both muscle and bone tissue are damaged, remain a challenge in the clinic. Gold standard treatment involves coverage of the bony defect with vascularized muscle flaps; however, large composite injuries leave scarce tissue viable to use for coverage. Vascular supply in these muscle flaps has been shown to be crucial in the healing process. In this study, we test if we can substitute tissues that provide vascular supply with pre-formed microvascular constructs. We implanted these constructs into a composite segmental bone defect and volumetric muscle loss model in two distinct locations: around the bone, similar to a periosteal substitute, or within the muscle defect, similar to a muscle flap substitute. We find that the microvascular constructs placed around the bone defect resulted in higher revascularization at day 7 post-injury, but this treatment deterred bone formation when implanted with our rhBMP-2 hybrid delivery system. On the other hand, the microvascular constructs placed within the muscle defect as a flap substitute did not significantly facilitate revascularization at 7 days post-injury but did improve muscle and bone functional metrics. Taken together, microvascular constructs do have potential in tissue engineering strategies for composite extremity injuries, though vascularization may not play the only role in facilitating regeneration.

## 7.2 Introduction

Open fractures, in which a large soft tissue injury is sustained with a bone fracture or defect, are associated with a high rate of complications, such as osteomyelitis, delayed or persistent non-union, and muscle flap loss [221]. Approximately 82% of all fractures in the military are open fractures [1]. In the civilian population, a large number of open fractures are caused by motor vehicle accidents and falls from large heights. Though the incidence rate of open long bone fractures is low and ranges from 11.5 to 21 per 100,000 people per year, these type of injuries are associated with a high rate of complication of up to 32% from infection, implant failure, and delayed union [222, 223]. Additionally, fractures and open fractures are frequently components of polytrauma, in which patients suffer from injuries to multiple body regions [224]. Polytraumatic patients that suffer from additional extremity injuries experience pain, impaired functional abilities, and a decreased quality of life [225].

The clinical gold standard for treating open fractures uses muscular flaps to cover the bone, but this treatment can be complicated by flap necrosis or partial flap necrosis, which can result in delayed amputation [226]. In injuries involving a large loss of soft tissue, availability of muscle flaps for transfer may be limited, and functional donor site morbidity has been reported for the latissimus dorsi, a muscle commonly used for muscle flap treatment [227, 228]. Patients that elect to salvage open fractures in the lower limbs often experience pain and issues with motility years after the injury and sometimes do not regain normal function of their extremity despite higher chances of re-hospitalization, osteomyelitis, and repeat surgeries than patients that elect to amputate the limb [30, 102]. Even with treatment and limb salvage, patients have significant levels of disability that lead to similar long-term functional outcomes as amputated lower extremities [229].

Despite limitations of availability and donor site morbidity for muscle flap treatments and the lack of full limb recovery, there are currently no tissue engineering strategies for composite injuries of bone and muscle.

The sizeable injuries that our defect models involve present a harsh environment with challenged mass transfer of nutrients, which prevents efficient regeneration within the large defect. Clinically, an important consideration for musculocutaneous or muscle flaps is the vascularity of the flap [190, 191, 230]. Not only is the vascular supply crucial for the survival and viability of the muscle flap, these soft tissue flaps also serve as a source of vascular supply [35]. To this end, muscle is a preferred flap over fasciocutaneous tissue due to its greater vascularity, and this clinical observation was confirmed in a murine tibial fracture model [138]. The vascularization of intact periosteum also plays a large role in the healing of bone fracture, and the removal of periosteum during fracture healing delays or prevents bone union [231]. Vascularization is important in aiding mass transfer in both muscle and bone tissues, and insufficient vasculature has been implicated for delayed healing [140]. In our model of composite muscle and bone injury, as discussed in section 3.2, the addition of the muscle injury to a bone defect resulted in a delayed early revascularization of the leg, possibly due to cross-talk between the muscle and the bone through vasculature [104]. These data suggest that a vascular therapy may be able to aid in regeneration of both the muscle and bone.

Microvascular constructs made with adipose-derived microvessels comprise of randomly aligned microvessel networks that quickly integrate with tissues and result in perfusion-capable vasculature when implanted subcutaneously in a mouse and in a rat VML model [204, 205]. With the increased perfusion that the microvascular constructs

could provide, the defect region could be replenished of nutrients and possible growth factors as well as be more amenable for cell delivery, providing a greater likelihood for regeneration. Our previous work (Section 4.2) showed that the implantation of microvascular constructs with myoblasts, or muscle stem cells, into a biceps femoris VML resulted in a higher vascular volume compared to the empty VML defect, suggesting that the constructs inosculate *in vivo* and can increase vascularity in a muscle defect space.

Given the importance of vascularization in tissue regeneration and the lack of early revascularization in our composite model, a tissue engineering strategy that provides a vascular supply may have an influence on the regeneration of the muscle and bone. **The objective of this study is to examine the regenerative and angiogenic potential of microvascular constructs on composite bone & muscle defects.** *We hypothesize that microvascular constructs implanted into composite injuries at the muscle-bone junction will aid in revascularization and regeneration of both tissues.* In testing this hypothesis, we decided to implant preformed microvascular network constructs around the mesh surrounding the bone defect, mimicking a periosteal substitute, or preformed microvascular network constructs with myoblasts within the quadriceps defect, mimicking a vascularized muscle flap.

### 7.3 Materials/Methods

#### *Myoblast Isolation*

Myoblasts were isolated from GFP-transgenic Sprague Dawley rats. The soleus muscle was carefully isolated from each leg, weighed, and placed in a small volume of sterile PBS. The tissue was washed in sterile PBS and placed into 0.2% collagenase XI

(6mL for every 2 muscles). The tissue was minced manually using two sterile razor blades for 5 minutes and transferred into a 15mL conical tube. The tube was incubated in a 37°C water bath and incubated for 60 minutes, mixing once halfway through the incubation. Collagenase was then removed, and the homogenate was incubated in 6mL/2 muscles of dispase (2.4U/mL) at 37°C for 45 minutes. The dispase was then removed, and the cells were resuspended in growth medium (F10, 20% FBS, 1% penicillin/streptavidin, and 2.5ng/mL bFGF). The cells were then passed through a 100µm strainer (Steriflip, Millipore) and pre-plated for 30minutes to obtain a myoblast-enriched population.

#### *Microvessel Isolation*

Epididymal fat was isolated from Sprague-Dawley retired breeder rats. The fat was minced and digested with collagenase, after which vessels smaller than 500 microns and larger than 20 microns were isolated through filters. The microvessels with or without myoblasts (15,000 vessels per mL with or without  $10^6$  myoblasts per mL) were then suspended in a collagen gel (3mg/mL) around a polycaprolactone nanofiber mesh and cultured *in vitro* in serum-free media prior to implantation.

#### *Surgical Procedure for Creation of the Composite Defect*

All procedures were approved by the Georgia Institute of Technology Institutional Animal Care and Use Committee (protocol #A09039 and #12075). Thirteen week old female Sprague-Dawley rats (Charles River Labs, Wilmington, MA) were used for this study. Unilateral bone defects were surgically created in the femora of rats, as previously described [10, 151, 152]. Briefly, an anterior incision was made along the length of the femur and the muscle was then separated using blunt dissection. A modular fixation plate

was affixed to the femur using miniature screws (JI Morris Co., Part No. P0090CE250). A full-thickness segmental defect, 8 mm in length, was created in the diaphysis using a miniature oscillating saw. A perforated nanofiber mesh tube made of polycaprolactone (PCL) was then placed over the native bone ends surrounding the defect, and 150  $\mu$ l alginate hydrogel containing rhBMP-2 was then injected into the defect space [10]. Non-treated controls were not used in this study as previous studies have demonstrated that in the absence of rhBMP-2, the defect contains very little bone formation [150, 152]. Muscle defects were created through the full thickness of the quadriceps down to the femur using an 8 mm diameter biopsy punch. The defect encompassed regions of the rectus femoris, vastus lateralis, vastus medialis, and vastus intermedius. The bone defect was made first, then, once the incised muscles had been closed with 4-0 suture, the muscle defect was created. Animals were given buprenorphine post-surgery to manage pain (0.03 mg/kg 3x daily for the first 48 hours, then 0.01 mg/kg 3x for the next 24 hours).

For testing the microvascular constructs created around the nanofiber mesh to surround the bone defect, the collagen gel containing microvessels (150,000 vessels per mL) was solidified around the cylindrical nanofiber mesh and cultured *in vitro* for 10 days prior to implantation (Figure 35). All bone defects were treated with 150  $\mu$ l of RGD-functionalized alginate and 2  $\mu$ g of rhBMP-2 per defect. Half of the animals received a collagen/microvessel-coated nanofiber mesh (MV+ group) while the other half received a bare nanofiber mesh (MV- group). The muscle defect was untreated in this part of the study and left empty. A subset of animals (n=6) were euthanized at 1 week post-injury for

micro-CT angiography in order to analyze revascularization of the limb. Remaining animals underwent radiography and micro-CT at 4, 8, and 12 weeks (n=2-3).

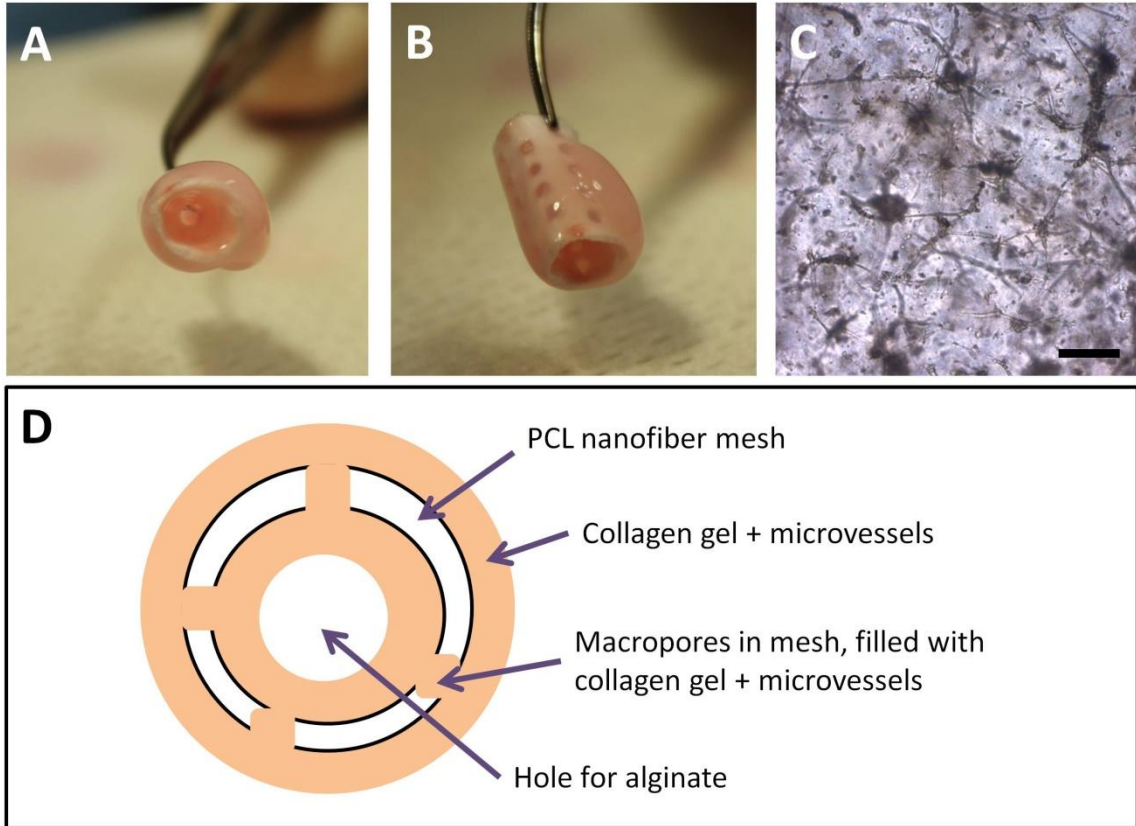


**Figure 35: Microvascular Construct Surrounding a Nanofiber Mesh.** Axial view (A) and side view (B) of the construct is shown. When grown *in vitro* for 8 days, microvessel fragments grow into networks (C). An axial view of the components of the microvessel construct is shown in the diagram (D).

To create the microvascular constructs for implantation into the quadriceps defect, microvessels and myoblasts were suspended in a collagen gel that was solidified around a flat polycaprolactone nanofiber mesh (Figure 36A, B, D). The nanofiber mesh was sutured on top of the quadriceps defect with the majority of the microvascular construct (collagen gel with microvessels and myoblasts) within the defect space (Figure 36C). All bone defects were treated with a perforated nanofiber mesh tube made of

polycaprolactone (PCL) placed over the native bone ends surrounding the defect, and 150  $\mu$ l alginate hydrogel containing 1 $\mu$ g rhBMP-2 was then injected into the defect space. Half of the animals received the microvascular construct within the quadriceps defect (MV+) while half of the animals received no treatment for the quadriceps defect (MV-). A subset of animals (n=6) were euthanized at 1 week post-injury for micro-CT angiography in order to analyze revascularization of the limb. Remaining animals underwent radiography and micro-CT at 4, 8, and 12 weeks (n=3-4).

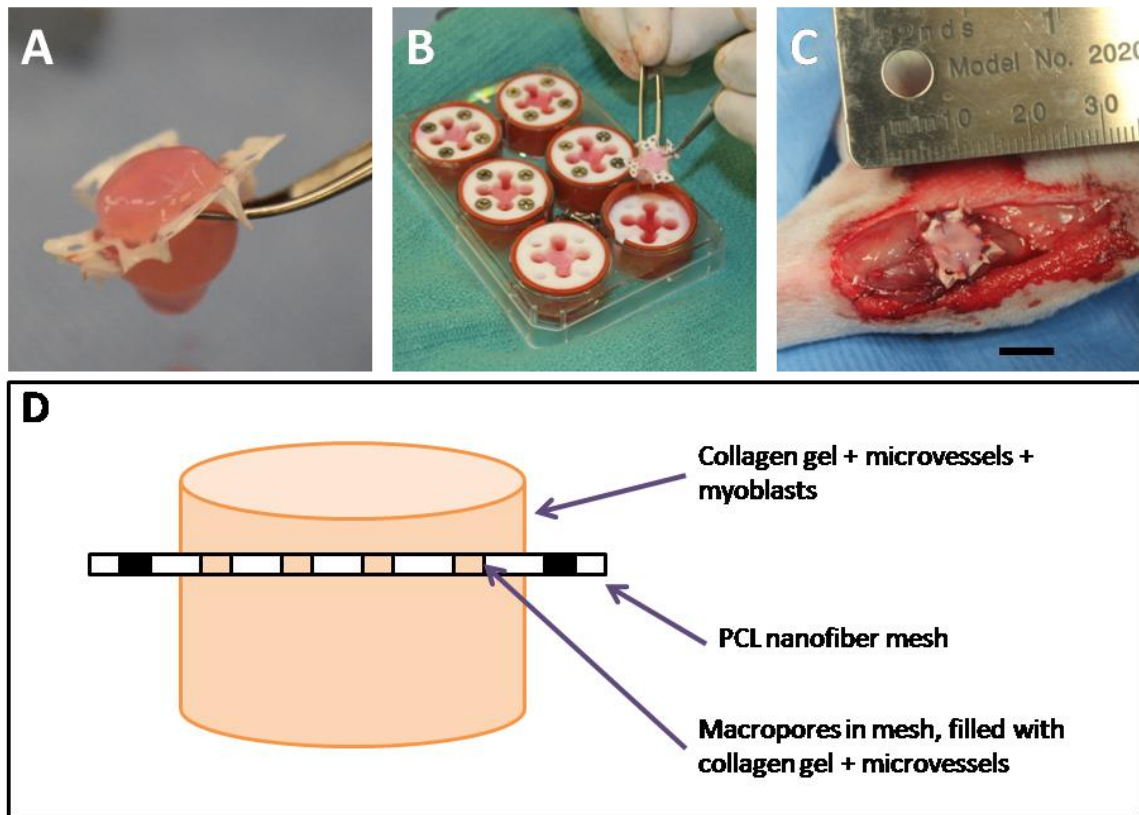


**Figure 36: Microvascular Construct for Filling of Quadriceps Defect.** Side view (A) and top view (B) of the construct is shown. The bulk of the microvascular construct was placed into the quadriceps defect space, and the nanofiber mesh was sutured around the defect (C). A side view of the components of the microvessel construct is shown in the diagram (D).

#### *Muscle Isometric Tetanic Torque Assessment*

Isometric tetanic torque production about the knee by the knee extensor muscles was measured at 12 weeks post-surgery using a custom built apparatus based on a previous design used for assessment of lower leg muscle function (Figure 9B) [113]. All measurements were made under isoflurane anesthesia during a terminal procedure immediately prior to euthanasia. A 2-cm long incision was made through the skin exposing the femoral triangle in the upper thigh. The posterior branch of the femoral nerve was carefully isolated and a nerve cuff was positioned surrounding that branch. The rat was then carefully secured to the platform of the apparatus. The animal was positioned so that the knee angle was at 90° and the ankle was secured to a force transducer (Isometric Transducer Model No. 60-2996, Harvard Apparatus). The knee extensor muscles were stimulated using a stimulator (GRASS S11 Stimulator, Grass Technologies) and the nerve cuff implanted on the femoral nerve. Stimulator pulse duration, frequency, and train duration were set to 0.5 ms, 175 Hz, and 500 ms, respectively; these settings elicited maximal isometric tetanic torque as determined in a pilot study. Measurements of injured muscles were normalized to contralateral intact muscle for each animal.

#### *Faxitron X-Ray Analysis*

Digital radiographs (Faxitron MX-20 Digital; Faxitron X-ray Corp.) of the defect region in the femur were performed at an exposure time of 15 s and a voltage of 25 kV. Animals received X-ray imaging at 2, 4, 8 and 12 weeks post-surgery.

#### *MicroCT Analysis*

MicroCT scans (VivaCT 40, Scanco Medical) were performed at 38.0 µm voxel size at a voltage of 55 kVp and a current of 109 µA. Scans were taken at 4 and 12 weeks

post-surgery. Bone tissue was segmented by application of a global threshold corresponding to 386 mg hydroxyapatite/cm<sup>3</sup> (roughly 50% of the native cortical bone density), and a low-pass Gaussian filter (sigma = 1.2, support=1) was used to suppress noise. Samples were contoured and evaluated over 146 slices taken from a central region within the defect in order to normalize between samples without including cortical bone. *Ex-vivo* analysis over the entirety of the defect region was also performed and showed the same differences among the groups as the *in vivo* data at 12 weeks.

### *Biomechanical Analysis*

Animals were euthanized by CO<sub>2</sub> inhalation 12 weeks post-surgery. This time point was chosen based on previous publications demonstrating that bone apposition reaches a plateau by this time [150]. Torsional testing was performed on extracted femurs. The femurs were cleaned of soft tissue and the ends potted in mounting blocks using Wood's metal (Alfa Aesar, Wood Hill, MA). After removal of the fixation plate, the specimens were tested (ELF 3200, Bose ElectroForce Systems Group, Minnetonka, MN) at a rotational rate of 3° per second. Maximum torque was measured at the failure point from the torque-rotation data. Torsional stiffness was calculated by fitting a straight line to the linear portion of the curve before failure.

### *Histology*

Histological analysis was performed at 12 weeks post-surgery on extracted quadriceps muscles and femurs. Samples were perfusion fixed then immersion fixed for 48 h at 4 °C with 10% neutral buffered formalin. Following paraffin processing, 5 µm-thick cross-sections were cut and stained with hematoxylin and eosin (H&E) or Masson's Trichrome (for muscle/fibrosis). Bright-field images were obtained with the

Axio Observer.Z1 microscope (Carl Zeiss, Thornwood, NY). Images were taken at 4x and 10x magnification using the AxioVision software (Carl Zeiss, Thornwood, NY).

## 7.4 Results

### 7.4.1 Microvascular Construct around the Bone Defect

#### *Early revascularization at 1 week post-injury*

Early revascularization was analyzed at 7 days post-injury and showed a significant increase in vascular volume of the leg in the microvessel/myoblast-treated group compared to the MV- group (Figure 37A). Despite the increased vascularization, representative images of the axial view of the thigh show that few vessels were present near or around the bone defect where the microvessels were implanted in the MV+ group (Figure 37B).

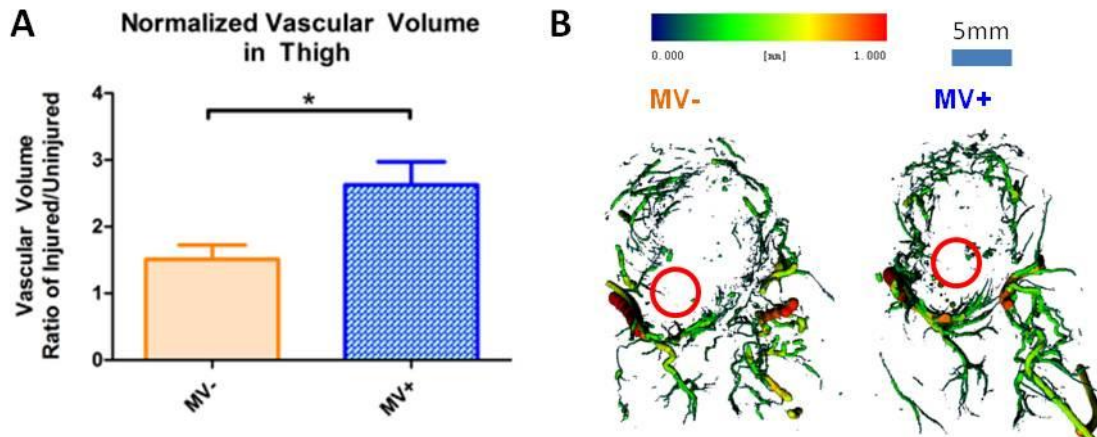


**Figure 37: Early Revascularization of Thigh near the Defect Area after Microvascular Treatment around Mesh.** CT angiography showed an increased normalized vascular volume in the thigh in the microvessels group (MV+) compared to the group without microvessels (MV-) (A). Representative images of the vasculature (B) showed that any increased vasculature in the MV+ group was not centered around the bone defect area (indicated by the red circle). Heat map shows thickness of vessels. \* $p < 0.05$ ,  $n = 6$ .

#### *Bone Regeneration*

At 8 and 12 weeks post-injury, micro-CT scans showed the MV- group had a significantly higher mineral volume compared to the MV+ group (Figure 3A). Representative radiographs supported the micro-CT data, showing a completely bridged defect in the MV- group and only a partially bridged defect in the MV+ group.

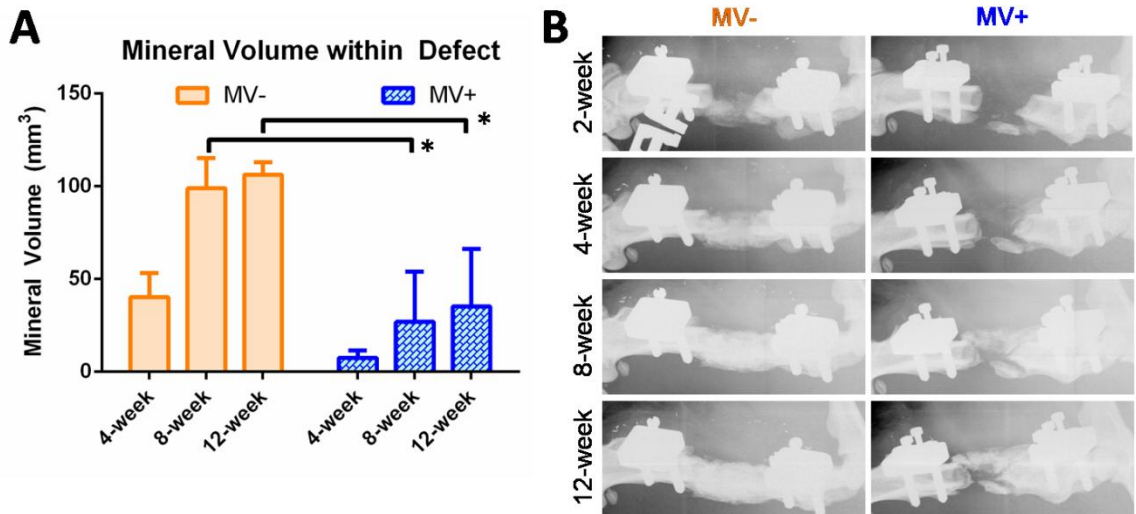


**Figure 38: Longitudinal Analysis of Bone Regeneration after Microvascular Treatment around Mesh.** (A) micro-CT scans showed significantly decreased mineral volume in the microvessels group compared to the alginate only group at 8 weeks (\* $p < 0.05$ ,  $n = 2-3$ ). (B) Radiographs showed full bridging in the alginate only group and partial bridging in the microvessels group by 8 weeks.

#### 7.4.2 Microvascular Construct in the Quadriceps Defect

##### *Early revascularization at 1 week post-injury*

CT angiography showed no difference in thigh vascular volume between the microvessel/myoblast-treated quadriceps group and the empty quadriceps defect group (Figure 39). Representative images of the microvessel/myoblast-treated (MV+) and empty (MV-) quadriceps defect groups do not show any obvious differences between the two groups.

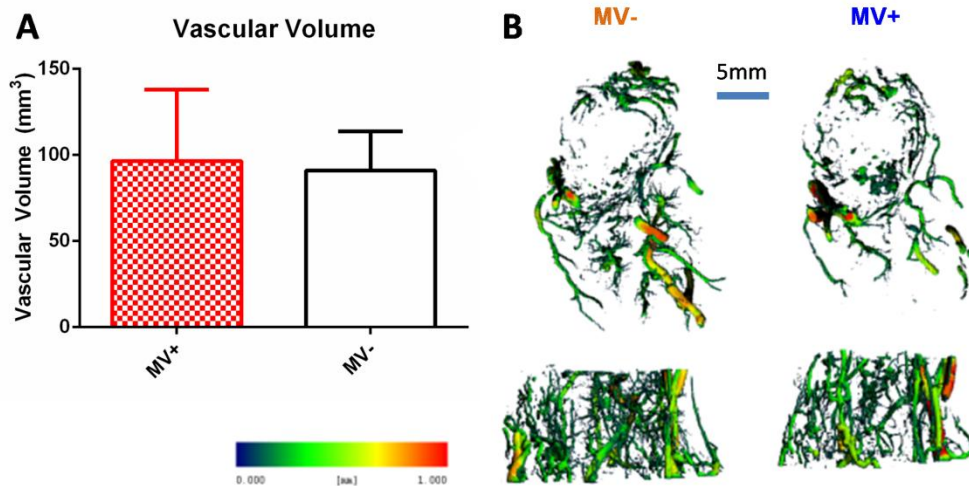


**Figure 39: Early Revascularization of Thigh near the Defect Area after Microvascular Treatment in the Quadriceps.** (A) CT angiography at 1 week post-injury showed no difference in thigh vascular volume in the microvessel/myoblast-treated and empty quadriceps defect groups. (B) Representative images of the microvessel/myoblast-treated (MV+) and empty quadriceps defect (MV-) groups are shown.

### *Bone Regeneration*

Longitudinal  $\mu$ CT quantification of mineral volume within the center of the bone defect showed no differences between the microvessel/myoblast-treated quadriceps group (MV+) and the empty quadriceps defect group (MV-) (Figure 40A). However, the mineral volume average was consistently higher in the MV+ group compared to MV-, as shown by representative radiographs at 2, 4, 8, and 12 weeks post-injury (Figure 40B).

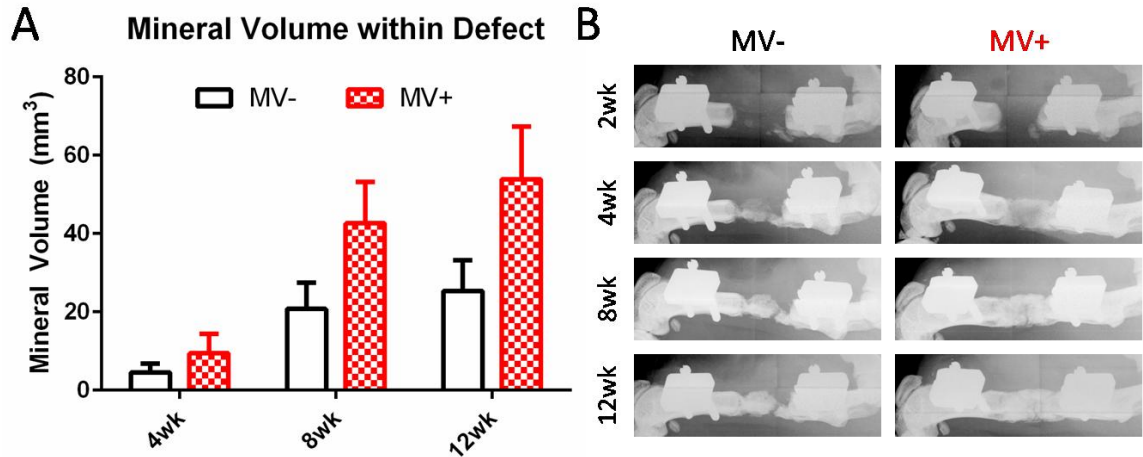


**Figure 40: Bone Mineral Volume and Radiograph Images after Microvascular Treatment in the Quadriceps.** (A) No significant differences were found in bone mineral volume between the microvessel/myoblast treated group (MV+) and the empty quadriceps defect group (MV-), though the MV+ group consistently had a higher mineral volume average at all time points. Representative radiographs (B) show bone formation at 2, 4, 8, and 12 weeks post-injury. n=3

Mechanical testing of the regenerated bones showed very similar results to the bone mineral volume measurements. Though the MV+ group had higher averages for failure strength (Figure 41A) and torsional stiffness (Figure 41B), these differences were not significant.

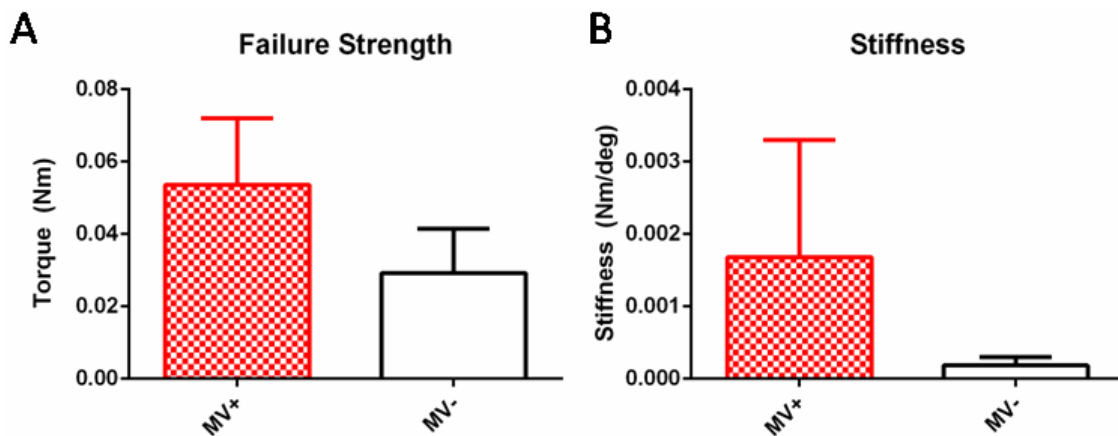


**Figure 41: Bone Postmortem Biomechanical Properties after Microvascular Treatment in the Quadriceps.** No significant differences were found in failure torque

(A) and torsional stiffness (B) between the microvessel/myoblast treated group (MV+) and the empty quadriceps defect group (MV-). n=3

### *Muscle Regeneration*

The contralateral uninjured control quadriceps muscles had a significantly higher muscle force and mass when compared to the microvessel/myoblast-treated quadriceps (MV+) group and the empty quadriceps defect (MV-) group at 12 weeks post-injury. The MV+ group had a significantly higher muscle mass compared to the MV- group, though muscle force between the two groups were not significantly different (Figure 42A, B). The MV+ group performed at about 30% of the contralateral control while the MV- group performed at around 10% of the contralateral control (Figure 42C). Similarly, the muscle mass in the MV+ group was 60% of the contralateral uninjured control while the muscle mass in the MV- group was 40% of the control (Figure 42D). Representative post-mortem images of the quadriceps muscles in both groups showed a noticeable difference in the size of the treated (MV+) versus untreated (MV-) quadriceps muscles (Figure 42E).

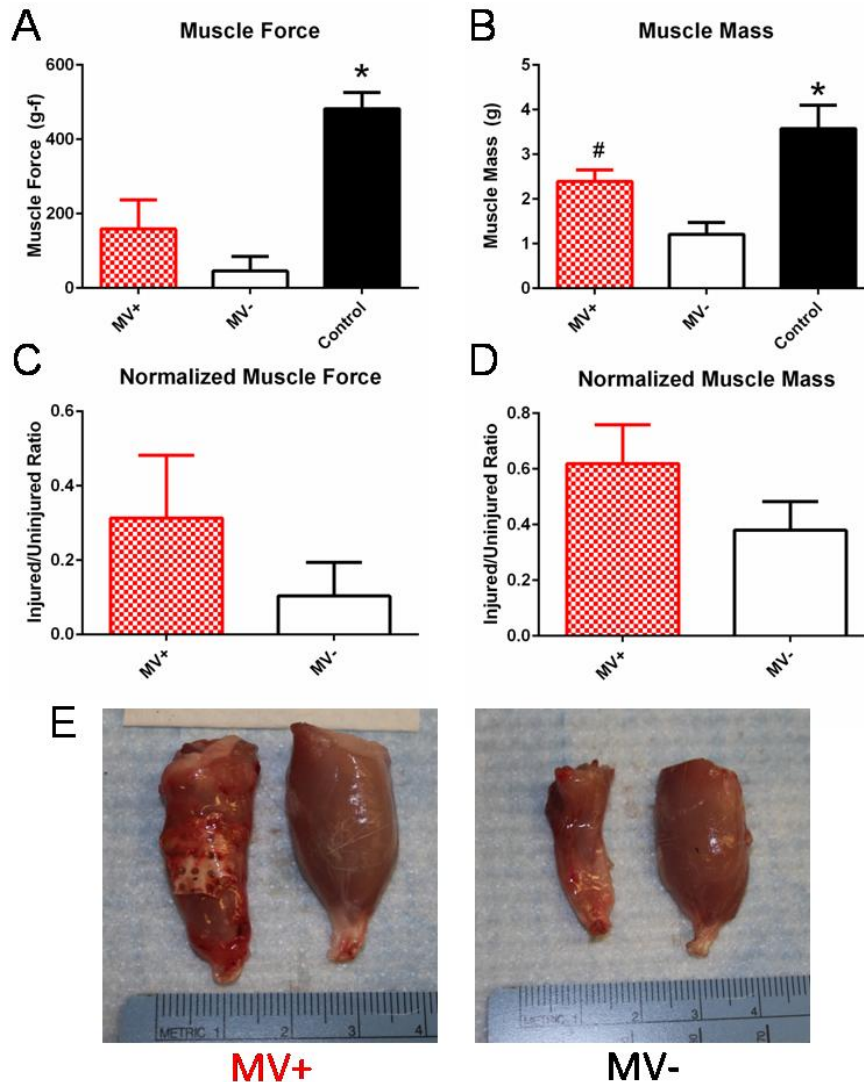


**Figure 42: Muscle regeneration after Microvascular Treatment in the Quadriceps.** Contralateral uninjured controls had significantly higher muscle force (A) and mass (B) compared to the microvessel/myoblast treated (MV+) and empty defect groups (MV-). The MV+ group had a significantly higher muscle mass compared to the MV- group. No significant differences were found in normalized muscle force (C) and muscle mass (D) between the microvessel/myoblast-treated quadriceps (MV+) and the empty quadriceps defect group (MV-). Representative postmortem images of the quadriceps muscles in both groups are shown (E). \* $p < 0.05$  compared to MV+ and MV-. # $p < 0.05$  compared to MV-.  $n = 3$  for injured groups,  $n = 6$  for controls.

## 7.5 Discussion

This work, to our knowledge, is the first to test microvascular construct treatment of composite bone and muscle defects. These microvascular constructs were first tested

for their regenerative potential positioned around the nanofiber mesh that is placed around the bone ends, enveloping the bone defect area in the place of the resected periosteum. The periosteum contributes greatly to bone repair, providing cellular, vascular, and structural support to the defect or fracture site [232-234]. The microvascular construct, though comprised of different cells and structure, can mimic a periosteal substitute, providing vasculature and cellular components for bone regeneration.

Microvessels are known to inosculate within a week when embedded subcutaneously in mice [204]. Our micro-CT angiography data suggest that our implanted microvascular networks surrounding the mesh did not fully inosculate, as there was a lack of vessels around the bone defect at day 7 even in the microvessel treated group. However, the microvessels did still have an overall effect on revascularization of the leg. It is likely that this increase in local vascularity, more so in the surrounding muscle than in the bone defect, could be a result of the paracrine effects of the implanted microvascular networks, influencing endogenous cell recruitment and angiogenesis.

CT measurements of mineral volume suggest that the microvascular constructs around the mesh may actually impede rhBMP2-mediated bone regeneration rather than facilitating it. Three plausible mechanisms can be proposed to explain this seemingly paradoxical observation: 1) The presence of the collagen matrix around the defect may deter or alter the release kinetics of rhBMP-2, disturbing the beneficial chemotactic, proliferative, and morphogenetic effects of the rhBMP-2. 2) The increased local blood perfusion in the surrounding muscle through the inosculated or newly formed microvascular networks could facilitate the local clearance of rhBMP-2 from within or

nearby the bone defect site, thus decreasing its bioavailability at the defect site. 3) The microvessels around the mesh may take up and use the rhBMP-2, which is known to induce formation of mature vascular systems, to create an amplified secondary pro-vascularization milieu, thus leaving insufficient quantities of rhBMP-2 to drive osteogenesis [235]. Further studies into the release of rhBMP-2 from the microvessel-impregnated construct will allow more insights into the proposed mechanisms. Thus, while we have shown a positive effect on early vascularization of the limb with the microvascular constructs, our hypothesis that this vascularization may aid tissue regeneration was rejected, possibly due to altering rhBMP-2 release kinetics *in vivo*.

We next tested an alternative method of incorporating microvascular networks that minimizes interference with rhBMP-2 release in this model by incorporating the microvascular construct within the quadriceps volumetric muscle loss injury. Clinically, muscle flaps are often used to cover bony injuries and defects, contributing cells, cytokines, growth factors, and a vascular supply for bone regeneration [35]. Additionally, studies have shown that intact muscle is more effective at promoting bone repair than injured muscle, suggesting that muscle regeneration within a composite defect may contribute to bone regeneration [8, 9].

Contrary to our hypothesis, the microvascular + myoblast constructs implanted into the quadriceps defect space did not result in an increased vascular volume at day 7 post-injury. Though networks were formed *in vitro* with the co-culture of microvessels and myoblasts in the collagen gel, these networks were not detected in the micro-CT angiography used to analyze vasculature at early time points. While it may be possible that the vascular networks are not inosculating, previous work (in Section 4.2) implanting

the microvessel/myoblast constructs into muscle defects resulted in an increased vascular volume, suggesting that these constructs do inosculate when implanted into damaged muscle. Limitations of the micro-CT angiography technique may also mask any differences in vascular volume with or without treatment. In this particular model, the vessels near and around the bone and quadriceps defects tend to be leaky, most likely due to a large amount of vasculature damage from creating the defects. Due to this, the contrast agent may escape the vasculature during perfusions at early time points, causing artifacts that artificially alter the vascular volume data. However, differences in vasculature are best seen in early time points, particularly within the first week of injury. For these reasons, we performed our micro-CT angiography at day 7. Though vascular volume in the composite defect was catching up to the bone defect only group by day 7 in our previous study, thereby making it difficult to detect differences between treated or untreated composite defect (in Chapter 3.2), day 3 micro-CT angiography tends to result in artifacts substantial enough to affect the vascular volume readings.

It is also possible that the implanted microvascular construct may have trouble surviving in the harsh environments around the defect site. As mentioned earlier, the microvascular constructs around the mesh may not have fully inosculated, suggesting that graft survival may be challenging. The large bone and muscle defects tend to result in large hematomas or edemas, as previously seen via MRI scans of the leg [176], which may act as a barrier to inosculature of the microvessels to the surrounding host vasculature. Additionally, it has been that in this segmental bone defect model at day 7, CD68-positive macrophages were present along with polymorphonuclear cells, indicating a large inflammatory response to the defect [236]. These inflammatory cells are likely to

be releasing cytokines, though the exact composition of this mixture is currently unknown within our bone defect. The presence of inflammatory cells and signals may create an environment that is not conducive for survival of all the microvascular fragments in the construct.

Despite the similar early revascularization between the microvessel/myoblast treated (MV+) and untreated (MV-) quadriceps groups, the MV+ group resulted in higher mineral volume averages, bone mechanical properties, muscle mass and function averages. None of these differences are significant, possibly due to the small sample size in the pilot study (n=3, post hoc power analysis showed a power of 0.45 at 12 weeks). However, these results are encouraging and suggest that the MV+ group is having a therapeutic effect on both the muscle and bone tissues. Though early vascular volumes were significantly increased in the MV+ group, there may be vascular or paracrine effects provided by the microvessels or myoblasts that could induce an endogenous response at the defect site. Also, the microvessels and myoblasts were delivered in a space-filling collagen gel, which may act as a conduit for endogenous cells to migrate into the defect space. Though this study did not have a collagen-only control, other studies have shown that collagen-only constructs do not induce increased vasculature or healing in the defect area, suggesting that the collagen by itself would not have resulted in such a large regenerative response [205]. The myoblasts within the constructs may also be contributing directly to muscle or bone regeneration by differentiating into myofibers that can fuse with endogenous cells or into osteoblasts that can aid in mineralizing bone. Further studies and histology at early time points will be needed to confirm whether the myoblasts are contributing to bone regeneration directly or if the contribution is through

regenerating the muscle and thus providing enough vascularization or cells in the muscle bed to facilitate bone regeneration.

In the attempt to facilitate regeneration of two different tissues, it is important to note that these two tissues may send contrasting signals to the graft that may deter the regeneration of the other tissue. For this study, rhBMP-2 was delivered in an alginate hydrogel within the bone defect to improve bone mineralization and healing, as has been shown in previous studies [10]. However, rhBMP-2 has an osteogenic effect on satellite cells and has been shown to suppress myogenic differentiation and deter the myoblasts from myotube formation [237, 238]. In this study, rhBMP-2 was delivered at a very low dose (1µg per defect), which may have been beneficial for determining the myogenic potential of the microvessel/myoblast constructs.

Large, multi-trauma injuries are challenging to heal in the clinic and often result in complications or functional deficits in the affected limbs. Our study analyzes the treatment of a very challenging composite injury with a vascular approach surrounding the bone, acting like a periosteum substitute, or within the muscle defect, similar to a muscle flap substitute. While this vascular approach can aid in counteracting the delayed revascularization in the defect space depending on the treated location, regeneration of the bone and muscle tissues did not seem to be wholly dependent on the revascularization of the defect. These results have implications on delivering biological components concurrently with the clinically available BMP2 used for bone fusion and repair of multi-tissue traumatic wounds to the extremities.

## CHAPTER 8 SUMMARY AND FUTURE DIRECTIONS

### 8.1 Overall Summary

Traumatic wounds to the extremities pose a serious challenge in the clinic. While recent advancements in reconstructive surgery have aided in reducing the number of complications in treating these traumatic wounds, large functional deficits still exist years after treatment, resulting in lowered quality of life and debilitating disabilities that sometimes prevent patients from returning to their original professions. In 2008, the Armed Forces Institute of Regenerative Medicine (AFIRM) was created as a federally-funded institution within the Department of Defense to direct the investigations of clinical therapies for military medical needs. One of the areas of research that benefit the therapy of injured soldiers is limb reconstruction, regeneration, and transplantation. With the increasing use of body armor and the rise in use of improvised explosive devices (IEDs) in recent US conflicts, military injuries are progressively dominated by traumatic injuries to the extremities with large defects within the muscle and bone. In a recent study by Cross et al. evaluating the records of wounded service members that were deemed unfit to continue serving, 76% of the injured had an orthopedic diagnosis that was the primary unfitting condition, indicating that orthopedic-related injuries often lead to disabilities that have a significant impact on the patient's well-being [239]. These data highlighting the high incidence of disability and lack of functional recovery underscore the importance of developing tissue engineering strategies to focus on improving functional outcomes.

Despite the need for therapeutic alternatives to the current clinical treatments, few therapies exist that can aid in healing such large complex injuries, and even fewer are

robust enough to be translated into the clinic. Additionally, while much research has been conducted in the field of tissue engineering/regenerative medicine (TE/RM) on single tissue injuries, very little research has delved into the complicated task of regenerating multiple tissues simultaneously, as would be necessary in traumatic extremity injuries. Thus, the main objective of this project is to examine the regenerative potential of engineered matrix constructs and stem cells on composite bone & muscle defects. The central hypothesis was that stem cells delivered on engineered matrix constructs into the muscle defect will aid in muscle regeneration and promote bone healing, ultimately resulting in superior functional limb recovery.

This dissertation first focused on the development and characterization of preclinical models that reproduce the challenging injuries seen in the clinic (Aim 1, Chapter 3.1 & 3.2). Our lab has previously developed a critically-sized segmental bone defect in the femur of a rat, which has been shown to heal to intact bone strength when treated with 5 $\mu$ g of rh-BMP-2 in a hybrid delivery system consisting of a macroporous cylindrical nanofiber mesh made of polycaprolactone and RGD-functionalized alginate that can be injected into the lumen of the mesh [10]. In this dissertation, we created a model of volumetric muscle loss (VML) in the quadriceps muscles of the rat, injuring all four muscles in the quadriceps (Aim 1, Chapter 3.1). Muscle autografts were tested in this model and were found to be insufficient for functional healing of the quadriceps defect, similar to clinical outcomes for VML injuries. We then combined this VML model with the segmental bone defect to create a composite injury model in which a large section of bone and muscle are resected to reproduce the injuries associated with severely injured limbs (Aim 1, Chapter 3.2). We demonstrated that this new preclinical model

recapitulated features of the compounded functional deficits that are commonly observed in polytraumatic injuries clinically. Additionally, further characterization of this composite defect model revealed a possible role of early revascularization in the healing of the bone defect. Thus, with this aim, we presented two new platforms on which to test tissue engineering strategies as well as biological models to study the interplay between the healing of muscle and bone tissues.

From the first aim of this dissertation, it was found that the quadriceps VML model was difficult to heal, even with autograft treatment. While this was beneficial in emulating the injury characteristics of a clinical VML wound, the challenging nature of the wound, due to the injury of multiple muscles and the possible injury of blood vessels and nerves, could preclude regeneration from tissue engineering constructs not designed to fix so many types of tissues. Thus, we developed a simplified VML model within the biceps femoris of the rat whereby one single planar muscle was injured with less damage to vasculature or nerves (Aim 2, Chapter 4,1). This model included both a negative control for regeneration (empty defect) that exhibited little to no regeneration of muscle fibers at the center of the defect as well as a positive control for regeneration (autograft), in which an autograft sutured in the center of the defect resulted in healthy muscle tissue after 4 to 8 weeks post-injury. From this model, we further investigated into possible differences between the negative and positive controls for regeneration and found a distinct difference in the revascularization of the defect site. While both the empty defect and autograft-treated defect muscles had a higher vascular volume than uninjured contralateral control muscles, the autograft-treated defect muscles had a significantly higher vascular volume than the empty defect.

We further investigated the effect of revascularization of the VML defect site by implanting a preformed microvascular network within the biceps femoris defect (Aim 2, Chapter 4.2). While this microvascular network quickly inoscultated with host vasculature and resulted in an elevated vascular volume compared to the empty defect and uninjured control, the effects of the vascularization on muscle regeneration were harder to discern. The microvascular treatment resulted in the formation of a large amount of fatty tissue in the defect space within the first month of recovery that eventually remodeled away to leave thin, fibrous tissue in the center of the defect space. Thus, while we were successful in inducing an increased vascular response at early time points after injury, the vasculature was not sufficient to promote muscle regeneration.

As mentioned in Aim 1, characterization of the composite injury model in which both muscle and bone were damaged showed a difference in early revascularization of the leg in the composite injury that may have led to attenuated bone formation. Thus, we developed two vascular constructs that could be used to substitute two important tissues that are crucial in the healing of traumatic limb injuries (Aim 3, Chapter 5). First, a microvascular construct was developed around the nanofiber mesh, surrounding the bone defect area, similar to a periosteum substitute. Second, a microvascular construct was developed to sit within the quadriceps defect, similar to a vascularized muscle flap that is commonly used to treat open fractures in the clinic. While the microvascular construct placed around the bone defect area resulted in an increase in vascular volume at day 7 post-injury, the construct seemingly deterred bone regeneration and resulted in less mineral volume than the untreated composite defect. This is most likely due to the effects that this microvascular construct around the bone had on the release kinetics of BMP-2,

suggesting that the BMP-2 in this case had a larger effect on bone regeneration than the microvascular construct itself. In contrast, the microvascular construct that acted as a vascularized muscle flap did not result in an increase in early revascularization, but it did increase the averages of mineral volume, bone function, and muscle function, though not by a statistically significant amount within the pilot study (n=3). These results suggested that while these microvascular networks could provide faster revascularization to the defect areas, the vascular networks alone may not be enough to aid in tissue regeneration.

Overall, this dissertation presented multiple preclinical platforms for testing tissue engineering strategies as well as models that can be used to gain insights on the healing of VML and composite VML/bone defects. From some of these insights gained on the vascularization of the defect sites, a vascular treatment strategy was tested within these platforms and shown to have varying results in the treatment of complex multi-tissue injuries.

## **8.2 Development and Characterization of Preclinical Models that Reproduce Traumatic Limb Injuries**

In the attempt to develop and design tissue engineering strategies that can aid in regenerating musculoskeletal injuries, preclinical models must first be developed to test these therapies. While few volumetric muscle loss models existed at the start of this dissertation work, the field has quickly expanded in the last five years, with more than a dozen articles published in developing and treating VML models. In the majority of the developed VML models, the size of the defects have been relatively small, with the removal of 50-100mg of muscle in rat models. Our quadriceps VML model, in contrast, involves the removal of 250-400mg of muscle, resulting in a very large defect in a very

large muscle. Likewise, our muscle function data showed a larger loss in function than any other VML models that currently exist. Additionally, we analyzed the regenerative potential of administering an autograft within the defect, expecting the muscle to heal with the treatment as has been previously shown [41]. Instead, we found that the graft did not result in functional recovery of the muscle, emphasizing the severity of the muscle defect that we have created.

These results highlight the importance of defect size. In muscles of relatively small size, such as a mouse extensor digitorum longus muscle, the entire muscle can be removed, minced, and replaced within the muscle bed and regenerate within 4 months [41]. In contrast, our muscle treated with a minced autograft showed very little regeneration, with a reduced cross-sectional area and only half the strength of the uninjured contralateral control. It is well known that animals of smaller size, such as rodents, have a much quicker healing response to relatively large injuries. Thus, when therapies move from a rodent model to a larger animal model, few therapies demonstrate the same regenerative response in the larger animal. Likewise, this study showed that the size of the muscle defect matters. While smaller sized defects could possibly heal with an autograft treatment, a larger sized defect may not have the same regenerative response. This presents a very interesting scientific question: if a certain therapeutic induces a regenerative response in a small VML, would the same therapeutic induce the same response in a larger VML? It would be very beneficial and cost-efficient if a therapeutic can be tested within larger defects within rodent models before moving on to testing in large animal models.

Our characterization of the quadriceps VML model showed the formation of a hematoma and/or edema as visualized by MRI. This is a normal response that provides a biological matrix with which the body can start healing, and it is an important consideration in investigating the regeneration of different tissues. While a hematoma may be beneficial in fracture healing and bone regeneration [240], edemas and hematomas may cause swelling and compartment syndrome in muscle injuries, which results in pain and possible ischemia if not treated [241]. Thus, while hematomas may bring inflammatory cells, cytokines, and growth factors to the site that may aid in tissue regeneration, an excessive amount of hematoma/edema that results in massive swelling may occlude perfusion of blood, cells, and nutrients to and from the injury site.

While the literature in the VML field has expanded dramatically in the last few years, few models exist that include simultaneous bone and muscle injuries. Of the few that exist, none have been used to test new therapeutics for regenerating the tissues. Instead, the models are used to gain insights into crosstalk between muscle and bone healing. The main purpose of developing our model was to determine the effects of treating the defects in an effort to improve treatment strategies in traumatic limb injuries in which functional recovery is often poor. Thus, we focused on developing functional outcome analyses such as maximal tetanic force testing to determine muscle function and torsional tests to determine bone function.

Our composite injury model supported observations that have been made in the clinic; the addition of a muscle injury to a bone injury deters bone regeneration, thus validating the model. The muscle is considered a "secondary periosteum" and provides cellular, molecular, and structural support to bone healing. The periosteum is regarded as

an important factor in fracture healing, and periosteal stripping significantly decreases blood flow to fractures and thus impairs fracture healing [242]. In our model, with the removal of both the periosteum and the "secondary periosteum," a large amount of vascular supply and cells are resected, leaving a large avascular void that the body must fill. From histology, the quadriceps muscle seemed to collapse on itself and shrunk in cross-sectional area, thereby affecting its function that is closely related to the muscle structure. This may be the body's response to the reduced vasculature and its way of protecting the tissue from necrosis. Without a nearby vascular supply, bone healing was likely reduced, thereby partially causing the attenuation of rhBMP-2-mediated bone regeneration in our model.

In further characterizing the composite model, we discovered an important insight that was crucial in determining our treatment strategy for aim 3. The composite injury revascularization occurred slower than the bone injury alone. Though this difference was mainly evident within the first week of injury, the vascular profile and maturity within the bone defect were different at 2 weeks post-injury. These data supported the idea that vascularization plays a pivotal role in tissue regeneration [11]. Size, again, may play a role in this difference in revascularization. While the bone defect resulted in a void which must be filled through vascularization to avoid necrosis in the center of that void, the addition of the muscle defect doubled the volume of that void, thereby delaying the vascularization into the empty spaces. We further explored the effects of vascularization on tissue regeneration by developing and testing a vascular treatment in the composite model in the third aim.

### 8.3 Pursuit of a Critically-Sized VML Model

Because the field of volumetric muscle loss injuries is still relatively new, no set standard exists to define the exact size or severity of a VML injury. VML defect sizes in the rat range from 50 to 300mg in mass. In contrast, the bone regeneration field has a set standard for a critically-sized defect, in which any defect equal or greater than critical size would lead to capping of the bone ends and very little regeneration within the defect space. This allows for some standardization of the size of defects, which as mentioned before, plays a large role in the degree of tissue regeneration that may occur after injury. Likewise, a muscle defect should be deemed "critically-sized" if the center of the defect shows no signs of regeneration, with a "capping" of muscle at the edges of the defect.

No published VML model has exhibited this type of capped healing. On the other hand, our biceps femoris defect model gives a glimpse of what a "critical size" in the volumetric muscle loss field might look like. In the empty defect group, the biceps femoris VML resulted in minimal regeneration, with no evidence of myofibers present in the center of the defect even after 8 weeks post-injury. This, in part, is due to the fact that this injury is a full-thickness defect with no connected nearby muscles to contribute to its healing. Though we decided to use a 12-mm biopsy punch to create this biceps femoris defect in order to match the defect mass of the quadriceps defect, this 12-mm punch may be larger than needed to create a "critically sized" muscle defect. It would be useful for the field if various sizes of muscle defects were tested in order to define such a "critical size" so that various treatments can be tested and compared in different VML models. Since the biceps femoris model already exhibits signs of a "critically-sized" defect, a logical progression would be to test different sized biopsy punches to create varying

VML sizes in the biceps femoris to determine if there is a size at which the muscle can heal.

The reason for defining a "critical size" for a defect is again due to the fact that size considerations play a big role in the healing and regeneration of tissues. Not only does the size of the defect affect the amount of material and cells that need to encompass the created empty space to heal it, size also affects mass transfer properties and the amount of vascularity needed to provide nutrients to the tissue formed within the defect. The same therapeutic that may be able to regenerate one VML defect may not be able to regenerate a different sized defect. As mentioned before and confirmed by the differences in regeneration with minced autograft treatments of different VML models, testing treatments in different sizes of defects may give some insights to whether or not a treatment could work in a large animal model or in humans.

Though the biceps femoris VML model seems to present a suitable "critical size" defect based on histology, the lack of muscle functional data may preclude its use in testing therapeutics. While *in vivo* measurements of biceps femoris function have been plagued by large variability that occluded differences between the negative and positive controls for muscle regeneration, an *ex vivo* method in which a strip of muscle from the center of the defect site could possibly allow for functional readings that support the histological data. However, developing an *ex vivo* method is a big challenge. Because *ex vivo* testing would be conducted on a smaller sub-section of the muscle, small differences in the isolation of the tissue for functional testing could lead to large variability in the data. It would be difficult to standardize the exact number of myofibers isolated for the testing, which may contribute to the variability of the functional *ex vivo* data. The exact

location from which the muscle strip is taken from may also have a large influence on the functionality. Despite these challenges and possible increased variability in measurements, the testing of *ex vivo* muscle strips from the defect site should result in a larger difference between the positive and negative controls, since all myofibers not included within the defect could be excluded from the reading. Thus, for the biceps femoris model, further research and work could result in the development of a functional assay of the regenerated muscle (or lack thereof) at the defect site.

#### **8.4 Challenges in the Use of Microvascular Constructs for Regeneration of Musculoskeletal Tissues**

This dissertation demonstrated proof of concept that microvascular constructs, with or without myoblasts, are able to affect tissue regeneration in large extremity injuries. However, when these microvascular constructs were tested in three distinct ways in two different models (the biceps femoris VML and the composite model with a quadriceps VML combined with segmental bone defect), three different healing responses occurred. This section outlines a series of challenges that must be overcome before microvascular constructs can be a viable treatment in the healing and regeneration of musculoskeletal defects.

Microvascular constructs are comprised of viable tissues that are isolated from various animals and pooled into groups to minimize animal to animal variability. This variability presents various problems, as different animals may contribute different tissues that can have different potentials in grafting and regeneration. As mentioned in Aims 2 and 3, the microvascular constructs resulted in varying degrees of revascularization and muscle regeneration. While some of this may be due to the location

at which the microvascular constructs are implanted, some of these differences in host response may be due to the variability of the microvessels themselves. The microvessel isolation protocol, though optimized through repeated isolations and trials with different collagenase lots, mincing time, and digestion time, may need to be re-optimized if the characteristics of the isolated tissues vary. Thorough studies into plausible sources of variability may provide insight into the system that could allow for better control of the variability within the microvessel isolation and growth.

Possible causes for this variability may include age and gender. Age has been shown to influence vascularization in fracture healing, and it may very well have an effect on microvessel growth *in vitro* and inosculation *in vivo* [243]. A thorough study on the effects of age on the proliferation and networking of microvessels may help to isolate a possible cause of the variable effectiveness of the microvessels. Though we isolated microvessels from adipose tissue from male rats, this tissue could also be isolated from female rats as well, which may could influence the growth and characteristics of the microvessels. Estrogen is known to influence smooth muscle cells and endothelial cells in vasculature and can regulate vascular cell growth and migration, at least in humans [244-246]. Thus, the gender of the animal from which microvessels are isolated may also affect their growth and networking *in vitro*. Other relevant causes for microvessel isolation variability may include human variability in the mincing and digesting of the microvessels. However, these aspects of the isolation process could be standardized through the use of machines, thereby minimizing the variability in human actions.

In this dissertation, the microvascular constructs were grown for the same amount of time *in vitro* prior to implantation into the animal. However, if different batches of

microvessels grow at different rates, this may not be the ideal way of standardizing the implanted constructs. For example, it was necessary to reduce the microvascular growth time *in vitro* when completing experiments involving both microvessel-only constructs and microvessel + myoblasts constructs because the addition of myoblasts sped up the growth and subsequent contraction of the constructs. A superior method of standardizing the vascular networks implanted *in vivo* would be to quantify the vascular networks *in vitro* and to implant constructs with similar connectivity and growth. However, this method would be impractical and was not explored within the purview of this dissertation.

Within the composite injury model, rhBMP-2 was delivered in the bone defect to aid in bone regeneration. However, this may have adverse effects on the microvessels and/or myoblasts that are delivered nearby, as BMP-2 may cause myoblasts to differentiate down the osteoblastic lineage or prevent myotube formation [237, 238]. Additionally, microvessels themselves could influence the mechanism by which rhBMP-2 is inducing bone regeneration *in vivo*. Further research into the interplay between rhBMP-2 and microvessels could help explain the differences in healing responses seen when implanting the microvessels around the bone defect or in the muscle defect.

Because microvascular constructs provide a vascular therapy and thus necessitates analysis of the revascularization of the defect, the analysis method and timing greatly influences the chances of identifying the effects of the vascular therapy on vascularization. While micro-CT angiography is advantageous in that it allows for a method of quantifying and imaging vasculature, it has various limitations. The resolution for the micro-CT angiography method is determined by the resolution of the micro-CT

scan, which is linked to the sample size. We scanned whole rat legs in these studies, necessitating the use of a 37 $\mu$ m voxel size. However, if the tissue could be dissected into smaller parts and scanned, a higher resolution could be achieved. The resolution of the vasculature also depends on the contrast agent's ability to pervade into the vasculature. We used microfil contrast agent, which has a certain viscosity that may prevent its ability to flow into capillaries and small arterioles. It would be possible to perfuse the vasculature with barium sulfate, which may allow for a higher resolution of vasculature to be scanned [247]. In micro-CT angiography, the microfil contrast agent is perfused by forcing the contrast agent through the vasculature by pressure, which may result in artifacts in the scan if the pressure caused the microfil to escape leaky vessels in the healing defect. Additionally, because the contrast agent is delivered post-mortem through pressure perfusion, blood flow is not taken into account. A possible way to analyze actual perfusion within the body may be to inject fluorescent microspheres into a live animal and examine the locations of the microspheres via histology [248].

While the translation of microvascular treatment for healing of defects may have potential, large barriers exist that need to be surpassed to allow for the possibility of using microvessels in the clinic. Human microvessels have not yet been successfully grown *in vitro*, and their ability to form networks or inosculate *in vivo* have not yet been evaluated. Microvascular treatment clinically would most likely be autologous; however, it is unknown whether microvessels isolated from an ailing trauma patient with possible systemic pro-inflammatory responses to the trauma may have the same therapeutic potential as microvessels isolated from a healthy person. Additionally, the issues in variability of microvessels faced in preclinical testing, such as differing optimizations of

protocols for isolating microvessels, will also apply to isolating microvessels for clinical use. Clearly, much more research and work must be done before microvascular treatment can even be considered for clinical use.

## **8.5 Final Conclusions**

In conclusion, three models of extremity trauma (VML in quadriceps, VML in biceps femoris, and composite injury with segmental bone defect and VML) were developed and characterized. The models allow for quantitative measurements of functional outcomes in the affected tissues, making them excellent platforms for the screening of different therapeutics for functional recovery. From the characterization of these models, vascularization was found to play a role in the regeneration of the different tissues. Vascular therapy, in the form of microvascular constructs, was tested in the VML in biceps femoris and composite defect models and was found to have the ability to facilitate revascularization, though the regenerative potential was variable. Microvascular construct treatment of the quadriceps VML in the composite defect did influence bone regeneration, supporting the overall hypothesis that the treatment of muscle with engineered matrix constructs with stem cells could promote bone healing.

## APPENDIX

### A.1. Microvessel Isolation Protocol

#### A.1.1. Solutions (keep all solutions on ice or in fridge)

1x PBS (Ca and Mg free, Sigma Aldrich)

4x DMEM (GIBCO, with HEPES and NaHCO<sub>3</sub>)

1x DMEM (low glucose, with pyruvate)

BSA (Sigma Aldrich)

FBS (10% in 1x DMEM, used as culture media)

Petri dish (non-TC treated)

0.1% BSA PBS (cation free) – sterile filtered

1N NaOH – syringe filtered in 50mL conical

1N HCl – syringe filtered in 50mL conical

Collagenase Type I (Clostridial collagenase, Worthington Biochemicals)

#### A.1.2. Preparation of Collagenase

- Test lots of collagenase with empirical microvascular yield and quality assessment of in-vitro culture testing. Buy in bulk the selected lot (4-5grams).
- Total volume of digestion solution is about 1.5 times the fat volume in mL.
- Measure out lyophilized collagenase: 2 times the fat volume in mg.
- Measure out DNase: 1.5 times the fat volume in mg.
- Add 1.5 times the fat volume (in mL) of 0.1% BSA-PBS to the collagenase and DNase.
- Mix and sterile filter. Prepare right before use. Add to fat at room temperature.

### A.1.3. Fat Isolation

- Materials needed:
  - Large gauze (3 per animal) – sterile
  - Straight hemostats – sterile
  - Large scissors – sterile
  - Small scissors – sterile
  - Forceps – sterile
  - 20mL 0.1% BSA/PBS in 50mL conical (per 2 rats) – sterile
  - Male rats – retired breeders (as heavy/old as possible)
- After anesthetizing the animal with isoflurane, lay the animal down in the supine position. Put pressure on the middle of abdomen area with 2 fingers and swipe down to move testes. Wipe animal well with alcohol gauze in the pelvic area.
- Grip the animal with hemostats on the skin directly at the base of the penis.
- Cut the skin below the hemostat to expose the testes. Make 2 cuts from the first cut towards each hip. This should expose the testes.
- Carefully place sterile gauze distal to the cuts. Touch only corners/edges of the gauze, fold the gauze in half, and place the gauze over the skin next to the incision.
- Using the forceps to grip the outer muscle layer of the testes and make a cut with the smaller scissors to expose the testicles. Gently draw out the epididymal fat and vessels (laying it over the sterile gauze to preserve sterility), and harvest the fat only without severing the large testicular vessels or the epididymal head/tail. Place the fat into the BSA/PBS.
- Expose the animal's thorax and induce a hemo-pneumothorax to euthanize the animal.

#### **A.1.4. Microvessel Isolation from Fat**

- From the BSA-PBS conical tube containing the fat, estimate fat volume and calculate the appropriate collagenase, DNase, and BSA-PBS amounts for the digestion solution. Prepare this prior to mincing the fat. Sterile-filter solution before use.
- Manually mince the fat pads for about 6 minutes to get a homogenous mix that can be drawn up into a 10mL pipette.
- Add the digestion solution to the minced adipose tissue and manually stir with the pipette tip to create a homogenous mix. Transfer to a small Erlenmeyer flask (50-125mL) with a small Teflon stir bar. Digest in a 37°C water bath with agitation (6 minutes, manually shaking the flask to create turbulence).
- Stop the digestion by adding serum containing cold media to the digestion solution (at least 1:1 volume).
- Transfer the digestion solution into 50mL conical tubes and spin in a clinical centrifuge at 4000 rpm for 5 minutes.
- Aspirate the supernatant and wash the pellet in further BSA-PBS. Break the pellet and re-suspend it in the new wash buffer. Transfer the solution to 15mL tubes. Spin at 3000rpm for 4 minutes.
- Repeat the previous wash step again and spin down at 3000rpm for 3 minutes.
- Aspirate supernatant and resuspend pellet in BSA-PBS. Filter through a 500µm nylon membrane. Wash the membrane with 5mL BSA-PBS. Discard the membrane and retain the flow-through.
- Filter the flow-through through a 20µm filter, and collect the microvessel fragments retained on this mesh. Wash the mesh with 40-50mL of BSA-PBS and collect the solution (10mL at a time in a petri dish). Count a representative

volume (3 drops of 20 $\mu$ L) from a well-mixed suspension (use wide-bore 200 $\mu$ L tips).

- Pellet the microvessel fragments (3000rpm for 4 minutes), re-suspend the pellet in about 50 $\mu$ L of BSA-PBS using a wide-bore pipette tip.

#### **A.1.5. Suspending Microvessels in a Collagen Gel**

- KEEP ALL SOLUTIONS ON ICE --- collagen solution at this concentration will gel and polymerize at room temperature.
- The final concentration of collagen should be 3mg/mL in 1x DMEM.
- Make about 1-2mL more collagen than needed due to losses in preparation.
- Use about 8-12 mg/mL stock collagen I (Fisher Scientific, high-concentration collagen) and 4x DMEM. Dilute to the right concentration with deionized sterile water.
- Fragment density is 20,000 fragments per mL of collagen solution.
- Check pH by color before adding fragments. Purple is too basic, orange/yellow is too acidic. Add 1N NaOH or 1N HCl to adjust the pH.
- Mix collagen, 4x DMEM, and sterile water to make the collagen solution --- keep on ice! Use frozen pipette tips if possible.
- Mix the microvessels in ~50 $\mu$ L BSA-PBS well before adding the appropriate collagen solution amount to the tube containing the microvessels. Mix this solution a few times with a frozen pipette tip.
- Transfer the collagen/microvessel solution to the culture chamber and place in incubator. Allow for 30-45minutes for polymerization.
- Add media to the culture chamber after polymerization. Change media on day 3 and every other day thereafter.
- Angiogenic sprouts should be visible by day 3, and a microvessel network should be visible by day 7.

## **A.2. Myoblast Isolation Protocol**

### **A.2.1. Solutions for Myoblast Isolation & Culture**

- Primary myoblast growth medium: F10, 20% FBS, 1% pen/strep, bFGF
- bFGF (Promega G-5071, 25µg powder) – dissolve in 1mL sterile 1% BSA-PBS. Aliquot into 50µL and store at -20°C. Use at 2µL bFGF per 10mL growth media. Don't freeze thaw.
- Differentiation medium: DMEM, 2% horse serum, 1% pen/strep.
- 0.2% Collagenase XI (Sigma C9407) – prepare lyophilized powder (100mg) in 50mL PBS, aliquot in 5mL, store at -20°C. Don't freeze-thaw. Use at this concentration.
- Dispase II (Stem Cell Technologies, 5U/mL, 100mL solution) – Dilute 1:2 to get 2.5U/mL. Aliquot 5-10mL and store at -20°C. Don't freeze-thaw.
- Collagen – Make to final concentration of .08mg/mL (dilute in .1N acetic acid).  
USE ONLY COLLAGEN-COATED FLASKS FOR MYOBLAST EXPANSION. To collagen-coat, add excess collagen solution into flask, incubate at 37°C overnight, and remove excess collagen. Can re-use this solution. Allow flask to dry in incubator, and rinse with PBS before use.

### **A.2.2. Isolation of Soleus Muscle**

- Soleus muscle has the highest density of satellite cells, though any other muscles can be isolated for the isolation of myoblasts.
- Remove skin from lower half of the leg.
- Separate the hamstrings on the posterior side.
- Remove hamstrings muscles to reveal the gastrocnemius.
- Insert the tips of a small pair of forceps at the ankle under the gastrocnemius. Blunt dissect and cut.

- Lift the gastrocnemius muscle, and the soleus muscle is underneath (large white tendon).
- Weigh the soleus muscles in a sterile container prior to transferring to a petri dish containing sterile PBS.

### **A.2.3. Mechanical and Enzymatic Dissociation of the Muscle**

- Wash the tissue by transferring (with a sterile forceps) into a 100mm dish containing sterile PBS. Repeat this 2x.
- Remove the connective/fat tissue from the muscle with sterile instruments and re-weigh.
- Add 0.2% collagenase XI (Sigma C9407, 100mg in 50mL PBS, aliquot and store at -20°C) --- use 5mL per 2 rat soleus muscles.
- Mince the tissue using two sterile razor blades for 5 minutes (sterilize razor blades by wiping with alcohol pads).
- Use a wide bore pipette tip (break off end of 5mL pipette) to transfer the contents into a 15mL sterile conical tube.
- Rinse the dish with an additional 5mL of 0.2% collagenase and transfer into conical tube (final enzyme solution volume = 10mL per 2 muscles).
- Place tube into a 37°C water bath and incubate for 2x30minutes. Triturate every 30 minutes by pipetting up and down (wide-bore pipette if necessary).
- Spin down cells (1400g for 4 minutes; 2800rpm for 15mL conical in the Guldberg cell culture room centrifuge) and aspirate off the collagenase.
- Add 3mL/animal of dispase II (Stem Cell Technologies, 5U/mL diluted 1:2 to get 2.5U/mL) and incubate at 37°C for 45 minutes. Triturate mixture after the 45 minute incubation.
- Spin down cells at 1400g for 4 minutes and aspirate off the dispase.
- Resuspend cells in 10mL prewarmed growth media.

- Pass resuspended cells through a vacuum 100µm strainer (Steriflip, Millipore).
- Spin down cells for 4 minutes at 1400g.
- Remove supernatant and resuspend in growth media with bFGF.
- Pass the resuspended extract through a 23G needle with a 10mL syringe (pull in extract and dispense extract). Dispense directly into appropriate dish for plating.
- You can also preplate the cells --- transfer cells onto uncoated dish, incubate at 37°C for 30 minutes, then transfer supernatant to a collagen coated dish.
- Maintain at 20% to 70% confluency. Change media every 2-3 days.

## REFERENCES

1. Owens, B.D., et al., *Characterization of extremity wounds in Operation Iraqi Freedom and Operation Enduring Freedom*. J Orthop Trauma, 2007. 21(4): p. 254-7.
2. Franken, J.M., P. Hupkens, and P.H. Spauwen, *The treatment of soft-tissue defects of the lower leg after a traumatic open tibial fracture*. European journal of plastic surgery, 2010. 33(3): p. 129-133.
3. Choudry, U., S. Moran, and Z. Karacor, *Soft-tissue coverage and outcome of gustilo grade IIIB midshaft tibia fractures: a 15-year experience*. Plastic and reconstructive surgery, 2008. 122(2): p. 479-85.
4. Jupiter, J.B., et al., *Treatment of segmental defects of the radius with use of the vascularized osteoseptocutaneous fibular autogenous graft*. The Journal of bone and joint surgery. American volume, 1997. 79(4): p. 542-50.
5. Melnyk, M., et al., *Revascularisation during fracture healing with soft tissue injury*. Archives of orthopaedic and trauma surgery, 2008. 128(10): p. 1159-65.
6. Claes, L., et al., *Moderate soft tissue trauma delays new bone formation only in the early phase of fracture healing*. Journal of orthopaedic research : official publication of the Orthopaedic Research Society, 2006. 24(6): p. 1178-85.
7. Landry, P.S., et al., *Effect of soft-tissue trauma on the early periosteal response of bone to injury*. The Journal of trauma, 2000. 48(3): p. 479-83.
8. Utvag, S.E., et al., *Poor muscle coverage delays fracture healing in rats*. Acta orthopaedica Scandinavica, 2002. 73(4): p. 471-4.

9. Utvag, S.E., et al., *Influence of extensive muscle injury on fracture healing in rat tibia*. Journal of orthopaedic trauma, 2003. 17(6): p. 430-5.
10. Kolambkar, Y.M., et al., *An alginate-based hybrid system for growth factor delivery in the functional repair of large bone defects*. Biomaterials, 2011. 32(1): p. 65-74.
11. Auger, F.A., L. Gibot, and D. Lacroix, *The pivotal role of vascularization in tissue engineering*. Annu Rev Biomed Eng, 2013. 15: p. 177-200.
12. Borrelli, J., Jr., *Management of soft tissue injuries associated with tibial plateau fractures*. J Knee Surg, 2014. 27(1): p. 5-9.
13. Grogan, B.F., J.R. Hsu, and C. Skeletal Trauma Research, *Volumetric muscle loss*. J Am Acad Orthop Surg, 2011. 19 Suppl 1: p. S35-7.
14. Alessandrino, F. and G. Balconi, *Complications of muscle injuries*. J Ultrasound, 2013. 16(4): p. 215-22.
15. Kao, L.S., et al., *Local variations in the epidemiology, microbiology, and outcome of necrotizing soft-tissue infections: a multicenter study*. Am J Surg, 2011. 202(2): p. 139-45.
16. Hakkarainen, T.W., et al., *Moving beyond survival as a measure of success: understanding the patient experience of necrotizing soft-tissue infections*. J Surg Res, 2014. 192(1): p. 143-9.
17. Park, J.J., et al., *Updates in the management of orthopedic soft-tissue injuries associated with lower extremity trauma*. Am J Orthop (Belle Mead NJ), 2012. 41(2): p. E27-35.

18. Machen, S., *Management of traumatic war wounds using vacuum-assisted closure dressings in an austere environment*. US Army Med Dep J, 2007: p. 17-23.
19. Mathieu, L., et al., *Soft tissue coverage of war extremity injuries: the use of pedicle flap transfers in a combat support hospital*. Int Orthop, 2014. 38(10): p. 2175-81.
20. Giannoudis, P.V., et al., *Long-term quality of life in trauma patients following the full spectrum of tibial injury (fasciotomy, closed fracture, grade IIIB/IIIC open fracture and amputation)*. Injury, 2009. 40(2): p. 213-9.
21. Castillo, R.C., et al., *Prevalence of chronic pain seven years following limb threatening lower extremity trauma*. Pain, 2006. 124(3): p. 321-9.
22. Matsuoka, T., et al., *Long-term physical outcome of patients who suffered crush syndrome after the 1995 Hanshin-Awaji earthquake: prognostic indicators in retrospect*. J Trauma, 2002. 52(1): p. 33-9.
23. Mimata, Y., et al., *Limb function after excision of a deltoid muscle sarcoma*. J Shoulder Elbow Surg, 2013. 22(12): p. e1-5.
24. Ziegler-Graham, K., et al., *Estimating the prevalence of limb loss in the United States: 2005 to 2050*. Arch Phys Med Rehabil, 2008. 89(3): p. 422-9.
25. Higgins, T.F., J.B. Klatt, and T.C. Beals, *Lower Extremity Assessment Project (LEAP)--the best available evidence on limb-threatening lower extremity trauma*. Orthop Clin North Am, 2010. 41(2): p. 233-9.
26. Masini, B.D., et al., *Resource utilization and disability outcome assessment of combat casualties from Operation Iraqi Freedom and Operation Enduring Freedom*. J Orthop Trauma, 2009. 23(4): p. 261-6.

27. Stinner, D.J., et al., *Prevalence of late amputations during the current conflicts in Afghanistan and Iraq*. *Mil Med*, 2010. 175(12): p. 1027-9.
28. Huh, J., et al., *Infectious complications and soft tissue injury contribute to late amputation after severe lower extremity trauma*. *The Journal of trauma*, 2011. 71(1 Suppl): p. S47-51.
29. Caudle, R.J. and P.J. Stern, *Severe open fractures of the tibia*. *The Journal of bone and joint surgery. American volume*, 1987. 69(6): p. 801-7.
30. Rossiter, N., T. Higgins, and I. Pallister, *(ii) The mangled extremity: limb salvage versus amputation*. *Orthopaedics and Trauma*, 2014. 28(3): p. 137-140.
31. Doukas, W.C., et al., *The Military Extremity Trauma Amputation/Limb Salvage (METALS) study: outcomes of amputation versus limb salvage following major lower-extremity trauma*. *J Bone Joint Surg Am*, 2013. 95(2): p. 138-45.
32. Cole, P., *Open tibia fracture: amputation versus limb salvage. OPINION: limb salvage*. *J Orthop Trauma*, 2007. 21(1): p. 68-9.
33. Dougherty, P.J., *Open tibia fracture: amputation versus limb salvage. Opinion: below-the-knee amputation*. *J Orthop Trauma*, 2007. 21(1): p. 67-8.
34. Hallock, G.G., *Evidence-based medicine: lower extremity acute trauma*. *Plast Reconstr Surg*, 2013. 132(6): p. 1733-41.
35. Chan, J.K., et al., *Soft-tissue reconstruction of open fractures of the lower limb: muscle versus fasciocutaneous flaps*. *Plast Reconstr Surg*, 2012. 130(2): p. 284e-295e.

36. Will, R.E., et al., *Low Complication Rate Associated With Raising Mature Flap for Tibial Nonunion Reconstruction*. The Journal of trauma, 2011.
37. Napierala, M.A., et al., *Infection reduces return-to-duty rates for soldiers with Type III open tibia fractures*. J Trauma Acute Care Surg, 2014. 77(3 Suppl 2): p. S194-7.
38. Graham, B., et al., *Major replantation versus revision amputation and prosthetic fitting in the upper extremity: a late functional outcomes study*. J Hand Surg Am, 1998. 23(5): p. 783-91.
39. Scott, D.J., et al., *Patient-based outcomes and quality of life after salvageable wartime extremity vascular injury*. J Vasc Surg, 2014. 59(1): p. 173-9 e1.
40. Rosenbloom, B.N., et al., *Systematic review of persistent pain and psychological outcomes following traumatic musculoskeletal injury*. J Pain Res, 2013. 6: p. 39-51.
41. Bierinx, A.S. and A. Seville, *Mouse sectioned muscle regenerates following autografting with muscle fragments: a new muscle precursor cells transfer?* Neurosci Lett, 2008. 431(3): p. 211-4.
42. Rossi, C.A., et al., *In vivo tissue engineering of functional skeletal muscle by freshly isolated satellite cells embedded in a photopolymerizable hydrogel*. FASEB J, 2011. 25(7): p. 2296-304.
43. Page, R.L., et al., *Restoration of skeletal muscle defects with adult human cells delivered on fibrin microthreads*. Tissue Eng Part A, 2011. 17(21-22): p. 2629-40.

44. Sicari, B.M., et al., *A murine model of volumetric muscle loss and a regenerative medicine approach for tissue replacement*. Tissue Eng Part A, 2012. 18(19-20): p. 1941-8.
45. Wu, X., et al., *A standardized rat model of volumetric muscle loss injury for the development of tissue engineering therapies*. Biores Open Access, 2012. 1(6): p. 280-90.
46. Nakabayashi, A., et al., *In vivo bioluminescence imaging of magnetically targeted bone marrow-derived mesenchymal stem cells in skeletal muscle injury model*. J Orthop Res, 2013. 31(5): p. 754-9.
47. Merritt, E.K., et al., *Functional assessment of skeletal muscle regeneration utilizing homologous extracellular matrix as scaffolding*. Tissue Eng Part A, 2010. 16(4): p. 1395-405.
48. Manini, T.M., et al., *Reduced physical activity increases intermuscular adipose tissue in healthy young adults*. Am J Clin Nutr, 2007. 85(2): p. 377-84.
49. Vettor, R., et al., *The origin of intermuscular adipose tissue and its pathophysiological implications*. Am J Physiol Endocrinol Metab, 2009. 297(5): p. E987-98.
50. Melnyk, M., et al., *Revascularisation during fracture healing with soft tissue injury*. Arch Orthop Trauma Surg, 2008. 128(10): p. 1159-65.
51. Claes, L., et al., *Moderate soft tissue trauma delays new bone formation only in the early phase of fracture healing*. J Orthop Res, 2006. 24(6): p. 1178-85.
52. Landry, P.S., et al., *Effect of soft-tissue trauma on the early periosteal response of bone to injury*. J Trauma, 2000. 48(3): p. 479-83.

53. Landry, P.S., et al., *Bone injury response. An animal model for testing theories of regulation.* Clin Orthop Relat Res, 1996(332): p. 260-73.
54. Utvag, S.E., et al., *Influence of extensive muscle injury on fracture healing in rat tibia.* J Orthop Trauma, 2003. 17(6): p. 430-5.
55. Stein, H., et al., *The muscle bed--a crucial factor for fracture healing: a physiological concept.* Orthopedics, 2002. 25(12): p. 1379-83.
56. Liu, R., A. Schindeler, and D.G. Little, *The potential role of muscle in bone repair.* J Musculoskelet Neuronal Interact, 2010. 10(1): p. 71-6.
57. Pfeifer, R., et al., *Cumulative effects of bone and soft tissue injury on systemic inflammation: a pilot study.* Clin Orthop Relat Res, 2013. 471(9): p. 2815-21.
58. Garg, K., et al., *Transplantation of devitalized muscle scaffolds is insufficient for appreciable de novo muscle fiber regeneration after volumetric muscle loss injury.* Cell Tissue Res, 2014.
59. Corona, B.T., et al., *The promotion of a functional fibrosis in skeletal muscle with volumetric muscle loss injury following the transplantation of muscle-ECM.* Biomaterials, 2013. 34(13): p. 3324-35.
60. Turner, N.J., et al., *Xenogeneic extracellular matrix as an inductive scaffold for regeneration of a functioning musculotendinous junction.* Tissue Eng Part A, 2010. 16(11): p. 3309-17.
61. Turner, N.J., et al., *Biologic scaffold remodeling in a dog model of complex musculoskeletal injury.* J Surg Res, 2012. 176(2): p. 490-502.
62. Gillies, A.R. and R.L. Lieber, *Structure and function of the skeletal muscle extracellular matrix.* Muscle Nerve, 2011. 44(3): p. 318-31.

63. Wolf, M.T., et al., *Biologic scaffold composed of skeletal muscle extracellular matrix*. *Biomaterials*, 2012. 33(10): p. 2916-25.
64. Gillies, A.R., et al., *Method for decellularizing skeletal muscle without detergents or proteolytic enzymes*. *Tissue Eng Part C Methods*, 2011. 17(4): p. 383-9.
65. Sicari, B.M., et al., *An acellular biologic scaffold promotes skeletal muscle formation in mice and humans with volumetric muscle loss*. *Sci Transl Med*, 2014. 6(234): p. 234ra58.
66. Mase, V.J., Jr., et al., *Clinical application of an acellular biologic scaffold for surgical repair of a large, traumatic quadriceps femoris muscle defect*. *Orthopedics*, 2010. 33(7): p. 511.
67. Palmer, E.M., et al., *Human helper T cell activation and differentiation is suppressed by porcine small intestinal submucosa*. *Tissue Eng*, 2002. 8(5): p. 893-900.
68. Allman, A.J., et al., *The Th2-restricted immune response to xenogeneic small intestinal submucosa does not influence systemic protective immunity to viral and bacterial pathogens*. *Tissue Eng*, 2002. 8(1): p. 53-62.
69. Valentin, J.E., et al., *Macrophage participation in the degradation and remodeling of extracellular matrix scaffolds*. *Tissue Eng Part A*, 2009. 15(7): p. 1687-94.
70. Badylak, S.F., et al., *Macrophage phenotype as a determinant of biologic scaffold remodeling*. *Tissue Eng Part A*, 2008. 14(11): p. 1835-42.

71. Shi, M., et al., *Acceleration of skeletal muscle regeneration in a rat skeletal muscle injury model by local injection of human peripheral blood-derived CD133-positive cells*. Stem Cells, 2009. 27(4): p. 949-60.
72. Mori, R., et al., *Promotion of skeletal muscle repair in a rat skeletal muscle injury model by local injection of human adipose tissue-derived regenerative cells*. J Tissue Eng Regen Med, 2012.
73. Machingal, M.A., et al., *A tissue-engineered muscle repair construct for functional restoration of an irrecoverable muscle injury in a murine model*. Tissue Eng Part A, 2011. 17(17-18): p. 2291-303.
74. Corona, B.T., et al., *Further development of a tissue engineered muscle repair construct in vitro for enhanced functional recovery following implantation in vivo in a murine model of volumetric muscle loss injury*. Tissue Eng Part A, 2012. 18(11-12): p. 1213-28.
75. Corona, B.T., et al., *Implantation of in vitro tissue engineered muscle repair constructs and bladder acellular matrices partially restore in vivo skeletal muscle function in a rat model of volumetric muscle loss injury*. Tissue Eng Part A, 2014. 20(3-4): p. 705-15.
76. VanDusen, K.W., et al., *Engineered Skeletal Muscle Units for Repair of Volumetric Muscle Loss in the Tibialis Anterior Muscle of a Rat*. Tissue Eng Part A, 2014.
77. Merritt, E.K., et al., *Repair of traumatic skeletal muscle injury with bone-marrow-derived mesenchymal stem cells seeded on extracellular matrix*. Tissue Eng Part A, 2010. 16(9): p. 2871-81.

78. Longo, U.G., et al., *Tissue engineered strategies for skeletal muscle injury*. Stem Cells Int, 2012. 2012: p. 175038.
79. Schultz, E., D.L. Jaryszak, and C.R. Valliere, *Response of satellite cells to focal skeletal muscle injury*. Muscle Nerve, 1985. 8(3): p. 217-22.
80. Ferrari, G., et al., *Muscle regeneration by bone marrow-derived myogenic progenitors*. Science, 1998. 279(5356): p. 1528-30.
81. Tidball, J.G., *Inflammatory processes in muscle injury and repair*. Am J Physiol Regul Integr Comp Physiol, 2005. 288(2): p. R345-53.
82. Lu, H., et al., *Macrophages recruited via CCR2 produce insulin-like growth factor-1 to repair acute skeletal muscle injury*. FASEB J, 2011. 25(1): p. 358-69.
83. Mourkioti, F. and N. Rosenthal, *IGF-1, inflammation and stem cells: interactions during muscle regeneration*. Trends Immunol, 2005. 26(10): p. 535-42.
84. Joe, A.W., et al., *Muscle injury activates resident fibro/adipogenic progenitors that facilitate myogenesis*. Nat Cell Biol, 2010. 12(2): p. 153-63.
85. Tedesco, F.S., et al., *Repairing skeletal muscle: regenerative potential of skeletal muscle stem cells*. J Clin Invest, 2010. 120(1): p. 11-9.
86. Levenberg, S., et al., *Engineering vascularized skeletal muscle tissue*. Nat Biotechnol, 2005. 23(7): p. 879-84.
87. Koffler, J., et al., *Improved vascular organization enhances functional integration of engineered skeletal muscle grafts*. Proc Natl Acad Sci U S A, 2011. 108(36): p. 14789-94.

88. Frey, S.P., et al., *VEGF improves skeletal muscle regeneration after acute trauma and reconstruction of the limb in a rabbit model*. Clin Orthop Relat Res, 2012. 470(12): p. 3607-14.
89. Borselli, C., et al., *Functional muscle regeneration with combined delivery of angiogenesis and myogenesis factors*. Proc Natl Acad Sci U S A, 2010. 107(8): p. 3287-92.
90. Borselli, C., et al., *The role of multifunctional delivery scaffold in the ability of cultured myoblasts to promote muscle regeneration*. Biomaterials, 2011. 32(34): p. 8905-14.
91. Richards, R.R. and E.H. Schemitsch, *Effect of muscle flap coverage on bone blood flow following devascularization of a segment of tibia: an experimental investigation in the dog*. J Orthop Res, 1989. 7(4): p. 550-8.
92. Schemitsch, E.H., et al., *The relative importance of intramedullary, intracortical, and extraosseous soft-tissue blood flow to the repair of devascularized canine tibial cortex*. Ann Plast Surg, 1997. 38(6): p. 623-31.
93. Harry, L.E., et al., *Comparison of the healing of open tibial fractures covered with either muscle or fasciocutaneous tissue in a murine model*. J Orthop Res, 2008. 26(9): p. 1238-44.
94. Hamrick, M.W., et al., *Recombinant myostatin (GDF-8) propeptide enhances the repair and regeneration of both muscle and bone in a model of deep penetrant musculoskeletal injury*. J Trauma, 2010. 69(3): p. 579-83.
95. Oest, M.E., et al., *Quantitative assessment of scaffold and growth factor-mediated repair of critically sized bone defects*. J Orthop Res, 2007. 25(7): p. 941-50.

96. MacKenzie, E.J., et al., *Health-care costs associated with amputation or reconstruction of a limb-threatening injury*. J Bone Joint Surg Am, 2007. 89(8): p. 1685-92.
97. MacKenzie, E.J., et al., *Characterization of patients with high-energy lower extremity trauma*. J Orthop Trauma, 2000. 14(7): p. 455-66.
98. Fischer, M.D., R.B. Gustilo, and T.F. Varecka, *The timing of flap coverage, bone-grafting, and intramedullary nailing in patients who have a fracture of the tibial shaft with extensive soft-tissue injury*. J Bone Joint Surg Am, 1991. 73(9): p. 1316-22.
99. Godina, M., J. Bajec, and A. Baraga, *Salvage of the mutilated upper extremity with temporary ectopic implantation of the undamaged part*. Plast Reconstr Surg, 1986. 78(3): p. 295-9.
100. Pollak, A.N., M.L. McCarthy, and A.R. Burgess, *Short-term wound complications after application of flaps for coverage of traumatic soft-tissue defects about the tibia. The Lower Extremity Assessment Project (LEAP) Study Group*. J Bone Joint Surg Am, 2000. 82-A(12): p. 1681-91.
101. Gopal, S., et al., *Fix and flap: the radical orthopaedic and plastic treatment of severe open fractures of the tibia*. J Bone Joint Surg Br, 2000. 82(7): p. 959-66.
102. MacKenzie, E.J., et al., *Long-term persistence of disability following severe lower-limb trauma. Results of a seven-year follow-up*. J Bone Joint Surg Am, 2005. 87(8): p. 1801-9.

103. Huh, J., et al., *Infectious complications and soft tissue injury contribute to late amputation after severe lower extremity trauma*. J Trauma, 2011. 71(1 Suppl): p. S47-51.
104. Willett, N.J., et al., *Attenuated human bone morphogenetic protein-2-mediated bone regeneration in a rat model of composite bone and muscle injury*. Tissue Eng Part C Methods, 2013. 19(4): p. 316-25.
105. Deumens, R., et al., *The CatWalk gait analysis in assessment of both dynamic and static gait changes after adult rat sciatic nerve resection*. J Neurosci Methods, 2007. 164(1): p. 120-30.
106. Bozkurt, A., et al., *CatWalk gait analysis in assessment of functional recovery after sciatic nerve injury*. J Neurosci Methods, 2008. 173(1): p. 91-8.
107. Uhrig, B.A., et al., *Characterization of a composite injury model of severe lower limb bone and nerve trauma*. J Tissue Eng Regen Med, 2012.
108. Hamers, F.P., et al., *Automated quantitative gait analysis during overground locomotion in the rat: its application to spinal cord contusion and transection injuries*. J Neurotrauma, 2001. 18(2): p. 187-201.
109. Lee, Y.S., et al., *Serial MR imaging of intramuscular hematoma: experimental study in a rat model with the pathologic correlation*. Korean J Radiol, 2011. 12(1): p. 66-77.
110. Duda, G.N., et al., *Biomechanical, microvascular, and cellular factors promote muscle and bone regeneration*. Exerc Sport Sci Rev, 2008. 36(2): p. 64-70.
111. Winkler, T., et al., *Time course of skeletal muscle regeneration after severe trauma*. Acta Orthop, 2011. 82(1): p. 102-11.

112. Lowe, D.A., et al., *Muscle function and protein metabolism after initiation of eccentric contraction-induced injury*. J Appl Physiol, 1995. 79(4): p. 1260-70.
113. Warren, G.L., et al., *Functional recovery of the plantarflexor muscle group after hindlimb unloading in the rat*. Eur J Appl Physiol, 2004. 93(1-2): p. 130-8.
114. Burke, R.E., et al., *Physiological types and histochemical profiles in motor units of the cat gastrocnemius*. J Physiol, 1973. 234(3): p. 723-48.
115. Zhang, F., et al., *Comparison of muscle mass preservation in denervated muscle and transplanted muscle flaps after motor and sensory reinnervation and neurotization*. Plast Reconstr Surg, 1997. 99(3): p. 803-14.
116. Oswald, T.M., et al., *Muscle flap mass preservation with end-to-side neurorrhaphy: an experimental study*. J Reconstr Microsurg, 2004. 20(6): p. 483-8.
117. Yoshitatsu, S., et al., *Muscle flap mass preservation by sensory reinnervation with end-to-side neurorrhaphy: an experimental study in rats*. J Reconstr Microsurg, 2008. 24(7): p. 479-87.
118. Kaariainen, M. and S. Kauhanen, *Skeletal muscle injury and repair: the effect of disuse and denervation on muscle and clinical relevance in pedicled and free muscle flaps*. J Reconstr Microsurg, 2012. 28(9): p. 581-7.
119. Carlson, B.M. and E. Gutmann, *Development of contractile properties of minced muscle regenerates in the rat*. Exp Neurol, 1972. 36(2): p. 239-49.
120. Meyer, G.A. and R.L. Lieber, *Elucidation of extracellular matrix mechanics from muscle fibers and fiber bundles*. J Biomech, 2011. 44(4): p. 771-3.

121. Zahir, K.S., et al., *Ischemic preconditioning improves the survival of skin and myocutaneous flaps in a rat model*. *Plast Reconstr Surg*, 1998. 102(1): p. 140-50; discussion 151-2.
122. Zahir, T.M., et al., *Ischemic preconditioning of musculocutaneous flaps: effects of ischemia cycle length and number of cycles*. *Ann Plast Surg*, 1998. 40(4): p. 430-5.
123. Zahir, K.S., et al., *Comparison of the effects of ischemic preconditioning and surgical delay on pedicled musculocutaneous flap survival in a rat model*. *Ann Plast Surg*, 1998. 40(4): p. 422-8; discussion 428-9.
124. Corona, B.T., et al., *Autologous minced muscle grafts: A tissue engineering therapy for the volumetric loss of skeletal muscle*. *Am J Physiol Cell Physiol*, 2013.
125. Edwards, C.C., et al., *Severe open tibial fractures. Results treating 202 injuries with external fixation*. *Clin Orthop Relat Res*, 1988(230): p. 98-115.
126. Gustilo, R.B., R.L. Merkow, and D. Templeman, *The management of open fractures*. *J Bone Joint Surg Am*, 1990. 72(2): p. 299-304.
127. Krettek, C., P. Schandelmaier, and H. Tscherne, *Nonreamed interlocking nailing of closed tibial fractures with severe soft tissue injury*. *Clin Orthop Relat Res*, 1995(315): p. 34-47.
128. Oestern, H.J. and H. Tscherne, *[Pathophysiology and classification of soft tissue damage in fractures]*. *Orthopade*, 1983. 12(1): p. 2-8.
129. Bosse, M.J., et al., *An analysis of outcomes of reconstruction or amputation after leg-threatening injuries*. *N Engl J Med*, 2002. 347(24): p. 1924-31.

130. Masquelet, A.C., *Muscle reconstruction in reconstructive surgery: soft tissue repair and long bone reconstruction*. Langenbecks Arch Surg, 2003. 388(5): p. 344-6.
131. Harry, L.E., et al., *Comparison of the healing of open tibial fractures covered with either muscle or fasciocutaneous tissue in a murine model*. Journal of Orthopaedic Research, 2008. 26(9): p. 1238-1244.
132. Helgeson, M.D., et al., *Risk factors for and results of late or delayed amputation following combat-related extremity injuries*. Orthopedics, 2010. 33: p. 669.
133. Russell, W.L., et al., *Limb salvage versus traumatic amputation. A decision based on a seven-part predictive index*. Ann Surg, 1991. 213(5): p. 473-80; discussion 480-1.
134. Georgiadis, G.M., et al., *Open tibial fractures with severe soft-tissue loss. Limb salvage compared with below-the-knee amputation*. J Bone Joint Surg Am, 1993. 75(10): p. 1431-41.
135. Owens, B.D., et al., *Combat wounds in operation Iraqi Freedom and operation Enduring Freedom*. J Trauma, 2008. 64(2): p. 295-9.
136. Liu, B., *Potential for Muscle in Bone Repair*. 2010.
137. Hamrick, M.W., P.L. McNeil, and S.L. Patterson, *Role of muscle-derived growth factors in bone formation*. J Musculoskelet Neuronal Interact, 2010. 10(1): p. 64-70.
138. Harry, L.E., et al., *Comparison of the vascularity of fasciocutaneous tissue and muscle for coverage of open tibial fractures*. Plast Reconstr Surg, 2009. 124(4): p. 1211-9.

139. Carano, R.A. and E.H. Filvaroff, *Angiogenesis and bone repair*. Drug Discov Today, 2003. 8(21): p. 980-9.
140. Hausman, M.R., M.B. Schaffler, and R.J. Majeska, *Prevention of fracture healing in rats by an inhibitor of angiogenesis*. Bone, 2001. 29(6): p. 560-4.
141. Lieberman, J.R., A. Daluiski, and T.A. Einhorn, *The role of growth factors in the repair of bone. Biology and clinical applications*. J Bone Joint Surg Am, 2002. 84-A(6): p. 1032-44.
142. Chan, X.C., J.C. McDermott, and K.W. Siu, *Identification of secreted proteins during skeletal muscle development*. J Proteome Res, 2007. 6(2): p. 698-710.
143. Hashimoto, N., et al., *Osteogenic properties of human myogenic progenitor cells*. Mech Dev, 2008. 125(3-4): p. 257-69.
144. Gersbach, C.A., R.E. Guldborg, and A.J. Garcia, *In vitro and in vivo osteoblastic differentiation of BMP-2- and Runx2-engineered skeletal myoblasts*. J Cell Biochem, 2007. 100(5): p. 1324-36.
145. Liu, R., et al., *Myogenic progenitors contribute to open but not closed fracture repair*. BMC Musculoskelet Disord, 2011. 12: p. 288.
146. Claes, L., et al., *Moderate soft tissue trauma delays new bone formation only in the early phase of fracture healing*. Journal of Orthopaedic Research, 2006. 24(6): p. 1178-1185.
147. Hamrick, M.W., et al., *Recombinant myostatin (GDF-8) propeptide enhances the repair and regeneration of both muscle and bone in a model of deep penetrant musculoskeletal injury*. The Journal of trauma, 2010. 69: p. 579-83.

148. Utvag, S.E., et al., *Poor muscle coverage delays fracture healing in rats*. Acta Orthop Scand, 2002. 73(4): p. 471-4.
149. Histing, T., et al., *Small animal bone healing models: standards, tips, and pitfalls results of a consensus meeting*. Bone, 2011. 49(4): p. 591-9.
150. Boerckel, J.D., et al., *Effects of protein dose and delivery system on BMP-mediated bone regeneration*. Biomaterials, 2011. 32(22): p. 5241-51.
151. Kolambkar, Y.M., et al., *Spatiotemporal delivery of bone morphogenetic protein enhances functional repair of segmental bone defects*. Bone, 2011. 49(3): p. 485-92.
152. Oest, M.E., et al., *Quantitative assessment of scaffold and growth factor-mediated repair of critically sized bone defects*. Journal of Orthopaedic Research, 2007. 25(7): p. 941-50.
153. Boerckel, J.D., et al., *Mechanical regulation of vascular growth and tissue regeneration in vivo*. Proc Natl Acad Sci U S A, 2011. 108(37): p. E674-80.
154. Duvall, C.L., et al., *Quantitative microcomputed tomography analysis of collateral vessel development after ischemic injury*. Am J Physiol Heart Circ Physiol, 2004. 287(1): p. H302-10.
155. Uhrig, B.A., et al., *Recovery from hind limb ischemia enhances rhBMP-2-mediated segmental bone defect repair in a rat composite injury model*. Bone, 2013. 55(2): p. 410-7.
156. Chu, T.M., et al., *Segmental bone regeneration using a load-bearing biodegradable carrier of bone morphogenetic protein-2*. Biomaterials, 2007. 28(3): p. 459-67.

157. Lieberman, J.R., et al., *The effect of regional gene therapy with bone morphogenetic protein-2-producing bone-marrow cells on the repair of segmental femoral defects in rats*. J Bone Joint Surg Am, 1999. 81(7): p. 905-17.
158. Yasko, A.W., et al., *The healing of segmental bone defects, induced by recombinant human bone morphogenetic protein (rhBMP-2). A radiographic, histological, and biomechanical study in rats*. J Bone Joint Surg Am, 1992. 74(5): p. 659-70.
159. Angle, S.R., et al., *Healing of rat femoral segmental defect with bone morphogenetic protein-2: a dose response study*. J Musculoskelet Neuronal Interact, 2012. 12(1): p. 28-37.
160. Brown, K.V., et al., *Improving bone formation in a rat femur segmental defect by controlling bone morphogenetic protein-2 release*. Tissue Eng Part A, 2011. 17(13-14): p. 1735-46.
161. Schindeler, A., R. Liu, and D.G. Little, *The contribution of different cell lineages to bone repair: exploring a role for muscle stem cells*. Differentiation, 2009. 77(1): p. 12-8.
162. Malizos, K.N. and L.K. Papatheodorou, *The healing potential of the periosteum molecular aspects*. Injury, 2005. 36 Suppl 3: p. S13-9.
163. Shapiro, F., *Bone development and its relation to fracture repair. The role of mesenchymal osteoblasts and surface osteoblasts*. Eur Cell Mater, 2008. 15: p. 53-76.
164. Dwek, J.R., *The periosteum: what is it, where is it, and what mimics it in its absence?* Skeletal Radiol, 2010. 39(4): p. 319-23.

165. Einhorn, T.A., *Enhancement of fracture-healing*. J Bone Joint Surg Am, 1995. 77(6): p. 940-56.
166. Gross, T.S., et al., *The effect of muscle dysfunction on bone mass and morphology*. J Musculoskelet Neuronal Interact, 2010. 10(1): p. 25-34.
167. Pedersen, B.K. and M.A. Febbraio, *Muscles, exercise and obesity: skeletal muscle as a secretory organ*. Nat Rev Endocrinol, 2012.
168. Aliprantis, A.O., et al., *Transient muscle paralysis degrades bone via rapid osteoclastogenesis*. FASEB J, 2012. 26(3): p. 1110-8.
169. Ausk, B.J., et al., *Cortical bone resorption following muscle paralysis is spatially heterogeneous*. Bone, 2012. 50(1): p. 14-22.
170. Mann, C.J., et al., *Aberrant repair and fibrosis development in skeletal muscle*. Skelet Muscle, 2011. 1(1): p. 21.
171. Evans, W.J. and W.W. Campbell, *Sarcopenia and age-related changes in body composition and functional capacity*. J Nutr, 1993. 123(2 Suppl): p. 465-8.
172. Perrini, S., et al., *The GH/IGF1 axis and signaling pathways in the muscle and bone: mechanisms underlying age-related skeletal muscle wasting and osteoporosis*. J Endocrinol, 2010. 205(3): p. 201-10.
173. Yazar, S., C.H. Lin, and F.C. Wei, *One-stage reconstruction of composite bone and soft-tissue defects in traumatic lower extremities*. Plast Reconstr Surg, 2004. 114(6): p. 1457-66.
174. Nauth, A., et al., *Managing bone defects*. J Orthop Trauma, 2011. 25(8): p. 462-6.
175. Boerckel, J.D., et al., *Effects of in vivo mechanical loading on large bone defect regeneration*. Journal of Orthopaedic Research, 2011.

176. Li, M.T., et al., *Functional analysis of limb recovery following autograft treatment of volumetric muscle loss in the quadriceps femoris*. J Biomech, 2014. 47(9): p. 2013-21.
177. Collins, C.A., et al., *Stem cell function, self-renewal, and behavioral heterogeneity of cells from the adult muscle satellite cell niche*. Cell, 2005. 122(2): p. 289-301.
178. Montarras, D., et al., *Direct isolation of satellite cells for skeletal muscle regeneration*. Science, 2005. 309(5743): p. 2064-7.
179. Nesti, L.J., et al., *Differentiation potential of multipotent progenitor cells derived from war-traumatized muscle tissue*. J Bone Joint Surg Am, 2008. 90(11): p. 2390-8.
180. Haury, B., et al., *Debridement: an essential component of traumatic wound care*. Am J Surg, 1978. 135(2): p. 238-42.
181. Rath, E.M., et al., *Gluteus minimus necrotic muscle debridement diminishes heterotopic ossification after acetabular fracture fixation*. Injury, 2002. 33(9): p. 751-6.
182. Basu, S., et al., *Necrotic but not apoptotic cell death releases heat shock proteins, which deliver a partial maturation signal to dendritic cells and activate the NF-kappa B pathway*. Int Immunol, 2000. 12(11): p. 1539-46.
183. Kono, H. and K.L. Rock, *How dying cells alert the immune system to danger*. Nat Rev Immunol, 2008. 8(4): p. 279-89.
184. Tabbaa, S., et al., *Role of vascularity for successful bone formation and repair*. Critical Reviews™ in Biomedical Engineering.

185. Cierny, G., 3rd, H.S. Byrd, and R.E. Jones, *Primary versus delayed soft tissue coverage for severe open tibial fractures. A comparison of results.* Clin Orthop Relat Res, 1983(178): p. 54-63.
186. Gerber, C., J.W. Mast, and R. Ganz, *Biological internal fixation of fractures.* Arch Orthop Trauma Surg, 1990. 109(6): p. 295-303.
187. Godina, M., *Early microsurgical reconstruction of complex trauma of the extremities.* Plast Reconstr Surg, 1986. 78(3): p. 285-92.
188. Richards, R.R., et al., *The influence of muscle flap coverage on the repair of devascularized tibial cortex: an experimental investigation in the dog.* Plast Reconstr Surg, 1987. 79(6): p. 946-58.
189. Koshima, I., et al., *The vasculature and clinical application of the posterior tibial perforator-based flap.* Plast Reconstr Surg, 1992. 90(4): p. 643-9.
190. Nojima, K., et al., *Defining vascular supply and territory of thinned perforator flaps: Part I. Anterolateral thigh perforator flap.* Plastic and reconstructive surgery, 2005. 116(1): p. 182-193.
191. Schaverien, M. and M. Saint-Cyr, *Perforators of the lower leg: analysis of perforator locations and clinical application for pedicled perforator flaps.* Plast Reconstr Surg, 2008. 122(1): p. 161-70.
192. Lieber, R.L. and J. Friden, *Functional and clinical significance of skeletal muscle architecture.* Muscle Nerve, 2000. 23(11): p. 1647-66.
193. Armstrong, R.B. and R.O. Phelps, *Muscle fiber type composition of the rat hindlimb.* Am J Anat, 1984. 171(3): p. 259-72.

194. Lieber, R.L. and S.C. Bodine-Fowler, *Skeletal muscle mechanics: implications for rehabilitation*. Phys Ther, 1993. 73(12): p. 844-56.
195. Sacks, R.D. and R.R. Roy, *Architecture of the hind limb muscles of cats: functional significance*. J Morphol, 1982. 173(2): p. 185-95.
196. Tanzer, M.L. and C. Gilvarg, *Creatine and creatine kinase measurement*. J Biol Chem, 1959. 234: p. 3201-4.
197. Adams, J.E., 3rd, D.R. Abendschein, and A.S. Jaffe, *Biochemical markers of myocardial injury. Is MB creatine kinase the choice for the 1990s?* Circulation, 1993. 88(2): p. 750-63.
198. Bischoff, R. and C. Heintz, *Enhancement of skeletal muscle regeneration*. Dev Dyn, 1994. 201(1): p. 41-54.
199. van Deursen, J., et al., *Skeletal muscles of mice deficient in muscle creatine kinase lack burst activity*. Cell, 1993. 74(4): p. 621-31.
200. Sillau, A.H. and N. Banchero, *Effects of hypoxia on capillary density and fiber composition in rat skeletal muscle*. Pflugers Arch, 1977. 370(3): p. 227-32.
201. Chang, C.C., et al., *Determinants of microvascular network topologies in implanted neovasculatures*. Arterioscler Thromb Vasc Biol, 2012. 32(1): p. 5-14.
202. Ochoa, O., et al., *Delayed angiogenesis and VEGF production in CCR2<sup>-/-</sup> mice during impaired skeletal muscle regeneration*. Am J Physiol Regul Integr Comp Physiol, 2007. 293(2): p. R651-61.
203. Hoying, J.B., C.A. Boswell, and S.K. Williams, *Angiogenic potential of microvessel fragments established in three-dimensional collagen gels*. In Vitro Cell Dev Biol Anim, 1996. 32(7): p. 409-19.

204. Shepherd, B.R., et al., *Rapid perfusion and network remodeling in a microvascular construct after implantation*. *Arterioscler Thromb Vasc Biol*, 2004. 24(5): p. 898-904.
205. Pilia, M., et al., *Transplantation and perfusion of microvascular fragments in a rodent model of volumetric muscle loss injury*. *Eur Cell Mater*, 2014. 28: p. 11-23; discussion 23-4.
206. Gibot, L., et al., *A preexisting microvascular network benefits in vivo revascularization of a microvascularized tissue-engineered skin substitute*. *Tissue Eng Part A*, 2010. 16(10): p. 3199-206.
207. Mauro, A., *Satellite cell of skeletal muscle fibers*. *J Biophys Biochem Cytol*, 1961. 9: p. 493-5.
208. Rhoads, R.P., et al., *Satellite cell-mediated angiogenesis in vitro coincides with a functional hypoxia-inducible factor pathway*. *Am J Physiol Cell Physiol*, 2009. 296(6): p. C1321-8.
209. Murphy, M.M., et al., *Satellite cells, connective tissue fibroblasts and their interactions are crucial for muscle regeneration*. *Development*, 2011. 138(17): p. 3625-37.
210. Sambasivan, R., et al., *Pax7-expressing satellite cells are indispensable for adult skeletal muscle regeneration*. *Development*, 2011. 138(17): p. 3647-56.
211. Nunes, S.S., et al., *Implanted microvessels progress through distinct neovascularization phenotypes*. *Microvasc Res*, 2010. 79(1): p. 10-20.

212. Asakura, A., M. Komaki, and M. Rudnicki, *Muscle satellite cells are multipotential stem cells that exhibit myogenic, osteogenic, and adipogenic differentiation*. *Differentiation*, 2001. 68(4-5): p. 245-53.
213. Uezumi, A., et al., *Mesenchymal progenitors distinct from satellite cells contribute to ectopic fat cell formation in skeletal muscle*. *Nat Cell Biol*, 2010. 12(2): p. 143-52.
214. Williams, J.T., et al., *Cells isolated from adult human skeletal muscle capable of differentiating into multiple mesodermal phenotypes*. *Am Surg*, 1999. 65(1): p. 22-6.
215. Shepherd, B.R., J.B. Hoying, and S.K. Williams, *Microvascular transplantation after acute myocardial infarction*. *Tissue Eng*, 2007. 13(12): p. 2871-9.
216. Contreras-Shannon, V., et al., *Fat accumulation with altered inflammation and regeneration in skeletal muscle of CCR2<sup>-/-</sup> mice following ischemic injury*. *Am J Physiol Cell Physiol*, 2007. 292(2): p. C953-67.
217. Warren, G.L., et al., *Chemokine receptor CCR2 involvement in skeletal muscle regeneration*. *FASEB J*, 2005. 19(3): p. 413-5.
218. Pinho, R.A., et al., *Imbalance in SOD/CAT activities in rat skeletal muscles submitted to treadmill training exercise*. *Cell Biol Int*, 2006. 30(10): p. 848-53.
219. Siu, P.M., et al., *Citrate synthase expression and enzyme activity after endurance training in cardiac and skeletal muscles*. *J Appl Physiol (1985)*, 2003. 94(2): p. 555-60.
220. Zhou, W., et al., *Angiogenic gene-modified myoblasts promote vascularization during repair of skeletal muscle defects*. *J Tissue Eng Regen Med*, 2013.

221. Tampe, U., et al., *Lower extremity soft tissue reconstruction and amputation rates in patients with open tibial fractures in Sweden during 1998-2010*. BMC Surg, 2014. 14(1): p. 80.
222. Enninghorst, N., et al., *Population-based epidemiology of femur shaft fractures*. J Trauma Acute Care Surg, 2013. 74(6): p. 1516-20.
223. Kovar, F.M., et al., *Incidence and analysis of open fractures of the midshaft and distal femur*. Wien Klin Wochenschr, 2013. 125(13-14): p. 396-401.
224. Nicola, R., *Early Total Care versus Damage Control: Current Concepts in the Orthopedic Care of Polytrauma Patients*. ISRN Orthop, 2013. 2013: p. 329452.
225. Banerjee, M., et al., *Epidemiology of extremity injuries in multiple trauma patients*. Injury, 2013. 44(8): p. 1015-21.
226. Neale, H.W., et al., *Complications of muscle-flap transposition for traumatic defects of the leg*. Plast Reconstr Surg, 1983. 72(4): p. 512-7.
227. Adams, W.P., Jr., et al., *Functional donor site morbidity following latissimus dorsi muscle flap transfer*. Ann Plast Surg, 2004. 53(1): p. 6-11.
228. Zook, E.G., R.C. Russell, and M. Asaadi, *A comparative study of free and pedicle flaps for lower extremity wounds*. Ann Plast Surg, 1986. 17(1): p. 21-33.
229. Momoh, A.O. and K.C. Chung, *Measuring outcomes in lower limb surgery*. Clin Plast Surg, 2013. 40(2): p. 323-9.
230. Kryger, Z., et al., *Effects of VEGF administration following ischemia on survival of the gracilis muscle flap in the rat*. Ann Plast Surg, 1999. 43(2): p. 172-8.
231. Macnab, I. and W.G. De Haas, *The role of periosteal blood supply in the healing of fractures of the tibia*. Clin Orthop Relat Res, 1974(105): p. 27-33.

232. Colnot, C., *Skeletal cell fate decisions within periosteum and bone marrow during bone regeneration*. J Bone Miner Res, 2009. 24(2): p. 274-82.
233. Dimitriou, R., E. Tsiridis, and P.V. Giannoudis, *Current concepts of molecular aspects of bone healing*. Injury, 2005. 36(12): p. 1392-404.
234. Zhang, X., et al., *A perspective: engineering periosteum for structural bone graft healing*. Clin Orthop Relat Res, 2008. 466(8): p. 1777-87.
235. Roedersheimer, M., et al., *A bone-derived mixture of TGF beta-superfamily members forms a more mature vascular network than bFGF or TGF-beta 2 in vivo*. Angiogenesis, 2005. 8(4): p. 327-38.
236. Dosier, C.R., et al., *Effect of Cell Origin and Timing of Delivery for Stem Cell-Based Bone Tissue Engineering Using Biologically Functionalized Hydrogels*. Tissue Eng Part A, 2014.
237. Katagiri, T., et al., *Bone morphogenetic protein-2 converts the differentiation pathway of C2C12 myoblasts into the osteoblast lineage*. J Cell Biol, 1994. 127(6 Pt 1): p. 1755-66.
238. Ono, Y., et al., *BMP signalling permits population expansion by preventing premature myogenic differentiation in muscle satellite cells*. Cell Death Differ, 2011. 18(2): p. 222-34.
239. Cross, J.D., et al., *Battlefield orthopaedic injuries cause the majority of long-term disabilities*. J Am Acad Orthop Surg, 2011. 19 Suppl 1: p. S1-7.
240. Grundnes, O. and O. Reikeras, *The importance of the hematoma for fracture healing in rats*. Acta Orthop Scand, 1993. 64(3): p. 340-2.

241. Rooser, B., S. Bengtson, and G. Hagglund, *Acute compartment syndrome from anterior thigh muscle contusion: a report of eight cases*. J Orthop Trauma, 1991. 5(1): p. 57-9.
242. Utvag, S.E., O. Grundnes, and O. Reikeraos, *Effects of periosteal stripping on healing of segmental fractures in rats*. J Orthop Trauma, 1996. 10(4): p. 279-84.
243. Lu, C., et al., *Effect of age on vascularization during fracture repair*. J Orthop Res, 2008. 26(10): p. 1384-9.
244. Farhat, M.Y., M.C. Lavigne, and P.W. Ramwell, *The vascular protective effects of estrogen*. Faseb j, 1996. 10(5): p. 615-24.
245. Simoncini, T., *Mechanisms of action of estrogen receptors in vascular cells: relevance for menopause and aging*. Climacteric, 2009. 12 Suppl 1: p. 6-11.
246. White, R.E., *Estrogen and vascular function*. Vascul Pharmacol, 2002. 38(2): p. 73-80.
247. Lu, C., R. Marcucio, and T. Miclau, *Assessing Angiogenesis during Fracture Healing*. Iowa Orthop J, 2006. 26: p. 17-26.
248. Vincent, M.A., et al., *Skeletal muscle microvascular recruitment by physiological hyperinsulinemia precedes increases in total blood flow*. Diabetes, 2002. 51(1): p. 42-8.